

Modeling of micro- and nanostructures made of films and crystals/fibers arrays

Dissertation

zur Erlangung des akademischen Grades

Doktoringenieurin

(Dr.-Ing.)

von M.Sc. Anna Girchenko

geb. am 18.11.1985 in Mineralnyje Wody

genehmigt durch die Fakultät für Maschinenbau
der Otto-von-Guericke-Universität Magdeburg

Gutachter:

Prof. Dr.-Ing.habil. Dr.h.c. Holm Altenbach

Prof. Dr. Sci. (Phys.-Math) Andrey V. Nasedkin

Promotionskolloquium am 05.12.2013

Abstract

The aim of this work is the complex research of the behavior of a multilayer structure which has a chiral geometry on the joint of multiphysics in the field of coupled tasks. In particular, the multiphysics statement of the present work consists in the consideration of mechanical action, electric response and two-way interaction between fluid and structure with the reflection both the field variables distribution in the fluid and the spectrum of variables distribution in the body. Of course, this task is reasonably sophisticated, that requires to take into account few assumptions: the isothermal conditions of considered processes, the physical linearity of the model and principles of continuum mechanics. After that, the obtained results will be generalized to the arrays of chiral structures by the moving from micro- to macroscale without losing of generality. The simulation of the shell behavior under some external conditions is the main result of this work. Since environment type influences the shell behavior the study of different types of rheological models of the environment is required and the comparison of the appeared complex effects according to various rheological models, such as the Weissenberg effect, the thixotropy, etc., should be performed.

The modeling of the above described open issues can significantly influence the development of nanotechnology in the area of using shell-like helical structures and their assemblies. Thus, the set of the problems solved in the present work, allow to construct a complete model of helical nanostructures and to open new opportunities for their application in practice with development of the modern nanotechnologies.

Zusammenfassung

Das wesentliche Ergebnis der Dissertation ist die Entwicklung eines Analyseverfahrens für spirale piezoelektrische Nanofilme und Massive Filme-Kristalle. In Ergänzung wurde die Simulation ihres Verhaltens betrachtet, insbesondere mit Berücksichtigung des Einflusses des Umgebungsmediums. Derartige Untersuchungen erfordern die Verwendung von Programmpaketen für die Lösung von Anfangs-Randwertaufgaben bei komplexen konstitutiven Gleichungen, da analytische Lösungen in geschlossener Form kaum zu finden sind. In der vorliegenden Arbeit werden die Ergebnisse der Untersuchung der Modelle für Nanostrukturen mit der chiralen Elementen beschrieben.

Das Verhalten des Kristall-Arrays auf einem Substrat ist ebenfalls untersucht worden. In diesem Fall wurde die Bestimmung der funktionellen Eigenschaften der allgemeinen Struktur durchgeführt. Für die Abschätzung der funktionellen Eigenschaften sind die theoretischen Methoden der klassischen Mechanik und der zusammengesetzten Fraktaltheorie verwendet worden. Die fraktale Theorie passt für die Untersuchung der Nano-Array-Strukturen, weil die Agglomerate der Kristalle Eigenschaften einer fraktalen Struktur besitzen können.

Die Ergebnisse dieser Arbeit können für den Entwurf einer Metamaterialstruktur mit chiralen Eigenschaften und für die Vorhersage der mechanischen und elektrischen Antwort verwendet werden.

Acknowledgements

Firstly I would like to express my gratitude to Prof. Holm Altenbach and Prof. Victor A. Eremeyev from the Institute of Mechanics Otto von Guericke University Magdeburg for revealing me as a researcher three years ago and for their guidance and encouragements (throughout this work) during all this period. Also I would like to thank the Research Institute of Mechanics and Applied Mathematics SFU Rostov an Don for supporting this research.

Specially I would like to mention Natalija Altenbach for her supporting and encouragement.



Contents

Contents	VII
1 Introduction and motivation	1
1.1 Motivation	1
1.2 Nanostructures – synthesis and applications	6
1.3 Thesis overview	11
2 Basic equations	15
2.1 Governing equations of elastopiezoelectricity	15
2.1.1 Material independent equations	15
2.1.2 Constitutive equations	22
2.1.3 Boundary and initial conditions	24
2.2 Fluid mechanics	26
2.2.1 Basics and classical models of fluids	26
2.2.2 Rheological models for a viscous incompressible fluid	28
2.2.3 Fluid-structure interaction model	30
3 Computational facilities and numerical aspects	33
3.1 Overview of the computational tools	33
3.2 Applications of finite element and finite volume methods	35
3.3 Numerical methods for the fluid-structure interaction problems	36
4 Spiral nanofilms with piezoelectric properties	39
4.1 Modeling of multi-layer nanofilms	39
4.1.1 Problem statement	40

4.1.2	Results: Eigenmodes of a two-layer shell	42
4.1.3	Results: External medium, preliminary discussion . . .	44
4.2	Interaction of a helical shell with a non-linear viscous fluid . . .	46
4.2.1	Problem statement	46
4.2.2	Results: Complex effects of non-linear environment . .	49
4.3	Instability of a piezoelectric helix	55
4.3.1	Problem statement	55
4.3.2	Stability of helical springs	57
4.3.3	Results: Buckling problem in the case of IPE	63
4.3.4	Piezoelectric response of investigated materials	67
5	Investigation of metamaterials with chiral elements	71
5.1	Problem statement	71
5.2	Results: Behavior of the chiral material	74
6	Crystal/fiber arrays on multilayer substrates	83
6.1	Problem statement	84
6.1.1	Case of quasi-periodic array of nanocrystals	85
6.1.2	Stochastic array of nanocrystals	88
6.2	Results: Analysis of applied methods	91
7	Conclusions	95
7.1	Summary	95
7.2	Outlook	97
	Bibliography	99

Introduction and motivation

1.1 Motivation

Currently, the development of nanotechnologies produces a wide range of nanomaterials, including well-known materials, such as nanoshells and nanosprings (fullerenes¹, single-walled and multi-walled nanotubes, etc.) with piezoelectric properties [94, 95, 98, 100], Fig. 1.1. One of the most promising concept for the creation of nanoscale sensors and actuators is the design of multilayer helical (chiral) nanostructures or similar nanoobjects, which are based on the technology of layering of materials with different properties on a solid substrate. Then a separation of the active layer is the result of the existing stresses in this layer [98]. These helical-like structures have a number of attractive properties for various applications. For example, the high flexibility, piezoelectric characteristics, and other principal particularities make these structures suitable for creation of the nanosensors, nanoswitches, propulsion systems and other nanoelectromechanical systems (NEMS)², see Fig. 1.2 [64, 65, 125].

In addition, semiconductor nanowires and nanorods are used as components for nano-scale electronic and photonic device applications [127]. The nanoneedle arrays can be used as the field emitters because of experiments on field emission of onedimensional ZnO nanostructures, such as nanowires, nanorods, nanopins and nanoneedles (Fig. 1.1). The experimental data have

¹Fullerenes are the any molecule composed entirely of carbon, in the form of a hollow sphere, ellipsoid or tube [15].

²Nanoelectromechanical systems (NEMS) are devices integrating electrical and mechanical functionality on the nanoscale [65].

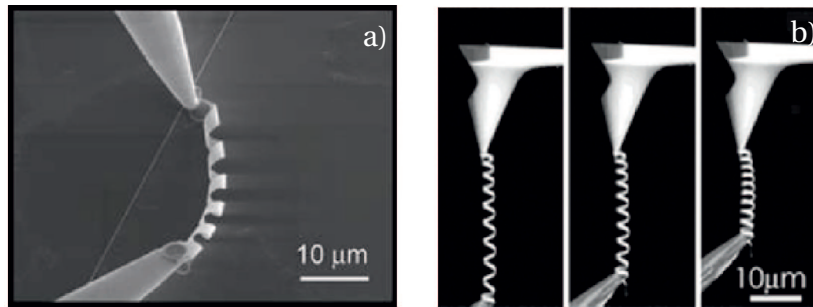


Figure 1.1: Piezoresistive helical nanobelts: a) Nanoelectromechanical sensors; b) Tensile elongation of large range helical nanobelts [64, 65] c) Nano-helices composed of ZnO [123]

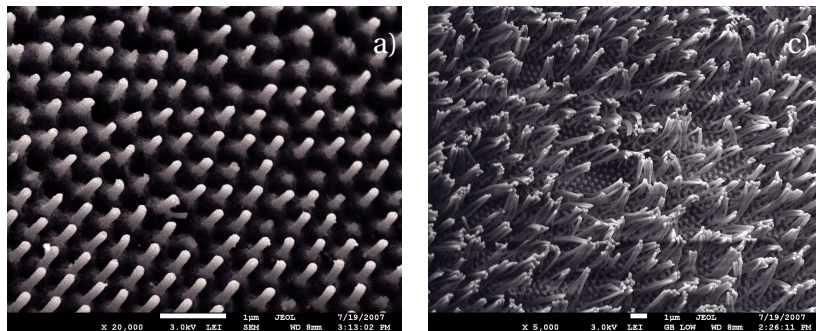


Figure 1.2: Examples of investigated nanostructures: a) Ordered nanocrystals array (by courtesy of S. Grimm); b) Disordered nanocrystals array (by courtesy of S. Grimm)

attracted considerable interest [49, 127]. Nanostructures arouse attention for solid-state gas sensors with a great potential for overcoming fundamental limitations due to their ultrahigh surface-to-volume ratio, see [122, 123, 127].

Conducting nanostructures propose the possibility of connecting molecular-scale constitution in a molecular computer. Scattering of conducting nanowires in different polymers (or another types of medium) are being investigated for the use as transparent electrodes for flexible flat-screen displays. Because of their high Young's moduli and other particular mechanical properties, their use in mechanically enhancing composites is being investigated [122]. They may be used as tribological additives to improve friction characteristics and reliability of electronic transducers and actuators. Because of their high aspect ratio, nanowires are also uniquely suited to dielectrophoretic manipulation [75].

During the investigation of such structures one can have a wide range of complex issues as the different scales, geometric nonlinearity, size effects, which should be taken into account by the consideration of various types of nano-objects [15, 28]. One of the basic ways to study the functional properties of nanostructured materials and the behavior of single nanostructures is the experimental investigation. The experimental approach can be based, for example, on the measurement of natural frequencies with the help of the scanning probe or atomic force microscopy [42, 105]. In this case one can have the problem of the redistribution of the natural vibration frequencies of the system "cantilever - surface" between the intrinsic natural frequencies of the cantilever³ and the surface. This problem is well known in the micromechanics [28, 42, 122, 123, 124]. It can be partially solved by the construction of mathematical and numerical models of the processes under consideration, because the numerical simulation simplifies the development of nanotechnology on the base of various types of designed nanoelements.

The choice of studied nanostructures as a representative element of modern nanotechnology can be based on the possibilities of inorganic synthesis, big surface area (this is useful for a more effective transfer of active substances), possibilities of assembly in agglomerates, and huge potential for the integration in micro- and nanodevices. Of course, the choice of the active materials, forming the nanostructure is specified by practical applications. The most attractive properties are the optoelectric, photoelectric, and piezoelectric characteristics [12]. These properties have particular interest by the consideration of some composite structures as metamaterials⁴. According to the stated above, in the present work we investigate the piezoelectric shell-like structures and their assemblies as a metamaterials. Metamaterials are a special type of materials which have very perspective applications. Unlike to classical materials, the physical and mechanical properties of metamaterials are determined almost by their structure. A special type of metamaterials is the helical metamaterial which microstructure is based on helical elements, see e.g. [122]. Although the electric and magnetic properties of helical metamaterials are of greatest interest, the mechanical design of helical elements plays an important role in engineering. The application of such shell-like elements is limited by their durability and reliability. In recent years significant progress

³Cantilever is used as sensor of force interaction in the atomic force microscopy [28].

⁴Metamaterials are artificial materials engineered to have properties that may not be found in nature. They are assemblies of multiple individual elements fashioned from conventional microscopic materials. The components are usually arranged in periodic patterns. Metamaterials gain their properties not from their composition, but from their exactly-designed structures [29].

in synthesis of metamaterials with perspective and unusual functional properties is observed. In particular, the helical shell structures have found various applications, for example, in microelectromechanical and nanoelectromechanical systems (MEMS/NEMS), optics and medicine, see [16, 72, 85] among others.

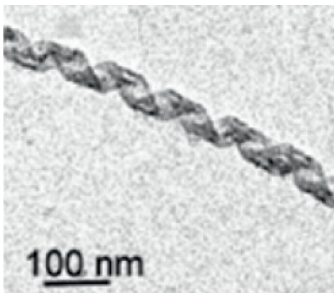
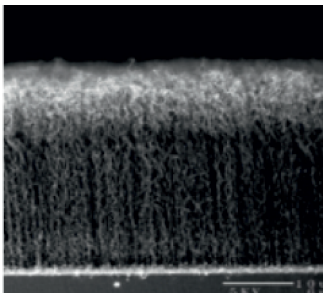
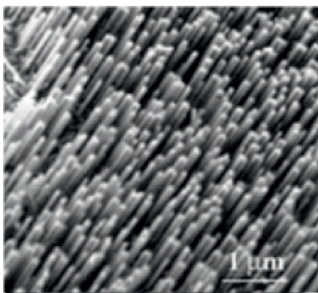
The complex materials can be synthesized by an insertion in a matrix of various periodic structures with different geometric shapes, which modify the functional properties of the composite material. An example of such structures is a periodic matrix with shells possessing a helical geometry sealed in a polymer matrix [97, 102]. By the synthesis of such complex structures a variation of different parameters of the material is possible (e.g. dimensions of the structure, shape, frequency, etc.). That makes possible to obtain significantly different properties of the resulting material and to find various areas of applications.

Here one can highlight two conjugate branches of research. The first one is concerned to the investigation of the single structure. The second one is dedicated to the determination of the agglomerates of such structures as some kind of metamaterial structures. The separation of the general investigation in the two branches is grounded on the necessity to pass from micro (scale of the devices components) to macro (area of fabricated devices work) view in the nanotechnology area. This point helps to understand more deeply the processes in the macromaterial, because the nanocomposite can be in particular cases be assembled from microelements, for example, helical nanoshells. However, not only functional properties of the metamaterials are interesting. The single nanocomponents of the nanocomposite reveal some area of possible applications, for example, in medicine (whole blood immunoassay, targeted drug delivery [67]), biotechnology [96], gas-sensors [102], etc. Examples of Bio-MEMS⁵ applications in medical and health related technologies are the Lab-On-Chip and MicroTotalAnalysis (biosensor, chemosensor) or embedded in medical devices, for instance, stents [96].

According to this point, the overlook on the applied aspects of performed results can be divided into the tasks for singular objects as a helical shell with the principal goal to study its behavior under some various types of load and tasks for an array of crystals/fibers on a substrate. The second branch of research is the generalization of the first part and connected with homogenization methods for composite structures.

⁵Microelectromechanical systems (MEMS) is the technology of very small devices; it merges at the nano-scale into nanoelectromechanical systems (NEMS) and nanotechnology [62].

Table 1.1: Example of the investigated structures

		
Delclos (2008)	Signo (2010)	Wang (2004)
Helical ribbon	ZnO nanowire	Carbon Nanotubes
MEMS, NEMS, optronics, medicine, solar battery	MEMS, NEMS, optronik, gas-sensor, ultracapacitors	MEMS, NEMS, optronics, gas-sensor, solar battery
Inorganic synthesis, sol-gel process, self-organization	Inorganic synthesis, self-organization	Inorganic synthesis, self-organization, stamp-process
Multilayer, semiconductor, piezoelectric, large surface area	Semiconductor, piezoelectric, anisotropic behavior	Semiconductor, piezoelectric, anisotropic behavior

The substances, which stand in a nano-modification, have large differences in mechanical, thermodynamic, magnetic and electric characteristics in comparison with bulk materials [59]. The unique characteristics of nanomaterials (wide band gap, piezoelectric effect) lend them the great potential for electromechanical devices and pressure sensing applications [61, 96]. As an example the MEMS gyroscope, which is a cheap way to the packaged similarly to other integrated circuits and may provide either analog or digital outputs. In many cases, a single part includes gyroscopic sensors for multiple axes.

Nanomaterials require precise structural and electrical characterization which is not easy due to their size. In order to use successfully various nanostructures in macro-scale devices, see Table 1.1, one should develop effective means to integrate nanostructures into a working device [61, 62]. One of the actual applications of MEMS and NEMS is the application in the micro-scale energy harvesting including piezoelectric, electrostatic and electromagnetic microharvesters [53]. Nanostructured materials become of a major significance and the technology of their production and use rapidly grow into a powerful industry [13, 118]. By the finite element modeling of various types

of mechanical problems the size-effect can be taken into account by recalculating the material properties by using the scaling law proposed in [28]. It should be noted that obtaining more accuracy by finite element simulation of the nano-objects properties is possible with the consideration of some range of physical effects as diffusion of charge carriers in semiconductor layers by using the appropriate transport equations [97].

1.2 Nanostructures – synthesis and applications

One of the methods of MEMS/NEMS creation is the using of multilayer shells made from semiconducting and piezoelectric materials, see for example, [61, 62, 63, 130]. Helical nanoshells can be used as elements of sensors and actuators [99]. The principal interest is the analysis of multilayer shells in the case of presence of a piezoelectric layer made from a material with a high electromechanical coupling coefficient.

As it is described in [22, 94, 97] this thin tape helixes and also some structures as nanorings, etc. can be synthesized by the epitaxial deposition on the substrate [103]. By the internal stresses this layer separates from the substrate and roll in a helix which result in anisotropic properties and a bending moment in this layer. It is also possible to laminate shells to each other. A result of such lamination is a multilayer composite with helical shape Fig. 1.3. According to Fig. 1.3, R is the radius of the rolling cylinder, t is the step of a spring winding, α is the helix ascent angle, b , a are the width and thickness

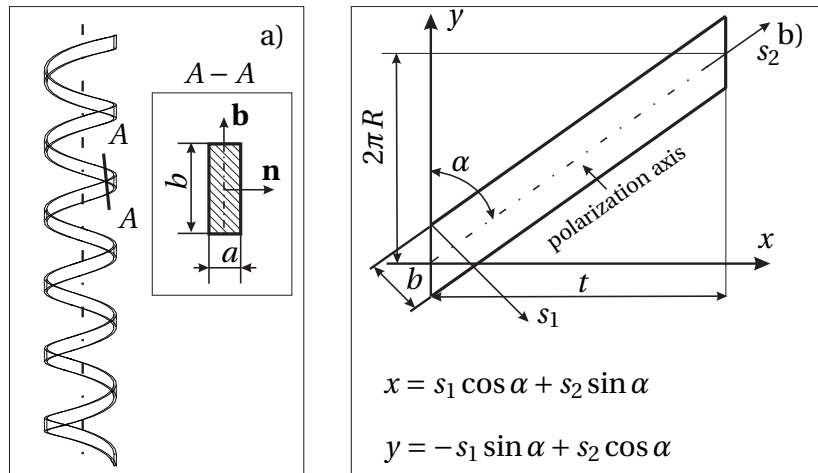


Figure 1.3: Geometric description of helices. Cylindrical shell with screw cuts: a) Helical spring shell; b) Part of the coil (median shell surface)

of the belt, respectively, Oxy is the system of principal coordinate axes, $s_1 s_2$ is the system of orthogonal coordinates. The formation of such nanostructures is a consequence of minimizing of the total energy contributed by spontaneous polarization and elasticity [100]. On this moment one can obtain such structures with a length to a few centimetres and with various functional properties. After forming of an array of helices this array can be sealed in a polymer matrix. The polymer matrix allows to keep the form, size and location of helices in the structure. The principal task of the matrix is the common work of inclusions, the homogenization of stress distribution and failure protection, see [99, 100, 101, 102] among others. Also the synthesis of nanobelts can be based on thermal evaporation of oxide powders under controlled conditions without the presence of a catalyst [123].

Many nanostructures can be obtained from the individual separate objects such as atoms and molecules by using the processes of self-formation and self-organization. In the technology of nano-objects there are two approaches in solids creation: "**top-down**" and "**bottom-up**".

"Top-down" is an approach of a cutting nanostructures from the source material, using lithography⁶, also it means an attrition or milling of structures, that involves the applications more specially in the nanocomposites and nano-grained bulk materials.

Approach of the "bottom-up" technique is a method, which uses a chemical synthesis and assembly nanoelements of individual atoms or molecules on the substrate. With the decrease in facilities and equipment to the size of the order of hundreds of atoms, the assembly method is more promising.

By the "bottom-up" method one can make the following phase classification:

- Gas (Vapor) Phase Fabrication, Pyrolysis⁷, Inert Gas Condensation, etc.
- Liquid Phase Fabrication: Solvothermal Reaction⁸, Sol-gel⁹, etc.

⁶Methods of mass production of integrated circuits, using lithography equipment source of extreme ultraviolet radiation with a wavelength of 13.5 nm, and the projection optical system based on reflective multilayer MoSi mirrors. In this way is expected to achieve miniaturization of integrated circuits 30 nanometers or less [97].

⁷Pyrolysis is the thermochemical decomposition of organic material at elevated temperatures without the participation of oxygen [71].

⁸Solvothermal reaction is the chemical reaction involving a solvent either in subcritical or supercritical conditions. Such a solvent can act as a chemical component or a fluid phase able through its physico-chemical properties to modify the reaction mechanisms [23, 86].

⁹Sol-gel is the process, which bases on a wet-chemical technique and can be widely used in the fields of materials science and ceramic engineering. Such methods are used for the fabrication of materials starting from a colloidal solution (sol) that acts as the precursor for an integrated network (or gel) of either discrete particles or network polymers [58].

Nano-objects, which can be formed by bending and folding-exempt bonds with the substrate of semiconductor strained shells are of particular interest. This method allows to create a class of semiconductor nanostructures: tubes, spirals, rings, etc. [101, 102]. This technological approach allows to scale the elements to molecular size and to overcome the limitations of lithography [70].

For the formation of three-dimensional structures strained-layer films (GaAs/InGaAs, GaAs is the outer layer) can be used [101, 102]. In this case the structure is locally grown on a substrate of gallium arsenide (GaAs) with a sacrificial layer of aluminum arsenide (AlAs). The structure rises applying the molecular beam epitaxy method. A thin film (few monolayers) is strained because the lattice constant of unstrained ternary compound indium gallium arsenide (InGaAs) layer is greater than that of GaAs (so the growth is obtained compressed layer InGaAs) and the separation from the substrate creates twists and eventually leads to collapse of the film. For separation of the bilayer-shell can be used a selective liquid reagent, which removes the sacrificial layer of AlAs without affecting other adhesion. One can minimize the obtained tube, which may consist of dozens of turns. By using monolayers of GaAs/InAs (mismatch of the lattice constants reaches 7%) one can obtain the semiconducting nanotubes with a diameter of 1 to 2 nm, which, in contrast to carbon nanotubes, can be formed at specific locations on a substrate with a given diameter by lithography. These free two-layer films consists of two atomic layers of different materials. This structure has a perfect atomic structure of inherent limitations of a flat film on the substrate surface [94, 97, 101, 102]. The above example illustrates the method, which is known as **Prinz-technology**¹⁰. This method is quite flexible and can be applied to many systems and plays the main role in the formation of three-dimensional helical nanostructures.

For the method presented in the thesis it is necessary to explain some simulations. By using **molecular beam epitaxy** (MBE)¹¹ the planar molecular monolayers grow with the highest atomic precision. Molecular beam epitaxy monolayer allows to grow monolayers for complex heterostructures, uniform from size [107]. However, the layers are fixed in the heterostructure and this limits their practical applications in nanodevices [75, 126].

¹⁰Prinz-technology is the method of a forming three-dimensional micro - and nanostructures based on separation of strained semiconductor films on a substrate and then rolling them into a spatial object. This technology is named in honor of the scientist working at the Institute of Semiconductor Physics Victor Ya. Prinz, who proposed this method in 1995 [97].

¹¹MBE is one of several methods of depositing single crystals. It was invented in the late 1960s at Bell Telephone Laboratories by J. R. Arthur and A. Y. Cho [18].

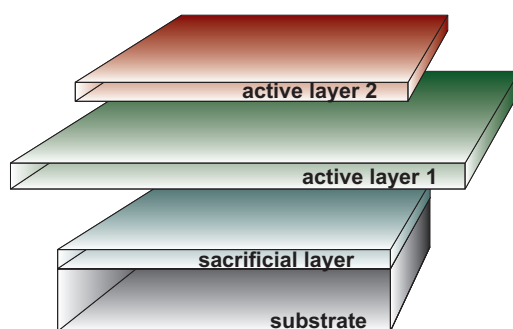


Figure 1.4: Formation of nanoobjects: molecular beam epitaxy. Precipitation of evaporated in the molecular source of matter on the crystal substrate

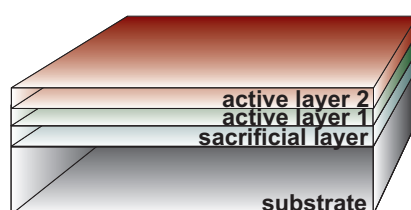


Figure 1.5: Formation of nanoobjects: the crystal lattice of thin layers adapt to the substrate lattice in the epitaxial growth (pseudomorphic growth condition)

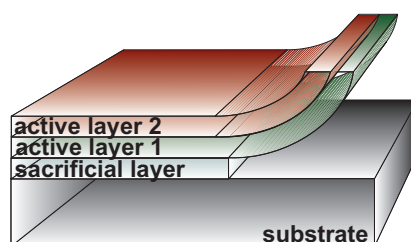


Figure 1.6: Formation of nanoobjects: removal of the sacrificial layer and folding itself into a chiral two-layer film structure

For the formation of the nanoobjects according to the methods described above should be performed the following items:

- Active layers grown on the substrate, Fig. 1.4;
- Thin film (few monolayers) is strained because the crystal lattice constant of the unstrained active layer 2 is greater than the respective value of the active layer 1 (the growth is obtained in the compressed layer of the active layer 2), Fig. 1.5;
- Bending of the two-layer film by its separation from the substrate after the selective removal of the sacrificial layer, Fig. 1.6.

Another process of nanostructure creation is based on the so-called thermal evaporation of the oxide powders under controlled conditions without any catalyst [123].

For the experimental investigation of the nanohelices, nanosprings of piezoelectric nanobelts and other structures are usually used microscopy tools:

- Atomic force microscopy (**AFM**);
- Scanning electron microscopy (**SEM**);
- High-resolution transmission electron microscopy (**HRTEM**);
- Near-field scanning optical microscopy (**NSOM**).

At present time the great progress in size reducing of the active regions and the creation of nanostructures is achieved. However, the transition from MEMS to NEMS is not enough to reduce only the feature size of devices, it is also necessary to achieve precision in the manufacturing of components.

By the numerical modeling of the various types of the mechanical problems the size-effect can be taking into account by the recalculation of the material properties by using the proposed in [28] scaling law. It should be noted that obtaining more accuracy by finite element simulation of the nano-objects properties is possible with the consideration of some range of physical effects as a diffusion of charge carriers in semiconductor layers by using the appropriate transport equations [97].

The fact that a decrease of the size of devices influences many characteristics takes a crucial part in microelectronics devices work. However, the other parameters of the structure as the wavelength of the electrons, the phase coherence length, the mean free path should be taken into account.

In microelectronics devices for switching from one state to another the current flow of one million electrons is required, at the same time the switching in NEMS requires only one electron. A new approach is the creation of quantum devices by using quantum effects, such as resonant tunneling¹², the interference of electron waves, the quantization of conductance, Coulomb blockade¹³, spin phenomena, etc. The methods of nanopiezoelectronics are used for the creation of new electronic components, which combine piezoelectric and semiconducting properties of materials [12]. For example, in a one-dimensional piezoelectric transistor, made from the ZnO oxide nanostructure by a small strain one can change the distribution of electric charges

¹²Resonant tunneling is the penetration of light particles (electrons, protons) in the area, inaccessible to them [47, 88].

¹³Coulomb blockade is the increased resistance at small bias voltages of an electronic device comprising at least one low-capacitance tunnel junction [47].

micro- to macroscale without losing of generality. The simulation of the shell behavior under some external conditions is the main result of this work. Since environment type influences the shell behavior the study of different types of rheological models of the environment is required and the comparison of the appeared complex effects according to various rheological models, such as the Weissenberg effect, the thixotropy, etc., should be performed, see Section 4.2. To achieve the goal the following **subtasks of research** are successfully completed:

- **Construction** of a model of chiral one- and multi-layer shells with the perfect consistency of the tied layers according to the conditions of nano-size effect and other additional conditions for the modeling of the real structure, Section 4.1.
- **Solution** of the complex multiphysics problem, which consists of the solution of the following subtasks, see Sections 4.2 and 4.3:
 - Fluid-Structure Interaction analysis of the elastic-piezoelectric shell with a special type of the nonlinear environment, see Section 4.2;
 - Fluid-Structure Interaction analysis of a moving solid shell in a pseudoplastic fluid with the consideration of appearing particular effects as the Weissenberg effect, the thixotropy, etc., see Section 4.2;
 - Analysis of the direct and inverse piezoelectric effects in the case of static and dynamic problems. This includes the following items, see Section 4.3:
 - * Stability loss problem for the geometrically non-linear helical shell under electrical load;
 - * Investigation of the size-effect influence.
- **Investigation** of the particular properties of the nano-structured materials as composite materials, see Chapter 5:
 - Calculation of the averaged functional properties of the nano-structured composite with taking into account the inclusions' packing: twisting of the constituent helixes, size of the shells, etc.;
 - Propositions of shape and properties optimization by the synthesis of the nano-structured composite materials, according to the future applications in microelectromechanical systems or nanoelectromechanical systems (MEMS/NEMS).
- **Construction** of a model of chiral nanoshells and of a crystals' array on the substrate. Investigation of the appearing waves in the crystal-layer, comparison of the results with the classical theories, see Chapter 6.

The results of the presented thesis can be used in predicting of the material properties of the multilayer structures with complex geometry, prediction and exhibition of the shell-like structures behavior in order to avoid the expensive natural experiments and for the reduction of costs for the further application of shell-like structures objects in MEMS and NEMS.

According to the formulated goal and subtasks the outline of the thesis consists the following items. **Chapter 1** introduces the motivation and relevance of the current study, this determines the described and formulated above goal and subtasks of the research. This chapter describes the principal characteristics of nanostructures, the synthesis variants and possible applications of the models. These questions should be taken into account by the consideration of investigated structures, because it makes more obvious the choice of shell materials or types of environment resulting in the special nanoobjects behavior, shape and geometry of shells, etc. Here the main ideas and distinctive features of nanostructures, which play an important role in nanotechnology and current developments in this field, are summarized. In Chapter 1 are presented the principal definitions of the descriptive adjectives of the metamaterials and general structured electromagnetic materials.

Assuming the continuum theory applicability to nano-structures we use the classical postulates and formulas of continuum mechanics. A brief summary of principal equations and relations, which are used in the thesis, is given in **Chapter 2**. The chapter is divided into the consideration of the governing equations of the piezoelectricity with the closed problem statement of electroelastic task, Section 2.1, and into the problem statement for the fluid-structure interaction task, Section 2.2. This classical theory will find a direct application in all presented investigation tasks.

Chapter 3 presents the computational tools in order to explain the facilities of the solution of the presented tasks. In addition, Chapter 3 states the principal problems of the simulation and modeling of the studied structures in connection with CAD and CAE tools and gives a principal overview of the computational particularities.

The quintessence of the present studies in sense of solved problems starts from the **Chapter 4**. Based on ideas introduced in [68, 69] in Section 4.1 the identification of the eigenvalues of multilayer helical shells are used for the determination of the particular functional properties of geometrically similar objects to real nanoobjects. The important task of the influence of the environment is discussed in Section 4.2 devoted to the non-linear fluid interacting with a piezoelectric shell. Section 4.2 presents several rheological models of the possible environment. The questions are coupled by Fluid-Structure In-

teraction tools. At first Section 4.3 describes more accurately some questions about size effect which should be taking into account in view of microshells. According to this the large influence of the size-effect is shown. In addition, this section covers the stability loss problem under applied electrical load in the process of the inverse piezoelectric effect (IPE). The comparison of the classical theory of the stability loss problem of tape helixes and the buckling collapse by the IPE is made. Section 4.3 gives explanations concerning the choice of used materials and nature of the piezoelectric response in their behavior.

The **Chapters 5 and 6** are the generalization of the results of previous chapters in context with composite nano-structured materials. In particular Chapter 5 is dedicated to both the elastic and the principal electric properties of a chiral material. In this chapter the consideration of a composite structure made of a polymer matrix and anisotropic inclusions with taking into account the piezoelectric and dielectric properties of the designed material is given. The principal task is the estimation of the functional properties of nanostructured materials. In Chapter 6 the application of the classical mechanics of fiber composites [55, 117] is considered, taking into account the morphology and electrical properties of nanotubes. For irregular structures the fractal analysis is applied [10]. After the determination of effective properties the finite element analysis is performed using the commercial FE-package ABAQUS/CAE[®] [21]. As the result of the FEM-simulation results of the modal analysis and the modeling of the surface wave propagation in multilayered plates are obtained.

In **Chapter 7** the results of the previous chapters are generalized, general conclusions are given and, in addition, future work in this research field are briefly discussed.

Basic equations

2.1 Governing equations of elastopiezoelectricity

Piezoelectric materials can get mechanical deformations as a result of an applied electrical field and vice-versa. The piezoelectric effect is considered as a transfer between electrical and mechanical energy [83]. In this chapter we discuss the basic equations which describe the effect of piezoelectricity in solids. The starting point is the invariant representation of the coupled electrical and mechanical equations. The constitutive equations are limited by the assumption of physical linearity.

The main assumption is the hypothesis of continuum for the investigation of the nanoobjects. The approximate description of nanoobjects in the range $\Delta V < \Delta V^*$, Fig. 2.1, requires some additional conditions [83], which in Chapter 5 will be considered.

2.1.1 Material independent equations

Within the assumptions of the classical continuum theory we introduce the principal equations for the continuum. The continuum is a medium with the matter, which is continuously distributed and fills the entire region of space and can be continually sub-divided into infinitesimal elements with properties being those of the bulk material [115]. The basic differential equations, describing the properties of the continuous medium, can be obtained from the **integral balances** for physical quantities as mass, momentum, and energy, which characterize this medium. Hereby the balance equations and constitutive axiomatic relations are valid for arbitrary small volume of the body.

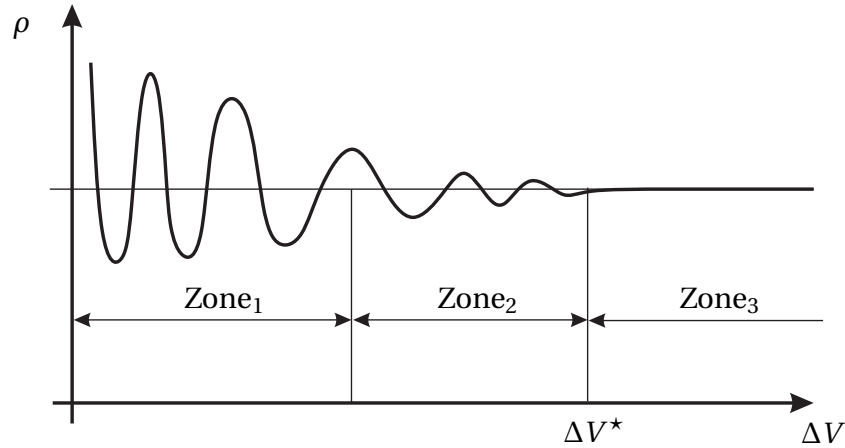


Figure 2.1: Density dependence of volume for different scales: Zone₁ is the scale of the molecular and atomic sizes; Zone₂ is the microcontinuum; Zone₃ is the classic continuum [83]

According to this the mass density ρ of a volume ΔV with the mass Δm is defined as:

$$\rho = \lim_{\Delta V \rightarrow 0} \frac{\Delta m}{\Delta V} \quad (2.1)$$

Equation (2.1) is the principal starting point for the continuum mechanics with a mathematically well-posed mass measure. Considering the elastopiezoelectric medium as a continuum the following axioms of continuum mechanics hold true [1, 4, 115]:

1. **Space-time axiom.** The continuum is a subspace of the Euclidean space [115]. The time is absolute and does not depend on the events.
2. **Continuity axiom.** The continuum is a material continuum at any time. This means that the concepts of mass and internal energy of each volume of the continuous medium are defined at any time point.
3. **Axiom of motion.** The function, which describes the motion of the continuum from the reference to the current configuration (mapping function $\xi(\cdot, t)$) is a homeomorphism, thus:
 - The material points forming a closed curve at any instant will always form a closed curve at any subsequent time point.
 - The material points forming a closed surface at any instant will always form a closed surface at any subsequent time point and the matter within the closed surface will always remain within this surface.
4. **Forces and energy** in the continuum mechanics [80]:

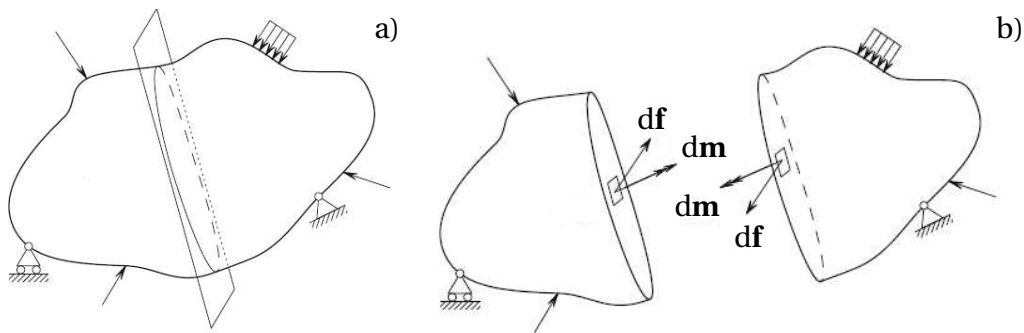


Figure 2.2: Arbitrary loaded body by external forces: a) Visualization of the cutting principle; b) Distribution of the resulting forces $d\mathbf{f}$ and moments $d\mathbf{m}$ on the surface element by the cutting principle [1]

- a) *Mass forces* are forces originating from sources outside of the body that act on the volume (or mass) of the body.
- b) *Surface forces* or contact forces can act either on the bounding surface as a result of mechanical contact or on imaginary internal surfaces that bound parts of the body as a result of the mechanical interaction between the parts of the body to either side of the surface (Euler-Cauchy's stress principle¹).
- c) *Flux across the surface* is the rate of energy flow across a unit area (e.g. heat) with the surface density as the magnitude.

5. **Balances.** For any representative volume of a continuum medium the following balances hold true [1]:

- a) Balance of mass,
- b) Balance of momentum,
- c) Balance of angular momentum,
- d) Balance of energy, and
- e) Balance entropy.

The principal task of the description of the body motion and deformation is the investigation of the transfer of all material points of a body in the space [83]. The region corresponding to the current configuration at time t is labeled with the help of the mapping function $\xi(\cdot, t)$. For this function it is necessary to apply the additional contingencies [74]:

- continuity over time (the body cannot be deformed instantly and at the same time point cannot exist more than one different deformations)

¹The action of one part of the body on the other is equivalent to the system of distributed forces and couples on the surface dividing the body, see Fig. 2.2 [1, 111, 115]. The influence of distributed couples will be ignored in this thesis.

state of continuum),

- existence of an inverse function (physically: the particle of the continuum cannot intersect itself),
- twice continuously differentiable or smooth of mapping function (physically: existence of the second continuous derivative for construction of differential equations describing the motion of continuum with continuous functions of velocity and acceleration of body).

Two approaches of the description of the body motion are well known [115]:

- **Eulerian description**

The spatial description or Eulerian description of motion in terms of the spatial coordinates, i.e. the current configuration is taken as the reference configuration, [80]. Characteristics of the medium are considered at, fixed points in the space. The motion of a continuum using the Eulerian description is expressed as:

$$\mathbf{X} = \boldsymbol{\xi}^{-1}(\mathbf{x}, t)$$

- **Lagrangian description**

According to the Lagrangian description of the position and physical properties of the particles are described in terms of the material or reference coordinates and time [80]. In this case the reference configuration is the configuration at initial point time t_0 . In the Lagrangian description the motion of a continuum body is expressed by the mapping function:

$$\mathbf{x} = \boldsymbol{\xi}(\mathbf{X}, t)$$

In particular, the axiom of motion allows to identify the particle of a continuum according to the reference configuration at the moment t_0 by the coordinates of the particle (X_1, X_2, X_3) .

Consider some field function $F(X_1, X_2, X_3, t)$, which characterizes some state of the continuum in the particle with coordinates X_1, X_2, X_3 . Consider the time derivative of the field function as it follows:

$$\frac{DF}{Dt} = \frac{\partial F}{\partial t} + \frac{\partial F}{\partial \mathbf{X}} \cdot \frac{\partial \mathbf{X}}{\partial t} = F_t + \mathbf{v} \cdot \nabla_{\mathbf{X}} F \quad (2.2)$$

The differential operator (2.2) called the total derivative.

For the simplicity of the representation of the classical elasticity theory one can assume that the origin of coordinate systems for the reference configuration \mathbf{X} and for the current \mathbf{x} are equal. Then the displacement vector of the body motion \mathbf{u} is defined as:

$$\mathbf{u} = \mathbf{x} - \mathbf{X} \quad (2.3)$$

This vector joints two points of a particle motion of the continuum in the reference configuration \mathbf{X} and deformed configuration \mathbf{x} .

After the definition of the displacement vector the deformation gradient tensors can be introduced as it follows

$$\begin{aligned}\mathbf{F} &= \nabla_{\mathbf{X}}\mathbf{x} \\ \mathbf{H} &= \nabla_{\mathbf{x}}\mathbf{X} \\ J &= \det\mathbf{F} > 0, \forall t\end{aligned}\tag{2.4}$$

where $\nabla_{\mathbf{X}}$ and $\nabla_{\mathbf{x}}$ are the Hamilton operator in the reference and current configuration. In Eq. (2.4) \mathbf{F} and \mathbf{H} called the material and spatial deformation gradient tensor, respectively. Kinematic relations and constitutive equations are necessary to complete the system of governing equations. Thus considering the deformation gradient tensors (2.4) the material displacement gradient tensor follows:

$$\nabla_{\mathbf{X}}\mathbf{u} = \mathbf{F} - \mathbf{I}\tag{2.5}$$

where the \mathbf{I} is the second order unit tensor. The strain tensor in the case of finite deformations with respect to the material displacement gradient tensor (2.5) can be presented as [80, 79]:

$$\boldsymbol{\varepsilon} = \frac{1}{2}(\nabla_{\mathbf{X}}\mathbf{u} + \nabla_{\mathbf{X}}\mathbf{u}^T + \nabla_{\mathbf{X}}\mathbf{u} \cdot \nabla_{\mathbf{X}}\mathbf{u}^T)\tag{2.6}$$

This strain tensor (2.6) is called Lagrangian finite strain tensor, Green-Lagrangian strain tensor or Green–St. Venant strain tensor [111, 115].

In many cases it is sufficient to describe the behavior of the continuum assuming small deformations. For infinitesimal deformations of the continuum, in which both the displacements and the displacement gradient are small, i.e., $\|\mathbf{u}\| \ll 1$ and $\|\nabla_{\mathbf{X}}\mathbf{u}\| \ll 1$, it is possible to perform a geometric linearization of the Lagrangian finite strain tensor.

$$\boldsymbol{\varepsilon} = \frac{1}{2}(\nabla_{\mathbf{X}}\mathbf{u} + \nabla_{\mathbf{X}}\mathbf{u}^T)\tag{2.7}$$

Regarding of continuity of motion by the smoothness of the mapping function $\xi(\cdot, t)$ the mass conservation law takes the form:

$$\int_V \left(\frac{d\rho}{dt} + \rho \nabla_{\mathbf{X}} \cdot \mathbf{v} \right) dV = 0\tag{2.8}$$

Under the arbitrariness of the volume one can rewrite (2.8) as:

$$\frac{d\rho}{dt} + \rho \nabla_{\mathbf{X}} \cdot \mathbf{v} = 0\tag{2.9}$$

where $\mathbf{v} = \frac{\partial \xi(X, t)}{\partial t}$ is the velocity of the particle, t is the time.

Let us consider a medium under action of distributed forces. The forces act to the surface of the body and/or to the interior of the medium. This decomposition into surface and body forces is necessary to put some tensor into operation, which describes the stresses in the body.

After deformation the material particles occupy the surface element defined by $\mathbf{n}dA$, where dA is the area and \mathbf{n} is the normal in the current configuration. Suppose that a force $d\mathbf{f}$ acts on the surface element (in the current configuration). Then by definition of the Cauchy stress [1]:

$$\begin{aligned} d\mathbf{f} &= \boldsymbol{\sigma} \cdot \mathbf{n}dA, \\ \mathbf{s} &= \frac{d\mathbf{f}}{dA}, \Rightarrow \mathbf{s} = \boldsymbol{\sigma} \cdot \mathbf{n} \end{aligned} \quad (2.10)$$

where \mathbf{s} is the Cauchy traction vector. The set of the components of the stress tensor forms the second-order tensor $\boldsymbol{\sigma}$, which takes the following matrix form:

$$\boldsymbol{\sigma} = \begin{bmatrix} \sigma_{11} & \sigma_{12} & \sigma_{13} \\ \sigma_{21} & \sigma_{22} & \sigma_{23} \\ \sigma_{31} & \sigma_{32} & \sigma_{33} \end{bmatrix}$$

where σ_{11} , σ_{22} , and σ_{33} are normal stresses and σ_{12} , σ_{13} , σ_{21} , σ_{23} , σ_{31} , σ_{32} are shear stresses. The main consequence of the conservation of angular momentum law is the symmetry of the stress tensor: $\boldsymbol{\sigma} = \boldsymbol{\sigma}^T$. Applying the symmetry of the stress tensor in the Voigt notation² the representation of the Cauchy stress tensor can be given as a six-dimensional vector with the components:

$$\left[\sigma_{11}, \sigma_{22}, \sigma_{33}, \sigma_{23}, \sigma_{13}, \sigma_{12} \right]^T = \left[\sigma_1, \sigma_2, \sigma_3, \sigma_4, \sigma_5, \sigma_6 \right]^T$$

Then the strain tensor can take the form [119]:

$$\left[\varepsilon_{11}, \varepsilon_{22}, \varepsilon_{33}, 2\varepsilon_{23}, 2\varepsilon_{13}, 2\varepsilon_{12} \right]^T = \left[\varepsilon_1, \varepsilon_2, \varepsilon_3, \varepsilon_4, \varepsilon_5, \varepsilon_6 \right]^T$$

The definition of the stress tensor completely determines the stress state and makes it possible to obtain the stress for every part of body.

After brief introduction of the stress and strain tensors and the definition of the surface and body forces one can consider the equation of body motion [115]:

$$\nabla_x \cdot \boldsymbol{\sigma} + \rho \mathbf{f}_m = \rho \frac{d^2 \mathbf{u}}{dt^2} \quad (2.11)$$

²The notation is named after physicist Woldemar Voigt and presented, for example, in [119].

Equation (2.11) describes the case of small deformations taking into account the strain tensor (2.7), where $\boldsymbol{\sigma}$ is the Cauchy stress tensor, ρ is the density of the continuum in the current configuration, \mathbf{f}_m is the vector of the mass density of the body forces acting on the continuum (the force per unit mass). This equation describes the momentum transport of any continuum and in particular cases also determines the motion of ideal fluid (Euler model of fluid) and viscous fluid (Navier–Stokes equations), which will be considered in Section 2.2.

In the case of finite deformations or by the consideration the large strain theory it is necessary to consider the Piola-Kirchhoff stress tensors, expressing the stresses relative to the forces in the reference configuration to areas in the reference configuration. The force in the reference configuration is obtained via a mapping that preserves the relative relationship between the force direction and the outer normal in the current configuration.

Then one can consider the following form of equation of motion:

$$\nabla_X \cdot [\boldsymbol{\sigma}_{\mathbf{P}_I} \cdot \mathbf{F}] + \rho_0 \mathbf{f}_m = \rho_0 \frac{d^2 \mathbf{u}}{dt^2} \quad (2.12)$$

It should be noted that in Eq. (2.12) the Hamilton operator ∇_X and density ρ_0 are refer to the the reference configuration, and the 1st Piola–Kirchhoff stress tensor $\boldsymbol{\sigma}_{\mathbf{P}_I}$, relates forces in the current configuration with areas in the reference configuration. The relation between the Cauchy and 1st Piola-Kirchhoff stress tensors with taking into account the deformation gradient tensor (2.4) takes the form:

$$\boldsymbol{\sigma}_{\mathbf{P}_I} = [\det \mathbf{F}] \boldsymbol{\sigma} \cdot \mathbf{F}^{-T} \quad (2.13)$$

The 1st Piola-Kirchhoff stress tensor is not symmetric: $\boldsymbol{\sigma}_{\mathbf{P}_I} \neq \boldsymbol{\sigma}_{\mathbf{P}_I}^T$.

Using the definition of the 2nd Piola-Kirchhoff stress tensor \mathbf{P}_{II} the equation of continuum motion can be written as [115]:

$$\nabla_X \cdot [\boldsymbol{\sigma}_{\mathbf{P}_{II}} \cdot \mathbf{F}] = \rho_0 \frac{d^2 \mathbf{u}}{dt^2} - \rho_0 \mathbf{f}_m \quad (2.14)$$

It should be noted that the relation between the Cauchy and 2nd Piola-Kirchhoff stress tensor with taking into account deformation gradient tensor (2.4) takes the form:

$$\boldsymbol{\sigma}_{\mathbf{P}_{II}} = [\det \mathbf{F}] \mathbf{F}^{-1} \cdot \boldsymbol{\sigma} \cdot \mathbf{F}^{-T} \quad (2.15)$$

The 2nd Piola-Kirchhoff stress tensor tensor is symmetric: $\boldsymbol{\sigma}_{\mathbf{P}_{II}} = \boldsymbol{\sigma}_{\mathbf{P}_{II}}^T$. It should be noted that for infinitesimal deformations or rotations, the Cauchy and the

Piola–Kirchhoff tensors are identical because the Lagrangian and Euler the deformation tensors are identical³.

For the system of material independent equations for piezoelectric continuum one should add the equations, which describe the electric fields and its relation with the electric charges and currents in the continuum mediums, thus [83]:

$$\nabla \cdot \mathbf{D} = q \quad (2.16)$$

$$\mathbf{E} = -\nabla\varphi \quad (2.17)$$

where \mathbf{E} is the electric field vector, φ is the electric potential, \mathbf{D} is the electric displacement vector and q is the electric charge.

It should be noted that the influence of magnetic components is ignored because this physical response is not significant of the presented in the thesis problems. In addition, the absence of the magnetic components in the governing equations allows to simplify the piezoelectric problem statement [66].

2.1.2 Constitutive equations

In order to describe the transport of such quantities as mass, energy, momentum, electric charges, etc., characterizing the continuum it is necessary to specify the relations of the material response. In the general case assuming linear-elastic material properties the stresses and strains are described using the second-order tensor. The well-known generalized Hooke's law connects these tensors and in the case of physical linearity one gets a tensorial linear equation introducing one elastic tensor of fourth order \mathbf{C} :

$$\boldsymbol{\sigma} = {}^{(4)}\mathbf{C} \cdot \boldsymbol{\varepsilon}$$

For the piezoelectric body a similar law describing the electric response of the material is necessary. The piezoelectricity combines effects of the electric and the elastic behavior of the material. The electric charge density displacement \mathbf{D} is defined by the electric field \mathbf{E} and the second-order tensor of the dielectric constants \mathbf{d} :

$$\mathbf{D} = \mathbf{d} \cdot \mathbf{E}$$

The mechanical response in a piezoelectric material is not only a result of the mechanical deformations, but also of the applied electric field. The constitutive equation for the stresses takes the following form:

$$\boldsymbol{\sigma} = {}^{(4)}\mathbf{C} \cdot \boldsymbol{\varepsilon} - {}^{(3)}\mathbf{e}^T \cdot \mathbf{E} \quad (2.18)$$

³From now we use the standardized form of the Hamiltonian operator as a result consideration, in general, the case of the small deformations and identity of the Lagrangian and Euler deformation tensors, unless the opposite is stated.

At the same time the electric response in the material is the reason for both the electric field and the mechanical deformations. This means that the relation for the electric displacement field should contain also a mechanical part and a relation for the electric charge density displacement:

$$\mathbf{D} = \boldsymbol{\varepsilon} \cdot \mathbf{E} + \mathbf{d} \cdot \mathbf{E} \quad (2.19)$$

The introduced third-order tensor of the piezoelectric parameters \mathbf{d} describes the piezoelectric properties of the material.

The general notation of the piezoelectric tensor in the matrix representation can given as it follows:

$$[\mathbf{d}] = \begin{bmatrix} d_{11} & d_{12} & d_{13} & d_{14} & d_{15} & d_{16} \\ d_{21} & d_{22} & d_{23} & d_{24} & d_{25} & d_{26} \\ d_{31} & d_{32} & d_{33} & d_{34} & d_{35} & d_{36} \end{bmatrix}, \quad [\mathbf{d}]^T = \begin{bmatrix} d_{11} & d_{21} & d_{31} \\ d_{12} & d_{22} & d_{32} \\ d_{13} & d_{23} & d_{33} \\ d_{14} & d_{24} & d_{34} \\ d_{15} & d_{25} & d_{35} \\ d_{16} & d_{26} & d_{36} \end{bmatrix} \quad (2.20)$$

For real materials we assume some kind of symmetry with respect to the material behavior. Then only a few components in the representation (2.20) are nonzero [119]. One example is the case of the orthorhombic symmetry mm2. In this case one can present the piezoelectric tensor considering the [100]-orientation as it follows (\cdot denotes zero values):

$$[\mathbf{d}] = \begin{bmatrix} d_{11} & d_{12} & d_{13} & \cdot & \cdot & \cdot \\ \cdot & \cdot & \cdot & d_{24} & \cdot & \cdot \\ \cdot & \cdot & \cdot & \cdot & d_{35} & \cdot \end{bmatrix}, \quad [\mathbf{d}]^T = \begin{bmatrix} d_{11} & \cdot & \cdot \\ d_{21} & \cdot & \cdot \\ d_{31} & \cdot & \cdot \\ \cdot & d_{42} & \cdot \\ \cdot & \cdot & d_{53} \\ \cdot & \cdot & \cdot \end{bmatrix} \quad (2.21)$$

Explaining the physical meaning of the parameters, which is necessary for the correct description of the metamaterial behavior. The physical meaning of the piezoelectric constants according to the matrix representation of the tensors considering the [100]-material orientation is the following one [119]:

- The modulus d_{11} is the induced polarization of the material in direction 1 per unit stress applied in direction 1 (directions 1-2-3 form a orthogonal triad in the space). The inverse piezoelectric effect induces strains in direction 1 per unit electric field applied in the direction 1.
- The modulus d_{21} is the induced polarization of the material in direction 1 per unit stress applied in direction 2. The inverse piezoelectric effect

induces strains in direction 2 per unit electric field applied in the direction 1.

- The modulus e_{31} is the induced polarization of the material in direction 1 per unit stress applied in direction 3. The inverse piezoelectric effect induces strains in direction 3 per unit electric field applied in the direction 1.
- The modulus e_{42} is the induced polarization of the material in direction 2 per unit shear stress applied in the 12-plane. The inverse piezoelectric effect induces shear strain in the 12-plane per unit electric field applied in the direction 2.
- The modulus e_{53} is the induced polarization of the material in direction 3 per unit shear stress applied in the 13-plane. The inverse piezoelectric effect induces shear strain in the 13-plane per unit electric field applied in the direction 3.

Considering the permittivity one can get the following representation of the dielectric matrix [119]:

$$[\mathbf{d}] = \begin{bmatrix} d_{11} & d_{12} & d_{13} \\ d_{21} & d_{22} & d_{23} \\ d_{31} & d_{32} & d_{33} \end{bmatrix} \quad (2.22)$$

For the [100] orientation this tensor in a matrix notation can be simplified:

$$[\mathbf{d}] = \begin{bmatrix} d_{11} & \cdot & \cdot \\ \cdot & d_{22} & \cdot \\ \cdot & \cdot & d_{33} \end{bmatrix} \quad (2.23)$$

where d_{11} is the permittivity for a dielectric displacement in the direction 1 and electric field in the direction 1 under constant stress, d_{22} is the permittivity for a dielectric displacement in the direction 2 and electric field in the direction 2 under constant stress, d_{33} is the permittivity for a dielectric displacement in the direction 3 and electric field in the direction 3 under constant stress, \cdot denotes zero values.

2.1.3 Boundary and initial conditions

The relation for the strain (2.7) and the electric field (2.17), the equation of motion (2.11), the quasistatic equation (2.16), the constitutive equations (2.18) and (2.19) form the system, which describes the mathematical model of the piezoelectric continuum under consideration. For the solution of this system it is necessary to prescribe boundary conditions and, in addition, in the case of non-stationary problems initial conditions.

At first we suppose a decomposition of the boundary Γ into parts:

$$\Gamma = \Gamma_u \cup \Gamma_\sigma \text{ and } \Gamma = \Gamma_\varphi^1 \cup \Gamma_\varphi^2 \cup \Gamma_q \quad (2.24)$$

On the boundary Γ_u the displacement vector \mathbf{u} is defined:

$$\mathbf{u}|_{\Gamma_u} = \mathbf{u}_1 \quad (2.25)$$

The condition (2.25) is usually called essential boundary condition or first-kind boundary conditions and defines the Dirichlet problem for the boundary value problem [115]. The natural boundary condition, which describes the action of the mechanical stress vector \mathbf{p} on the boundary Γ_σ with the external normal vector \mathbf{n} to this boundary can be presented as follows:

$$\mathbf{n} \cdot \boldsymbol{\sigma}|_{\Gamma_\sigma} = \mathbf{p} \quad (2.26)$$

The condition (2.26) is called second-kind boundary condition and defines the Neumann boundary value problem [111].

For the formulation of the electric boundary conditions we assume that $\Gamma_\varphi = \Gamma_\varphi^1 \cup \Gamma_\varphi^2$ is covered by infinitesimal electrodes, for example, the anode and the cathode are placed on Γ_φ^1 and Γ_φ^2 , respectively

$$\begin{aligned} \varphi|_{\Gamma_\varphi^1} &= \varphi_1, \\ \varphi|_{\Gamma_\varphi^2} &= \varphi_2 \end{aligned} \quad (2.27)$$

Then conditions (2.27) are similar to the first-kind boundary condition. The gradient of the electric potential between Γ_φ^1 and Γ_φ^2 is the reason for the mechanical response of interior forces as the result of the inverse piezoelectric effect [83]. The Neumann boundary value problem contains the condition on the area Γ_q :

$$-\mathbf{n} \cdot \mathbf{D}|_{\Gamma_q} = q \quad (2.28)$$

where q is the surface electric charge [83].

Other possible statements for the piezoelectricity tasks are reported in Table 2.1 [66, 89]. Here \mathbf{S} denotes the compliance matrix, \mathbf{g} , $\boldsymbol{\eta}$ and \mathbf{h} are representations of the piezoelectric tensors, $\boldsymbol{\beta}$ is the representation of the dielectric tensor. The relationship between the electric properties of a piezoelectric material can be presented in the following form [89]:

$$\mathbf{e} = \mathbf{C} \cdot \mathbf{g}, \quad \mathbf{g} = \boldsymbol{\varepsilon} \cdot \mathbf{h}, \quad \mathbf{h} = \mathbf{S} \cdot \boldsymbol{\eta}, \quad \boldsymbol{\beta} = \mathbf{d}^{-1}$$

In the case of non-stationary problems initial conditions should be prescribed:

$$\mathbf{u}|_{t=0} = \mathbf{u}_0 \quad (2.29)$$

Table 2.1: Constitutive equations and boundary conditions for various representations of the electro-elastic problem [89]

Problem	Constitutive equations	Boundary conditions
$[\mathbf{u} - \varphi]$	$\boldsymbol{\sigma} = {}^{(4)}\mathbf{C} \cdot \boldsymbol{\varepsilon} - \mathbf{e}^T \cdot \mathbf{E}, \mathbf{D} = \boldsymbol{\varepsilon} \cdot \mathbf{e} - \mathbf{d} \cdot \mathbf{E}$	$\mathbf{u} _{\Gamma_u} = \mathbf{u}_0, \varphi _{\Gamma_\varphi} = \varphi_0$
$[\boldsymbol{\sigma} - \mathbf{D}]$	$\boldsymbol{\varepsilon} = \mathbf{S} \cdot \boldsymbol{\sigma} + \mathbf{g}^T \cdot \mathbf{D}, \mathbf{E} = -\mathbf{g} \cdot \boldsymbol{\sigma} + \boldsymbol{\beta}^T \cdot \mathbf{D},$	$\mathbf{n} \cdot \boldsymbol{\sigma} _{\Gamma_\sigma} = \mathbf{p}, -\mathbf{n} \cdot \mathbf{D} _{\Gamma_q} = \mathbf{q}$
$[\boldsymbol{\sigma} - \varphi]$	$\boldsymbol{\varepsilon} = \mathbf{S} \cdot \boldsymbol{\sigma} + \boldsymbol{\eta}^T \cdot \mathbf{E}, \mathbf{D} = \boldsymbol{\eta} \cdot \boldsymbol{\sigma} + \mathbf{d}^T \cdot \mathbf{E},$	$\mathbf{u} _{\Gamma_u} = \mathbf{u}_0, -\mathbf{n} \cdot \mathbf{D} _{\Gamma_q} = \mathbf{q}$
$[\mathbf{u} - \mathbf{D}]$	$\boldsymbol{\sigma} = \mathbf{C} \cdot \boldsymbol{\varepsilon} - \mathbf{h}^T \cdot \mathbf{D}, \mathbf{E} = -\mathbf{h} \cdot \boldsymbol{\varepsilon} + \boldsymbol{\beta} \cdot \mathbf{D},$	$\mathbf{u} _{\Gamma_u} = \mathbf{u}_0, \varphi _{\Gamma_\varphi} = \varphi_0$

$$\dot{\mathbf{u}}|_{t=0} = \mathbf{v}_0 \quad (2.30)$$

where \mathbf{u}_0 is the initial displacement of the continuum medium and \mathbf{v}_0 is the initial velocity of the points of the continuum. The relations (2.7)–(2.19), the boundary conditions (2.25)–(2.28) and the initial conditions (2.29)–(2.30) form the classical initial-boundary problem for the linear elastopiezoelectricity [66].

2.2 Fluid mechanics

Fluid mechanics is a part of continuum mechanics studying the behavior of liquids and gases [74]. Fluid mechanics is divided into fluid statics, fluid kinematics, and fluid dynamics. Usually fluid mechanics is mathematically complex. A lot of applied problems cannot to be solved in analytically [67]. The fluid-structure interaction is a typical example. Here a movable or deformable structure with an internal or surrounding fluid flow is considered. For the solution of this complex problems only numerical methods, for example the finite volume method, can be applied. Another topic of research is the proper specification of the fluid properties, described by rheological models and material characteristics [51, 114]. Below we discuss some applied problems, based on some simplified assumptions about the fluid behavior (e.g. ideal fluid or Newtonian fluid, etc.) [7, 114]. This requires deep and well-founded analysis of the problems of the fluid mechanics.

2.2.1 Basics and classical models of fluids

As mentioned above the principal equations for the mathematical model of a fluid can be deduced from the general equations of continuum mechanics. A fluid is a continuum with special flow properties like viscosity, density, etc.

Fluids can be divided into two classes: compressible and incompressible fluids. One can consider ideal and real fluids. The model of an **ideal fluid** is based on the assumption that the friction between the particles, the viscosity and the heat conduction can be ignored. As a consequence, it does not oppose the tangential shear forces. A perfect or ideal fluid is completely incompressible. The closed system of equations for the incompressible ideal fluid takes the following form [74]:

$$\rho_f \frac{\partial \mathbf{v}}{\partial t} = -\nabla p + \mathbf{f} \quad (2.31)$$

$$\frac{\partial \rho_f}{\partial t} = 0 \quad (2.32)$$

$$\nabla \cdot \mathbf{v} = 0 \quad (2.33)$$

where ρ_f is the density of the fluid, \mathbf{v} is the velocity of the fluid, \mathbf{f} is the vector field of mass forces and p is the fluid pressure. Equation (2.31) is the Euler equation of the ideal fluid motion and Eq. (2.32) denotes the constancy of density of the fluid continuum. As a consequence from the general form of the continuity equation

$$\frac{\partial \rho_f}{\partial t} + \nabla \cdot \rho_f \mathbf{v} = 0,$$

hereafter we consider the fluid incompressibility by Eq. (2.33). The system of equations (2.31)–(2.33) allows to describe the ideal fluid motion (Euler model of the fluid motion).

Let us consider a fluid with a linear relationship between the shear stresses and velocity gradient. Such a continuum is called **Newtonian fluid** [50]. In contrast to the Euler model of the fluid motion (2.31)–(2.33) we assume the Navier–Stokes equation [7] for the description of the Newtonian fluid motion:

$$\rho_f \left[\frac{\partial \mathbf{v}}{\partial t} + (\mathbf{v} \cdot \nabla) \mathbf{v} \right] = -\nabla p + \mu \nabla \cdot (\nabla \mathbf{v}) + \mathbf{f} \quad (2.34)$$

where μ is the non-zero viscosity. In addition, we assume the incompressibility condition (2.33).

The next extension of the fluid model is the consideration of the non-linear dependence between the shear stresses and the velocity gradient. This viscous fluid called non-linear or **non-Newtonian fluid** [7, 74]. Thus, the equation of motion for a non-Newtonian fluids is given as follows [7]:

$$\rho_f \left[\frac{\partial \mathbf{v}}{\partial t} + (\mathbf{v} \cdot \nabla) \mathbf{v} \right] = -\nabla p + \mu \nabla \cdot (\nabla \mathbf{v}) + \nabla \mu \cdot \nabla \mathbf{v} + \mathbf{f} \quad (2.35)$$

Equation (2.35) is the extended Navier-Stokes equation (2.34). The non-classical term $\nabla \mu \cdot \nabla \mathbf{v}$ in (2.35) is related to the non-linear behavior of the fluid.

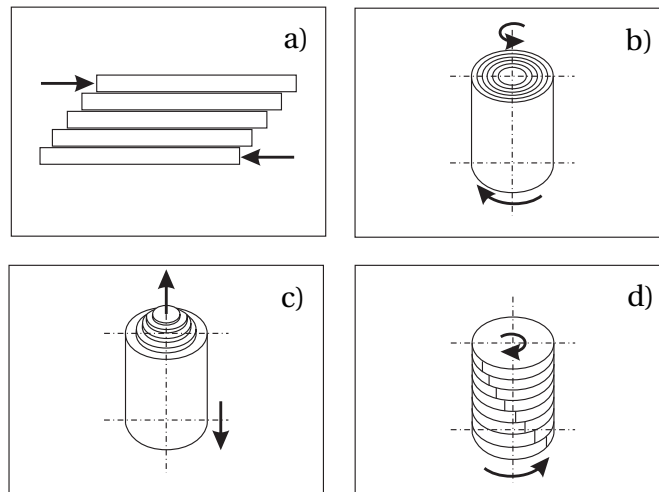


Figure 2.3: Types of laminar flow displacement: a) Elementary shear; b) Circular motion; c) Telescopic (translational) motion; d) Torsion [74]

For investigation of the fluid-structure interactions is important the type of the fluid motion because this defines additional conditions for the study. According to the rheology the fluid can reflect unusual effects, see the problem in Section 4.2. One can notice the types of fluid motion, which are depicted in Fig. 2.3 [7].

2.2.2 Rheological models for a viscous incompressible fluid

Various real media behave different under equal external conditions. This means that the described above equations are not enough for representing the motion of the continuum. The construction of the closed system, which describes the mathematical model of motion of some medium, is required. In particular, the rheological behavior of the continuum should be defined. This part is related to the rheology.

It is necessary to consider the various types of fluids according to their rheological behavior. For fluids in a shear flow the dependency of the shear stress on the shear strain rate is depicted in Fig. 2.4 a), while the viscosity depends on the shear strain rate as in Fig. 2.4 b). Here τ is the shear stress, $\dot{\gamma}$ is the shear strain rate, μ_0 and μ_∞ are the infimum and supremum of the viscosity μ , respectively.

The most commonly used types of generalized non-Newtonian fluids are [114]:

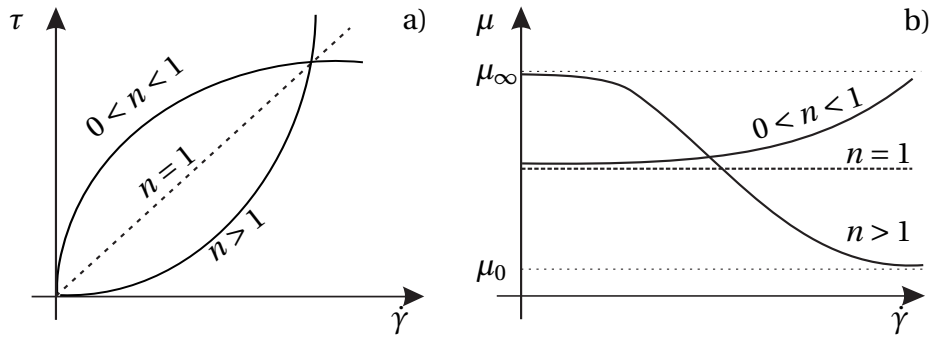


Figure 2.4: Constitutive behavior of various types of non-linear viscous fluids: a) Shear stress vs. shear strain rate; b) Viscosity vs. shear strain rate [114]

- Power-law fluid:

$$\mu = k \|\mathbf{J}\|^{n-1} \quad (2.36)$$

- Carreau fluid:

$$\mu = \mu_0 (1 + (\lambda \dot{\gamma})^2)^{\frac{n-1}{2}} \quad (2.37)$$

- Cross fluid:

$$\mu = \frac{\mu_0}{1 + \left(\frac{\mu_0 \dot{\gamma}}{\check{\tau}}\right)^{1-n}} \quad (2.38)$$

Hereafter $\mathbf{J} = \frac{1}{2}(\nabla \mathbf{v} + \nabla \mathbf{v}^T)$ is the tensor of the velocity gradient of the fluid flow, $\|\mathbf{J}\| = \sqrt{\text{tr}(\mathbf{J} \cdot \mathbf{J}^T)}$ is the norm of \mathbf{J} , \mathbf{v} is the velocity vector of the fluid, k is the consistency index, which describes the saturation degree of the non-linear fluid, λ is the time constant, $\check{\tau}$ is the natural time (i.e., the inverse of the shear rate at which the fluid changes from Newtonian to power-law behavior). The parameter n characterizes the non-Newtonian behavior of the fluid. The specific properties of rheological laws are presented by (2.36)-(2.38). According to the power law (2.36) the constitutive equation of the Newtonian fluid is obtained as a special case when $n = 1$. The pseudoplastic fluid behavior corresponds to $n < 1$, dilatant behavior to $n > 1$, see [7, 50]. At low shear rate

$$\dot{\gamma} \ll \frac{1}{\lambda}$$

or

$$\dot{\gamma} \ll \frac{1}{\mu_0 \check{\tau}}$$

the Carreau fluid and the Cross fluid (2.37) and (2.38), respectively, behave as a Newtonian fluid. For proving this fact it is enough to tend the terms with the shear rate to zero and one can have a constant value of the viscosity. This

corresponds to the definition of the Newtonian fluid. In general, the Carreau law (2.37) and Cross law (2.38) with the increase of the shear rate can become the power law (2.36). In the Eqs. (2.37) and (2.38) μ_0 denotes the accessible value of the viscosity at zero shear rate and can be considered as an entry parameter for the description of the fluid behavior. This is the principal difference with the generalized power law, because in the general case the power law can describe the constitutive fluid behavior with the viscosity as a function, which asymptotically tends to limit values (infimum and supremum of the viscosity function as function from shear strain rate), Fig. 2.4. For the general description and accurate modeling of the particular behavior of various suspensions it is necessary to take into account the possible limits of the viscosity function with possible values of the shear strain rate. According to this, in the present work will be used the power law for the description of non-linear behavior of the studied fluid.

For the description of the rheology of the generalized Newtonian fluid in the three-dimensional case will be used the following model:

$$\boldsymbol{\sigma}_f = -p\mathbf{I} + 2\mu(\mathbf{J})\mathbf{J}, \quad (2.39)$$

where the viscosity μ is given by the power law in form of Eq. (2.36), $\boldsymbol{\sigma}_f$ is the stress tensor of the fluid, p is the fluid pressure, \mathbf{I} is the unit tensor. The first term in the Eq. (2.39) defines the hydrostatic pressure without taking into account the motion of the fluid. It should be noted that the part of the stress tensor $2\mu(\mathbf{J})\mathbf{J}$ shows the influence of viscosity function on the resulting stress state.

Initial conditions for the fluid motion can be determined similar to the case of continuum motion:

$$\mathbf{u}_f|_{t=0} = \mathbf{u}_{f0} \quad (2.40)$$

$$\dot{\mathbf{u}}_f|_{t=0} = \mathbf{v}_{f0} \quad (2.41)$$

where \mathbf{u}_{f0} is the initial displacement of the fluid particle and \mathbf{v}_0 is the initial velocity of the flow.

2.2.3 Fluid-structure interaction model

Many physical problems require the solution of the interaction problem between fluids and elastic deformable bodies. The problem of a piezoelectric body - fluid combination is more complicated because this requires the consideration of the influence of the environment. The coupling is reflected by

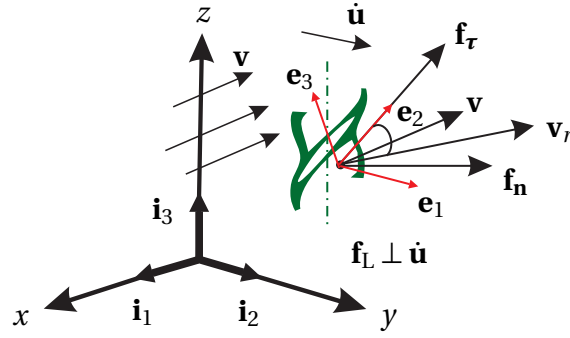


Figure 2.5: Constraining aerodynamic force [74]

the boundary conditions on the fluid-body interface. In Section 2.1 the relations (2.7)–(2.19) and respective boundary conditions (2.25)–(2.28) are considered. We add to this system of equations the relations (2.33), (2.35) and (2.39), which describe the fluid behavior.

However, the mathematical model of the fluid-structure interaction, which is presented by the coupled system of equations, should be supplemented by the boundary conditions on the body-fluid interface and conditions at infinity of the fluid domain. First of all we consider the constraining aerodynamic force \mathbf{F}_{CAF} , which influences the motion of the structure in the fluid. In general, this vector can be decomposed into three independent vectors (2.42), see Fig. 2.5:

$$\mathbf{F}_{\text{CAF}} = \mathbf{f}_n + \mathbf{f}_\tau + \mathbf{f}_L \quad (2.42)$$

where $\mathbf{f}_n = \mathbf{f}_n(\mathbf{v}_r)$ is the vector of the frontal force, $\mathbf{f}_\tau = \mathbf{f}_\tau(\mathbf{v}_r)$ is the vector of the tangential force, $\mathbf{f}_L = \mathbf{f}_L(\mathbf{v}_r)$ is the vector of the lift force, $\mathbf{v}_r = \mathbf{v} - \dot{\mathbf{u}}$ is the relative velocity, \mathbf{v} and $\dot{\mathbf{u}}$ are the velocity of the fluid and the body, respectively.

For the fluid it is necessary to accept the following boundary conditions:

$$\mathbf{v}_n|_{\Gamma_\infty} = 0 \quad (2.43)$$

$$\mathbf{v}_\tau|_{\Gamma_\infty} = 0, \text{ or } \mathbf{v}_\tau|_{\Gamma_\infty} = \mathbf{v}_{\text{wall}} \quad (2.44)$$

$$(\mathbf{v}, \mathbf{n})|_{\Gamma_{\text{in}}} = \mathbf{v}_n \quad (2.45)$$

$$\left\{ \begin{array}{l} \nabla(\mathbf{v}, \mathbf{n})|_{\Gamma_{\text{out}}} = \mathbf{0}, (\mathbf{v}, \mathbf{n}) \leq 0 \\ (\mathbf{v}, \boldsymbol{\tau})|_{\Gamma_{\text{out}}} = \mathbf{v}_\tau, (\mathbf{v}, \mathbf{n}) > 0 \\ p|_{\Gamma_{\text{out}}} = 0 \end{array} \right. \quad (2.46)$$

The relations (2.43)–(2.46) describe the flow behavior. The boundary conditions (2.43)–(2.44) describe the standard boundary conditions as “wall”-

condition [110] with a deceleration of the fluid particle near the abstract border by the definition of the tangential component v_τ and zeroing of the normal component v_n of the velocity vector of the flow. The condition (2.45) describes the inlet of the fluid particles with the $v_n > 0$ (“inlet”) in the abstract fluid area. Relations (2.46) present the free outlet of the flow from fluid area with zero fluid pressure.

The interaction of the moving deformable piezoelectric solid and the fluid flow should be described by the essential and natural boundary conditions on the body-fluid interface. Then, taking into account the constraining aerodynamic force in form (2.42), one can consider the following form of the boundary conditions:

$$\mathbf{n} \cdot \boldsymbol{\sigma}|_{\Gamma_{\text{body/fluid}}} = \mathbf{n} \cdot \boldsymbol{\sigma}_f = \mathbf{F}_{\text{CAF}} \quad (2.47)$$

$$\mathbf{v}|_{\Gamma_{\text{body/fluid}}} = \dot{\mathbf{u}} \quad (2.48)$$

where \mathbf{n} is the unit normal vector to the body-fluid interface boundary $\Gamma_{\text{body/fluid}}$, $\dot{\mathbf{u}}$ denotes the velocity vector of the solid. The condition (2.48) presents the effect of transfer of fluid particles on the motion in the flow of an elastic body.

Computational facilities and numerical aspects

3.1 Overview of the computational tools

For the investigation of nanoshells/fibers/crystals-like structures or systems of arrays of similar elements is necessary the consideration of various types of initial-boundary problems in multi-physics areas, for example, fluid dynamics, gas dynamics, stress analysis, etc. Both the model formulation and the simulation of complex processes requires the use of mathematical and numerical tools for solving practical problems.

The widespread applications of experimental methods and tools are primarily associated with the complexity, uniqueness, but also high costs of modern equipments. Only in this case physical processes can be reproduced in all their diversity. A possible alternative is the application of computer simulations based on high-end software packages. Below some elements of numerical analysis are discussed.

Computer-aided engineering (CAE) is one of the best possibilities for detailed modeling. This includes the visualization of the studied effects, the analysis and the comparison of the numerical and the theoretical results. The combination of reasonable opportunities of the adequate quantitative description and visual reproduction allows the study of the structures with the maximum quality of a representation and conditions, which are the similar to the laboratory experiment. In addition, the applications of CAE technique allows to compare the relevant theoretical researches, namely to perform a verification of the formulated theory.

The following tools of the **computer aided engineering** are applied:

- Stress analysis of components and assemblies using **Finite Element Analysis** (FEA);
- Thermal and fluid flow analysis using the **Computational fluid dynamics** (CFD);
- **Multibody dynamics** (MBD) and Kinematics.

Independently of the tool, the process of modeling requires the following steps:

- Pre-processing: determination of the model and environment factors and producing data for external software operators;
- Analysis solver;
- Post-processing of results.

In the thesis both numerical and analytical modelings possibilities of two-dimensional and three-dimensional problems are developed and investigated, taking into account the influence of specific changes of the properties at the nanoscale and the impact of the environment on the structural behavior. Numerical investigations help to avoid the expensive performance of experiments. For the numerical simulation of the coupled problem the combination of the finite element and finite volume methods via two-way exchange at each time step with the dynamically adapting of the re-meshing is applied.

The standard procedure of mathematical and numerical modeling of structures has the following steps:

- The geometrical problem is based on the design with the help of external programs (the so-called geometrical preprocessing) and by the import of the geometrical data into the finite-volume module. It should be noted that many of the finite-volume software systems work only with three-dimensional geometry, so two-dimensional models are special cases.
- Physical and mathematical formulation of the problem - the choice of model for interior points of the computational domain and setting limits of the boundary conditions design. The initial conditions for time-dependent problems should be determined.
- Input parameters of the grid according to the type of numerical method for the numerical solution of the problem.
- The derivation, analysis, and verification of the results.

For the Fluid Structure Interaction modeling we used several CFD-packages such as ANSYS CFX[®] [6], ABAQUS FSI[®] [21], FlowVision MpM[®] [110], etc. The main advantages of them can be considered as:

- Universal complex for the numerical solution of a large range of applications in multiphysics problems.

- All software systems are developed with intuitive interface and can be integrated into a variety of CAD/CAM/CAE systems.

The most standard way of **Computer-aided design** (CAD) is the export of the built geometry of studied structure and in the case of **Fluid-Structure Interaction** (FSI) the calculation domain for the engineering simulation software is conducted. Thus, by an implementation of the numerical simulation, the geometry of the investigated structures is exported in the neutral file formats, as an example *.sat or *.vrmf.

Due to the nature of the investigated structures the size, the chirality, the contact area, etc. are very important and should be accurate computer-aided designed. By the way, all geometry objects are constructed with the help of a CAD package and saved in the standard **3D ACIS[®] Modeler** (*.sat format). This format is chosen according to the broad area of an export/import data tools.

The fluid simulation also requires additional efforts in the CAD package in spite of the simplicity of the geometry. The reason of this is the need for distinguishing facets of the computational domain for assigning the different types of boundary conditions. For this realization is used the universal data format **Virtual Reality Modeling Language** (*.vrmf) is used, which allows such possibilities as predefined properties, for example, the color of facets.

3.2 Applications of finite element and finite volume methods

The basic methods for the computer simulation and numerical calculations are the **Finite Element Method** (FEM), the **Finite Volume Method** (FVM) and their coupling via an **Exchange Modul**. The FEM is a numerical algorithm for approximate solution of partial differential equations. It is based on the **Ritz method**, which is a special case of **Bubnov-Galerkin method** [108]. The solution approach is based on elimination of the spatial derivatives in the partial differential equations. This approximates the partial differential equations by a system of algebraic equations for steady state problems. If we have transient instead of the a system of the algebraic equations, we have a system of ordinary differential equations with respect to time.

The FVM is a method for representing and evaluating partial differential equations in the form of algebraic equations [76, 112]. This is close to the FEM, but unknown values are computed at discrete places as "finite volumes" with respect to the tessellated geometry. For the numerical solution of the ba-

sic equations within the FVM packages a method is used, which belongs to the so-called conservative schemes for unsteady partial differential equations. In comparison with the non-conservative schemes this method gives solutions, which exactly satisfy the conservation laws (in particular, the continuity equations).

The finite element partition in the domains Ω_{hj} approximating the domains Ω_j is performed. The unknown functions \mathbf{u} and φ on the grid are approximated as

$$\mathbf{u} \approx \mathbf{N}_{\mathbf{u}}^T(x) \cdot \mathbf{U}(t), \quad \varphi \approx \mathbf{N}_{\varphi}^T(x) \cdot \Phi(t) \quad (3.1)$$

where $\mathbf{N}_{\mathbf{u}}^T(x)$ is the shape function matrix for the displacement field \mathbf{u} and $\mathbf{N}_{\varphi}^T(x)$ is the row vector of the shape functions for the field of the electric potential φ . $\mathbf{U}(t)$ and $\Phi(t)$ are the global vectors of the corresponding nodal degrees of freedom. The finite element approximation of piezoelectric problems in the FEM package, including the boundary conditions, gives a system of ordinary differential equations.

3.3 Numerical methods for the fluid-structure interaction problems

The coupling of Finite Element and Finite Volume methods for the solution of the FSI can be implemented via off-site exchange modulus by means of direct common interface. In the general case, FSI simulation involves moving bodies, free surfaces, and conjugate heat exchange. The body rotation and translation are defined by the user. The computation grid is automatically rebuilt after each time step. The grid takes into account structural deformations calculated by FEM [21]. Grid generation process is fully automatic [110].

The most interesting task is to consider the problem of the coupled analysis as a FSI. Let us consider this task on the example of two effective software packages (FEM-package Simulia ABAQUS[®] [21] and Flow Vision[®] [110]). The implementation of the Fluid Structure Interaction analysis with help of coupling softwares Simulia ABAQUS[®] [21] and Flow Vision is based on the **SGGR** (Sub-Grid-Geometry-resolution) method used in FlowVision[®] [110] for grid generation. The SGGR method provides a natural link between finite volume grid and finite element mesh. The **MPM** (Multi-Physics-Manager) controls both FlowVision[®] and ABAQUS[®] during the simulation process. The data is exchanged using direct coupling providing optimal data transfer rates and accurate data exchange.

Let us introduce briefly the main items of simulations [110]:

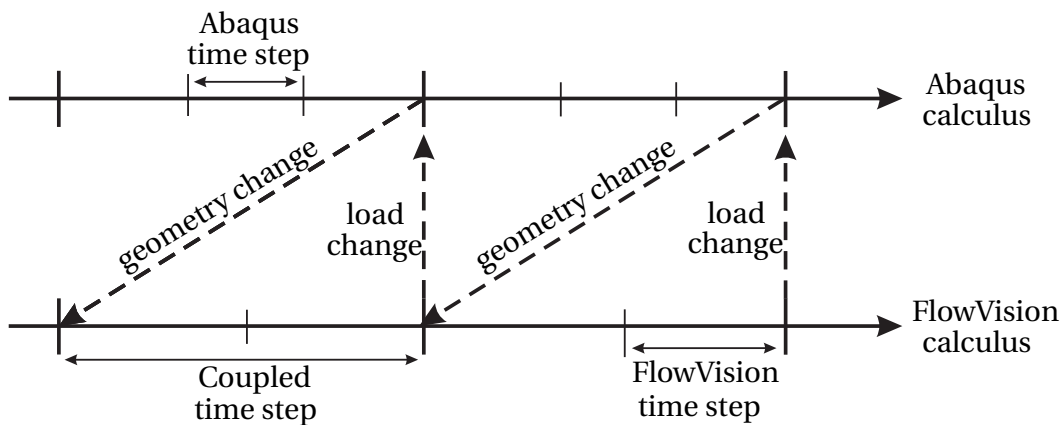


Figure 3.1: Scheme of the coupled numerical analysis [110]

- Sub-Grid Geometry Resolution (SGGR) method
 FlowVision-HPC adaptive grid generator is fully automatic and operates directly on 3D CAD data. A CAD model, defined by 3D surfaces is imported to FlowVision-HPC and surrounded by a Cartesian mesh. The computation domain is defined as result of the Boolean subtraction of the CAD model exterior boundaries and the Cartesian CFD mesh. On the boundary the original hexahedral CFD cells are trimmed by the initial CAD geometry in such a way that the exact geometry shape is maintained. The flow equations in the boundary cells are adapted to approximate the boundary conditions and take into account the cell shape.
- Natural link between CFD and FEA systems
 When the boundary of the computational domain is represented by the FE mesh, the link between the CFD grid and FE mesh is automatically established. FE mesh is matched with fluid cells allowing precise load transfer between fluid and structure, see Fig. 3.1. In this way coupled multi-physic problems as the fluid-structure interaction can be efficiently and accurately solved.
- Multi-Physics Manager (MPM) for Fluid-Structure Interaction (FSI)
 FSI simulation takes into account large structural deformations and moving bodies caused by the hydrodynamic loads imposed on the boundaries of the computation domain. The MPM module control and synchronize the operation of both FlowVision-HPC[®] and ABAQUS[®] (explicit or implicit).
- Moving bodies and free surfaces
 The FSI simulation supports of moving bodies (user defined rotation and translation) and tracking of free surfaces analysis. The grid genera-

tion process is fully automatically with rebuilding of the computational grid at each time step. The data are exchanged with ABAQUS[®] computing the structural deformations.

Spiral nanofilms with piezoelectric properties

4.1 Modeling of multi-layer nanofilms

The unique properties of spiral nanofilms make them very attractive in applications: planar microelectronics, various sensors, magnetic and optical recording and storage systems, micro- and nanoelectromechanical devices (MEMS/NEMS), optics, tribological engineering, for anticorrosion and high temperature protection coatings, and in other fields [13, 38, 39, 45, 51]. In particular, recent decades can be characterized by a considerable progress in submicro- and nanofilm technologies. The use of thin films is determined by their mechanical properties, strength and reliability [24]. In this context, the most important parameters are the thickness, the hardness, the Young's modulus, the internal stress in individual layers and the layer-to-layer adhesion [2, 34]. These characteristics are responsible for mechanical, tribological, electrical, optical and other functional properties of thin films as well as for the reliability of devices in which they are used. One way of designing micro- and nanoelectromechanical devices is to use multilayer films made of semiconductor and piezoelectric materials in helical structures (see, e.g., [34, 41]).

Spiral nanoshells serve as elements of sensors and actuators. Their analysis is of particular interest, especially, in the case of multilayer spirals with a piezoelectric layer having a high electromechanical coupling factor. In simulation of nanoobjects by continuum elements, the determination of their physical and mechanical properties become very important [32, 33, 35]. Certain aspects of this problem can be resolved by comparing data of natural and numerical experiments. The determination of several eigenfrequencies

of a spiral nanoshell can provide way to determine the bending stiffness of the film of which the shell is made [31, 32, 41, 68].

4.1.1 Problem statement

Let us consider the eigenvalue problem for the helical multilayer structure with a typical geometry as depicted in the Figs. 1.3 and 4.1. The geometry parameters are presented in Table 4.1.

Based on the Eqs. (2.11)–(2.28) presented in Chapter 2 the eigenfrequency analysis requires the solution of the following problem:

1. Equation of motion:

$$\nabla \cdot \boldsymbol{\sigma} = \rho \frac{d^2 \mathbf{u}}{dt^2} \quad (4.1)$$

2. Maxwell's relations for the electric displacement and electric field vectors, respectively:

$$\nabla \cdot \mathbf{D} = 0 \quad (4.2)$$

$$\mathbf{E} = -\nabla \varphi \quad (4.3)$$

Table 4.1: Typical geometry parameters for the helical shell shown in Figs. 1.3 and 4.1

Thickness of lower layer (substrate), h_1	11 nm
Thickness of upper layer, h_2	16 nm
Thickness, $a = h_1 + h_2$	27 nm
Width of helix belt, b	3 μm
Length helix coil, s	5 μm
Number of helix coils, i	9
Length helix, ℓ	$\frac{2\pi R i}{\cos \alpha}$
Radius, R	2 μm

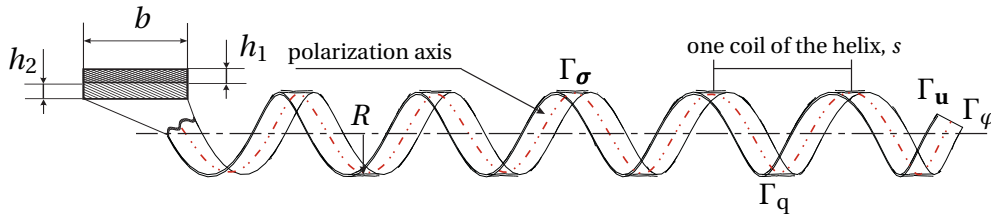


Figure 4.1: Model of two-layer helix

3. Relation for the strain tensor in the case of small deformations:

$$\boldsymbol{\varepsilon} = \frac{1}{2} (\nabla \mathbf{u} + \nabla \mathbf{u}^T) \quad (4.4)$$

4. Constitutive equations:

$$\boldsymbol{\sigma} = {}^{(4)}\mathbf{C} \cdot \boldsymbol{\varepsilon} - {}^{(3)}\mathbf{e}^T \cdot \mathbf{E} \quad (4.5)$$

$$\mathbf{D} = \boldsymbol{\varepsilon} \cdot {}^{(3)}\mathbf{e} - \mathbf{d} \cdot \mathbf{E} \quad (4.6)$$

5. Boundary conditions as shown in Fig. 4.1:

$$\mathbf{u}|_{\Gamma_u} = \mathbf{0} \quad (4.7)$$

$$\mathbf{n} \cdot \boldsymbol{\sigma}|_{\Gamma_\sigma} = \mathbf{0} \quad (4.8)$$

$$\varphi|_{\Gamma_\varphi} = 0 \quad (4.9)$$

$$\mathbf{n} \cdot \mathbf{D}|_{\Gamma_q} = 0 \quad (4.10)$$

The solution of the eigenvalue problem (4.1)–(4.10) can be found with the help of the two substitutions:

$$\begin{aligned} \mathbf{u}(\mathbf{x}, t) &= \mathbf{U}(\mathbf{x})e^{i\omega t} \\ \varphi(\mathbf{x}, t) &= \Phi(\mathbf{x})e^{i\omega t} \end{aligned} \quad (4.11)$$

where ω is the frequency. As usual only the determination of the first eigenfrequencies is of practical interest.

Below is presented the modal analysis of an $\text{In}_{0.14}\text{Ga}_{0.86}\text{As}/\text{PZT-5H}$ two-layer film structure with the properties indicated in Tables 4.2–4.5.

Piezoceramic materials compositions based on lead titanatezirconate (PZT) have the following properties: intrinsically strong piezoelectric effect,

Table 4.2: Properties of the substrate $\text{In}_{0.14}\text{Ga}_{0.86}\text{As}$ [128]

E [MPa]	ν	ρ_s $\left[\frac{\text{kg}}{\text{m}^3}\right]$
$8.06 \cdot 10^4$	0.32	5500

Table 4.3: Mechanical properties of the upper layer PZT-5H [37]

E_1 [MPa]	E_2 [MPa]	E_3 [MPa]	ν_{12}	ν_{13}	ν_{23}
$6.06 \cdot 10^4$	$4.83 \cdot 10^4$	$6.06 \cdot 10^4$	0.512	0.289	0.512

Table 4.4: Piezoelectric properties of upper layer PZT-5H [37]

$e_{41} \left[\frac{\text{m}}{\text{V}} \right]$	$e_{21} \left[\frac{\text{m}}{\text{V}} \right]$	$e_{22} \left[\frac{\text{m}}{\text{V}} \right]$	$e_{23} \left[\frac{\text{m}}{\text{V}} \right]$	$e_{35} \left[\frac{\text{m}}{\text{V}} \right]$
$741 \cdot 10^{-12}$	$-274 \cdot 10^{-12}$	$-593 \cdot 10^{-12}$	$-274 \cdot 10^{-12}$	$741 \cdot 10^{-12}$

Table 4.5: Permittivity properties of the upper layer PZT-5H [37]

d_{11}	d_{22}	d_{33}
$17.1 \cdot 10^2$	$14.7 \cdot 10^2$	$17.1 \cdot 10^2$

high Curie point, and higher coupling coefficient [37]. The considered parameters of the stiffness matrix in Table 4.3 can be recalculated by [2, 19]:

$$C_{ij} = E_i(v_{ji} + v_{ki}v_{jk})\gamma \quad (4.12)$$

where

$$\gamma = \frac{1}{1 - v_{12}v_{21} - v_{23}v_{32} - v_{31}v_{13} - 2v_{21}v_{32}v_{13}}, \frac{v_{ij}}{E_i} = \frac{v_{ji}}{E_j}, \sum : i \neq j \neq k = 1, 2, 3$$

4.1.2 Results: Eigenmodes of a two-layer shell

All objects are modeled as three-dimensional objects taking into account the piezoelectric properties of the material. The orientation of the piezoelectric layer is such that the polarization axis is tangential to the spiral turn, Figs. 1.3 and 4.1. These conditions correspond to the case where the shell is polarized before it takes on the form of a helical object. Thus, the curvilinear anisotropy of the shell can be considered [36]. For this purpose, a coordinate system for each finite element of the obtained triangulation is introduced to specify the orientation of the piezoelectric material such that the polarization axis would pass along the spiral turn. In other words, the local coordinate introduced at the n^{th} -step rotated together with a turn of helix that the z axis is outer normal to the surface.

In the finite element simulations are used eight-node prismatic finite elements in the hybrid approximation are used¹. The finite element grid consists of 13 104 elements corresponding to 34 858 nodes and 94 418 unknowns. In

¹The 8-node linear piezoelectric brick element is in ABAQUS[®] denoted by C3D8E [21].

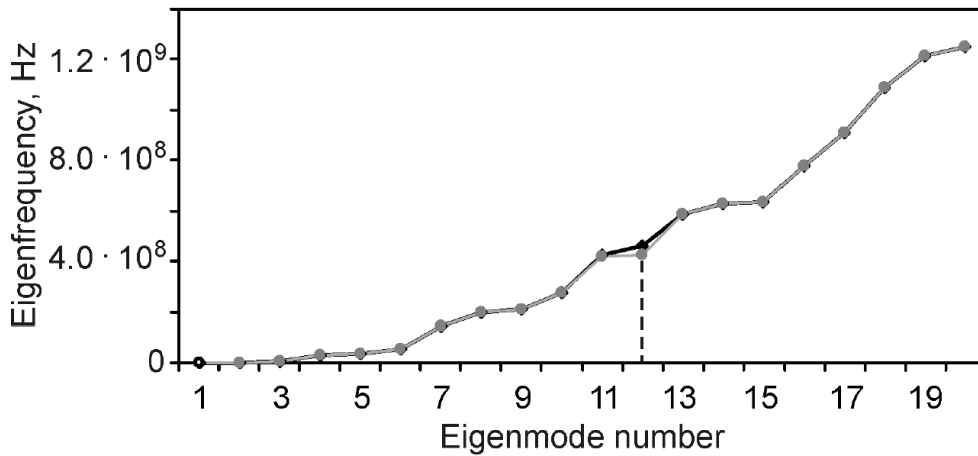


Figure 4.2: Eigenfrequencies vs. number of eigenmode

Table 4.6: Eigenfrequencies of a two-layered nanoshell with earthed left, right and both spiral faces

Mode number	Right end	Right + left ends	Left end
1.	$9.12261 \cdot 10^5$	$9.12259 \cdot 10^5$	$9.12298 \cdot 10^5$
2.	$9.56037 \cdot 10^5$	$9.56028 \cdot 10^5$	$9.56043 \cdot 10^5$
3.	$6.03050 \cdot 10^6$	$6.03048 \cdot 10^6$	$6.03056 \cdot 10^6$
4.	$3.18345 \cdot 10^7$	$3.18336 \cdot 10^7$	$3.18345 \cdot 10^7$
5.	$3.32418 \cdot 10^7$	$3.32417 \cdot 10^7$	$3.32420 \cdot 10^7$
6.	$5.42619 \cdot 10^7$	$5.42619 \cdot 10^7$	$5.42627 \cdot 10^7$
7.	$1.42982 \cdot 10^8$	$1.42982 \cdot 10^8$	$1.42983 \cdot 10^8$
8.	$1.99708 \cdot 10^8$	$1.99695 \cdot 10^8$	$1.99709 \cdot 10^8$
9.	$2.09541 \cdot 10^8$	$2.09537 \cdot 10^8$	$2.09545 \cdot 10^8$
10.	$2.73498 \cdot 10^8$	$2.73498 \cdot 10^8$	$2.73500 \cdot 10^8$
11.	$4.22775 \cdot 10^8$	$4.22775 \cdot 10^8$	$4.22777 \cdot 10^8$
12.	$4.60602 \cdot 10^8$	–	$4.60751 \cdot 10^8$
13.	$5.87122 \cdot 10^8$	$5.86844 \cdot 10^8$	$5.87126 \cdot 10^8$
14.	$6.26694 \cdot 10^8$	$6.26688 \cdot 10^8$	$6.26696 \cdot 10^8$
15.	$6.32586 \cdot 10^8$	$6.32118 \cdot 10^8$	$6.32589 \cdot 10^8$

the numerical experiment the comparative analysis of the eigenfrequencies and appropriate eigenmodes of the spiral nanoshell with one and two earthen spiral faces is performed. The eigenfrequencies of the nanoshell are compared in Fig. 4.2 and in Table 4.6.

The analysis of the data shows that, if both spiral ends are earthen (see

Table 4.6, second column), the eigenmode corresponding to the 12th eigenmode number is not excited, see Fig. 4.2. This can be explained by the piezoelectric properties of upper helical layer with special type of polarization, applied electrical boundary conditions and or appearance of aliquot eigenvalues. Based on the spectrum infinity of the eigenvalues one can make proposition that such losing of some eigenmodes can be occur in the case of higher order eigenvalues. Hereby one can consider the discharged (sparse) spectrum of the eigenfrequencies in devices with helical piezoelectric structures, which can find applications in high-Q resonators² with a sparse spectrum of natural vibrations [53]. At current moment such high-Q resonators find a broad area of applications:

- in microwave electronics as resonant and stabilizing systems of generators;
- in the measurement technique as the wave meter filters, measuring the spectrum of the signal, frequency discriminators;
- in electron paramagnetic resonance spectroscopy, etc.

These data calculated by the direct simulation are sufficiently consistent with the results obtained using the methodology presented in [31, 34].

4.1.3 Results: External medium, preliminary discussion

In the previous section we considered the eigenmodes and their appropriate eigenfrequencies of the $\text{In}_{0.14}\text{Ga}_{0.86}\text{As}/\text{PZT-5H}$ two-layer spiral shell. Of special interest is to analyze the frequencies with regard to an external medium, in particular, to external acoustic action, to determine its effect on the eigenfrequencies. The interest in this analysis is associated with the fact that the presence of an external medium can cause damping of oscillations by electromagnetic wave scattering at infinity. Moreover, the interaction between turns of the piezoelectric shell is possible due to the electromagnetic interaction. For this analysis, we simulate the following system: a two-layer structure is inscribed inside an external medium.

For the system to be as close to real conditions as possible, a section in the form of the spiral surface was made inside the external medium. This is necessary for consideration of the interaction of the medium and correct use of certain options of the Simulia ABAQUS[®] element package (e.g., consideration of the interaction between the surface of the external medium and the

²High Q microwave resonators are used to create high-quality source signals and radar navigation systems for the spectral and frequency measurements to measure the parameters of the materials for the particular physical researches.

Table 4.7: Comparison of eigenfrequencies of a bispiral shell with and without environment

Mode number	Bispiral/air Hz	Bispiral, Hz
1.	$2.19384 \cdot 10^5$	$9.12259 \cdot 10^5$
2.	$2.74099 \cdot 10^5$	$9.56028 \cdot 10^5$
3.	$4.64475 \cdot 10^6$	$6.03048 \cdot 10^6$
4.	$6.07333 \cdot 10^6$	$3.18336 \cdot 10^7$
5.	$1.05502 \cdot 10^7$	$3.32417 \cdot 10^7$

surfaces of spiral layers, triangulation with consistent geometry, etc.) [21]. The external medium approximates the air of normal atmospheric pressure at the temperature of 25°C.

Thus, in the numerical experiment we estimate eigenfrequencies of the spiral with one end rigidly fixed and embedded into the external medium. The obtained eigenfrequencies of the system are compared with those found earlier for a bilayer spiral shell consists of two layers made of different materials. The layers are adhesive butt-jointed [44].

Eight-node prismatic finite elements in the hybrid formulation are used in the finite element simulation. For the piezoelectric film, the finite elements are chosen with regard to the presence of electric degrees of freedom³. The external medium is modeled using acoustic finite elements⁴. The orientation of the piezoelectric layer is specified in the same way as in the previous case, see Fig. 4.1. The conditions correspond to the shell polarized before taking on a helical shape. The model analysis of the "air – bispiral" structure is performed in the Table 4.7. It is seen from the table that in the case of external medium action the eigenfrequencies decrease. This problem is directly related among other things to the simulation of nanosensors using variations in eigenfrequencies when other matters are acting on shells.

The simulation veracity can be confirmed by correctness of the properly posed eigenvalue problem, a numerical implementation in the approved software package with numerical stability by the increasing of the quantity of the finite elements and qualitative coincidence with the result in [68, 69]. However, the influence of the environment on the nanoshells can be particular considerable and requires deeper investigation as an independent problem. This issue will be considered in the following Section 4.2.

³The 8-node linear piezoelectric brick element is in ABAQUS® denoted by C3D8E [21].

⁴The 8-node linear acoustic brick element is in ABAQUS® denoted by AC3D8 [21].

4.2 Interaction of a helical shell with a non-linear viscous fluid

The need of mathematical and numerical simulations of coupled problems on fluid-structure interaction between the metamaterial and their individual component is obvious, see [41]. In addition, the problem of optimization of the design of helical shell-structures arises. The choice of material in design of shells may be defined with the chemical inertness, the possibility of decay and the presence of electric characteristics.

In design of such structures one should take into account the properties of the environment, in which the device is operating. An important aspect is to select the type of the environment with the required generalization of mathematical models that are more accurately describe its behavior. According to the possibilities of applications it is necessary to consider non-classical fluid models [106] because some real liquids have a significant non-linear behavior. Examples are blood, petroleum and various suspensions [7, 67, 114]. The present numerical investigation of the fluid-structure interaction (FSI) is focused on the analysis of the interaction of an elastic helical shell with a non-Newtonian fluid and of the motion of such structures in the laminar flow.

4.2.1 Problem statement

Let us consider the interaction of a helical elastic shell with a non-Newtonian fluid, Fig. 4.3. We restrict ourselves by the model of a non-linear viscous fluid (generalized Newtonian fluid), see Fig. 2.4. Figure 4.3 a) shows how the laminar flow of the non-linear viscous fluid is directed to the elastic shell clamped on the bottom end. The free shell motion in a laminar flow is shown in Fig. 4.3 b). In Subsection 2.2.3 is described the general statement for the investigation of the interaction between a fluid and an elastic body taking into account the equation of motion for non-Newtonian fluids (2.35), relations specifying the fluid behavior (2.33) and (2.39), boundary condition for the fluid domain (2.43)–(2.46) and boundary conditions on the body/fluid interface describing the interaction between the elastic body and the non-linear fluid (2.47) – (2.48).

Based on these relations the fluid-structure interaction problem requires the coupled solution of the following closed system of equations [66, 83]:

1. Equation of body motion:

$$\nabla \cdot \boldsymbol{\sigma} + \rho \mathbf{f}_m = \rho \frac{d^2 \mathbf{u}}{dt^2} \quad (4.13)$$

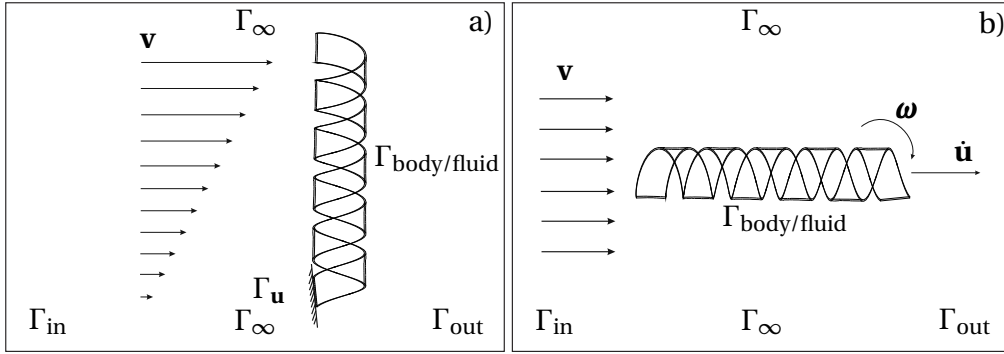


Figure 4.3: Models used in simulations: a) Coupled analysis of the fluid-structure interaction between an elastic piezoelectric shell and a laminar flow of a pseudoplastic fluid; b) Rigid shell motion in a laminar flow of a pseudoplastic fluid

2. Maxwell's relations for the electric displacement vector and electric field vector, respectively:

$$\nabla \cdot \mathbf{D} = q \quad (4.14)$$

$$\mathbf{E} = -\nabla \varphi \quad (4.15)$$

3. Small strain tensor:

$$\boldsymbol{\varepsilon} = \frac{1}{2} (\nabla \mathbf{u} + \nabla \mathbf{u}^T) \quad (4.16)$$

4. Constitutive equations:

$$\boldsymbol{\sigma} = {}^{(4)}\mathbf{C} \cdot \cdot \boldsymbol{\varepsilon} - {}^{(3)}\mathbf{e}^T \cdot \mathbf{E} \quad (4.17)$$

$$\mathbf{D} = \boldsymbol{\varepsilon} \cdot \cdot {}^{(3)}\mathbf{e} - \mathbf{d} \cdot \mathbf{E} \quad (4.18)$$

5. Equation of motion of the non-Newtonian fluid:

$$\rho_f \left[\frac{\partial \mathbf{v}}{\partial t} + (\mathbf{v} \cdot \nabla) \mathbf{v} \right] = -\nabla p + \mu \nabla \cdot (\nabla \mathbf{v}) + \nabla \mu \cdot \nabla \mathbf{v} + \mathbf{f}_m \quad (4.19)$$

6. Incompressibility condition:

$$\nabla \cdot \mathbf{v} = 0 \quad (4.20)$$

7. Rheological model for the fluid behaviour:

$$\mu = k \|\mathbf{J}\|^{n-1} \quad (4.21)$$

$$\boldsymbol{\sigma}_f = -p \mathbf{I} + 2\mu(\mathbf{J}) \mathbf{J} \quad (4.22)$$

$$\mathbf{J} = \frac{1}{2} (\nabla \mathbf{v} + \nabla \mathbf{v}^T) \quad (4.23)$$

Table 4.8: Properties of the elastic solid, GaAs [128]

C_{11} [MPa]	C_{12} [MPa]	C_{44} [MPa]	ρ_s $\left[\frac{\text{kg}}{\text{m}^3}\right]$	e $\left[\frac{\text{m}}{\text{V}}\right]$	d
$11.9 \cdot 10^4$	$5.34 \cdot 10^4$	$5.96 \cdot 10^4$	5317	$-2.69 \cdot 10^{-12}$	12.9

8. Boundary conditions for the solid, Fig. 4.3:

$$\mathbf{u}|_{\Gamma_u} = \mathbf{0} \quad (4.24)$$

$$\mathbf{n} \cdot \boldsymbol{\sigma}|_{\Gamma_{\text{body/fluid}}} = \mathbf{n} \cdot \boldsymbol{\sigma}_f = \mathbf{F}_{\text{CAF}} \quad (4.25)$$

$$\mathbf{v}|_{\Gamma_{\text{body/fluid}}} = \dot{\mathbf{u}} \quad (4.26)$$

9. Boundary conditions for the fluid domain, Fig. 4.3:

$$\mathbf{v}_n|_{\Gamma_\infty} = 0 \quad (4.27)$$

$$\mathbf{v}_\tau|_{\Gamma_\infty} = 0, \text{ or } \mathbf{v}_\tau|_{\Gamma_\infty} = \mathbf{v}_{\text{wall}} \quad (4.28)$$

$$(\mathbf{v}, \mathbf{n})|_{\Gamma_{\text{in}}} = v_n \quad (4.29)$$

$$\left\{ \begin{array}{l} \nabla(\mathbf{v}, \mathbf{n})|_{\Gamma_{\text{out}}} = \mathbf{0}, (\mathbf{v}, \mathbf{n}) \leq 0 \\ (\mathbf{v}, \boldsymbol{\tau})|_{\Gamma_{\text{out}}} = v_\tau, (\mathbf{v}, \mathbf{n}) > 0 \\ p|_{\Gamma_{\text{out}}} = 0 \end{array} \right. \quad (4.30)$$

10. Initial conditions:

$$\begin{aligned} \mathbf{u}|_{t=0} &= \mathbf{u}_0 \\ \dot{\mathbf{u}}|_{t=0} &= \mathbf{v}_0 \end{aligned} \quad (4.31)$$

Let us investigate on one-layer shell made from GaAs, Table 4.8⁵. The geometry of structure is defined by following values: layer thickness 29.6 nm, width of helix belt 6 μm , radius 5.5 μm , length of helix coils 5 μm , number of coils 4. Following [94, 98], GaAs is chosen as the basic piezoelectric material of the helical shell. The fluid properties are presented in Table 4.9. The properties of the fluid are close to the real human blood properties for the reason to find real applications of the present research [67]. This problem cannot be solved analytically in general, especially under consideration of anisotropy of the helical shell material and non-linear behavior of the fluid. The problem requires the numerical modeling of this initial boundary-value problem by FEM and FVM taking into account the fluid-solid interaction.

⁵Parameter d denotes the relative permittivity relatively the vacuum permittivity $d_0 = 8.854 \cdot 10^{-12} \left[\frac{\text{F}}{\text{m}}\right]$ (dimensionless property).

Table 4.9: Properties of the fluid [67]

μ_0	$\frac{\text{kg}}{\text{m}\cdot\text{s}}$	μ_∞	$\frac{\text{kg}}{\text{m}\cdot\text{s}}$	ρ_f	$\frac{\text{kg}}{\text{m}^3}$	k	$\frac{\text{kg}}{\text{m}}$	n	$ \mathbf{v} $ [$\frac{\text{m}}{\text{c}}$]
$3 \cdot 10^{-3}$		$5 \cdot 10^{-3}$		1060		$1 \cdot 10^{-3}$		0.5	1.0

4.2.2 Results: Complex effects of non-linear environment

For investigations of the influence of the non-Newtonian fluid on the elastic shell we use the finite-element package Simulia ABAQUS[®] together with the finite-volume package FlowVision[®] in a two-way exchange between the fluid and the structure, that allows to analyze with sufficient accuracy the effect of the laminar flow of the pseudoplastic fluid on the clamped elastic shell, see Fig. 4.3 a). For description of free motion of the helical shell and of the analysis of distribution of the velocity and the pressure we use only the finite-volume package FlowVision[®], Fig. 4.3 b). The details of the numerical modeling are discussed in Chapter 3.

With the help of software package Simulia ABAQUS[®] we create the model of the solid structure taking into account elastic and electric characteristics of the material as well as the curvilinear anisotropy. In particular, we specify the stiffness matrix for the orthotropic behavior, the matrix of piezoelectric parameters, the dielectric parameters and the general orientation of the material with respect to the local coordinate system rotating with the helix. We use three-dimensional prismatic 8-node finite elements, which possesses piezoelectric degrees of freedom. In the package Simulia ABAQUS[®] for these purposes is applied the element C3D8E allowing to derive the electric field and the distribution of the electric charge in the hydroelastic analysis. The implicit scheme of the exchange between the fluid and the solid shell for the numerical stability of the solution is used, see Fig. 3.1.

With the software package FlowVision[®] the computational domain of the laminar non-linear viscous flow is modeled. The computational area is chosen in such way that the behavior of the fluid near the external boundaries does not affect the behavior of the flow around the elastic shell. For the coupled hydroelastic analysis we used double coupling steps for FEM and FVM analysis, Fig. 3.1, which is provided by the multi-physics manager of FlowVision[®] and the possibility of a co-simulation within Simulia ABAQUS[®]. The results of the coupled dynamic FEM-FVM analysis (duration of 1 s) with time increments of 0.05 s in Figs. 4.4–4.10 are presented.

Figure 4.4 shows the distribution of the designated normalized scalar fields in the shell. The maximum and minimum values of the denoted variables are shown by the red and blue color, respectively. For the consideration of the variables distribution is chosen the middle time point. One can see that in the shell the minimal mechanical stresses are on the free face, Figs. 4.4 a), b). As the result one can consider the same behavior according to the electric response of the investigated material, Figs. 4.4 d), e). In Fig. 4.4 c) the distribution of the hydrodynamic pressure is shown, which is an indicator for the most liable areas influenced by the flow. Fixing one time point one can consider the distribution of the velocity vector magnitude presented in Fig. 4.4 f).

The changes of the flow velocity field as the result of the interaction with the shell is shown in Fig. 4.5. From Figs. 4.4 f) and 4.5 one can obtain the general representation of the helical shell motion. According to this field distribution one can imagine the elastic shell vibration under the influence of the flow. The helix motion in the fluid as the result of the described above bound-

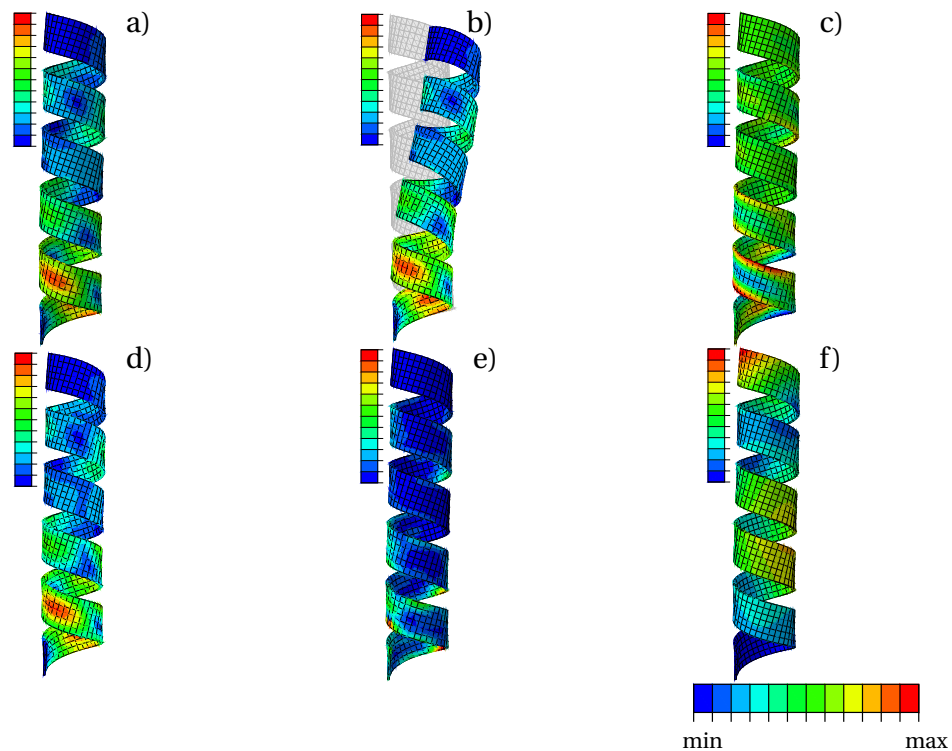


Figure 4.4: Coupled FEM-FVM analysis: a) von Mises stresses, b) Deformed state, c) Hydrodynamic pressure, d) Magnitude of the electric flux vector, e) Magnitude of the electric field vector, f) Magnitude of the shell velocity

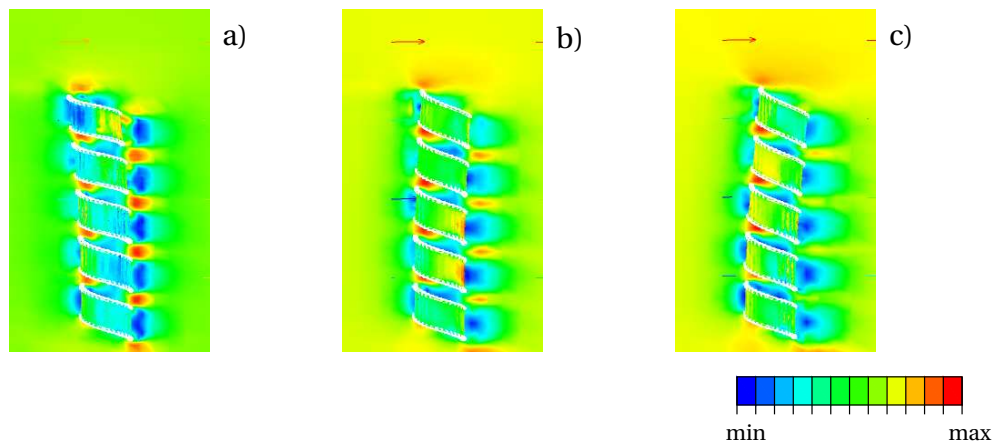


Figure 4.5: Velocity field at time steps: a) 0.20 s; b) 0.70 s; c) 0.90 s

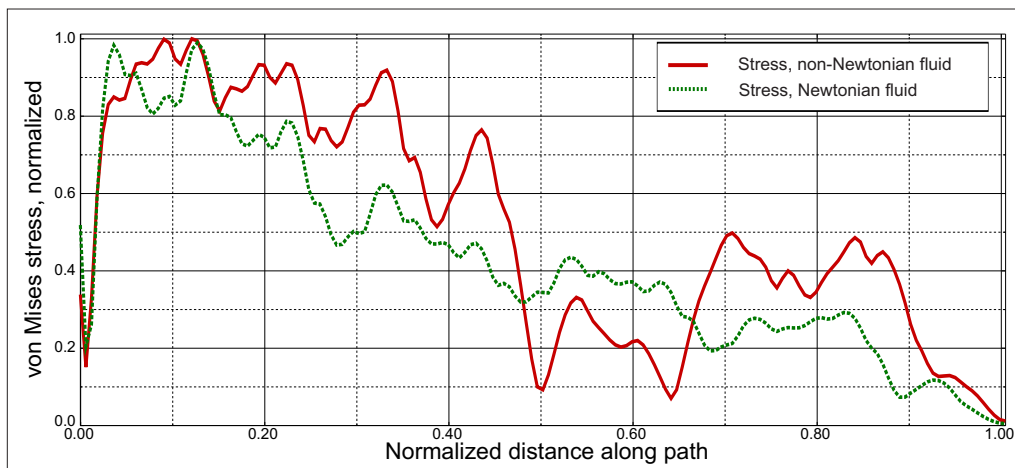


Figure 4.6: Comparison of the influence of non-Newtonian and Newtonian fluid models on the von Mises stress

ary conditions looks like the motion of seaweeds. The velocity of the flow particles changes corresponding to the deformations of the shell in every time point. As one can see in Fig. 4.5 the velocity of the fluid between the turns of the helix increases as well as the turns spacing decreases. The minimal velocity value of the fluid corresponds to the surfaces with the outer normal vector opposite to the direction of the velocity vector of the flow. These two facts can be observed with the help of the streamlines of the flow without separation of the elastic shell in investigated fluid.

Corresponding to the described above Figs. 4.4 and 4.5 the graphs in Figs. 4.6–4.10 show the changes of the above mentioned variables along the helical path (nodes of the finite elements) with respect to the considered fluid model

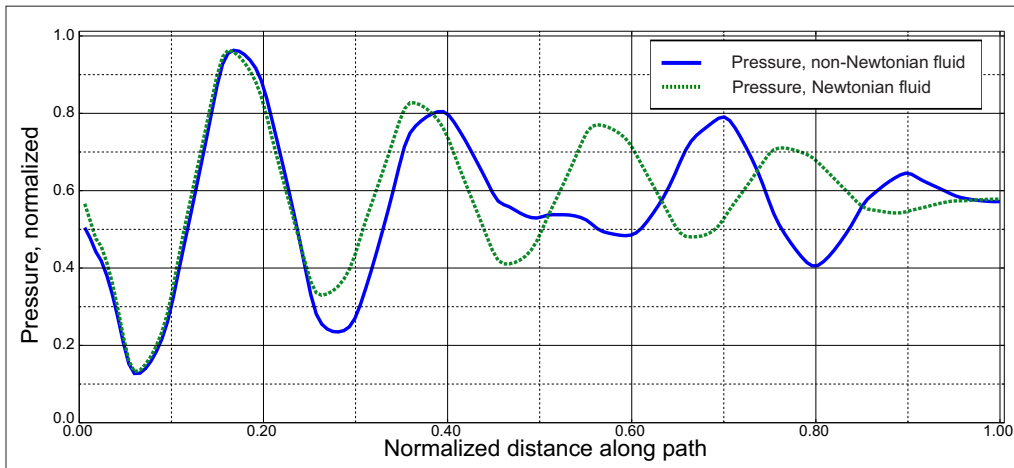


Figure 4.7: Comparison of influences of non-Newtonian and Newtonian fluid on the pressure variable

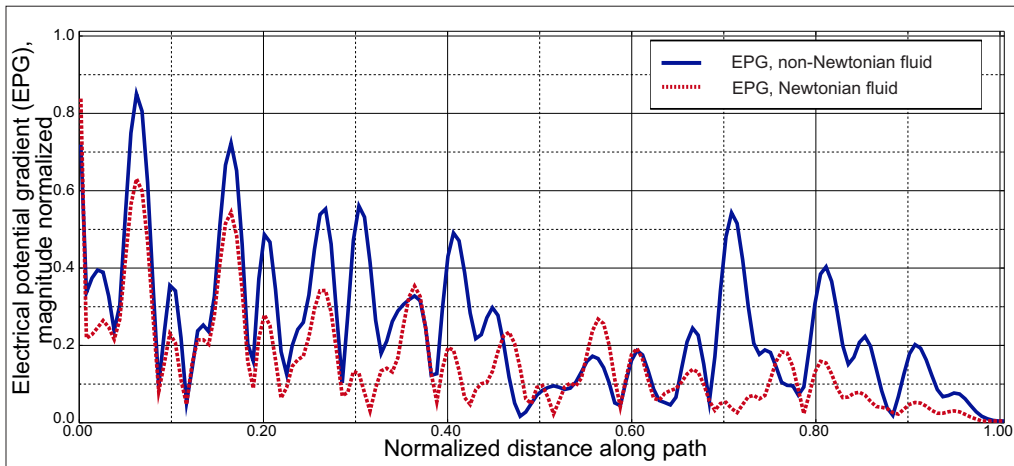


Figure 4.8: Comparison of the influence of non-Newtonian and Newtonian fluid models on the magnitude of the electric potential gradient

(non-Newtonian and Newtonian fluid). The consideration of non-linear viscosity of the fluid results in significant changes of the stresses and the electric fields in the shell, which can be explained by the direct piezoelectric effect. The influence is greater in the middle of the helix. In any case the Newtonian fluid has more smooth influence on the distributions of the considered variables. From the simulation follow the necessity of the taking into account the constitutive equation of non-Newtonian fluid (4.19). Let us note that the detection of the appeared electric fields in such analysis can be explained by the onset of the direct piezoelectric effect. This means that the deformations in

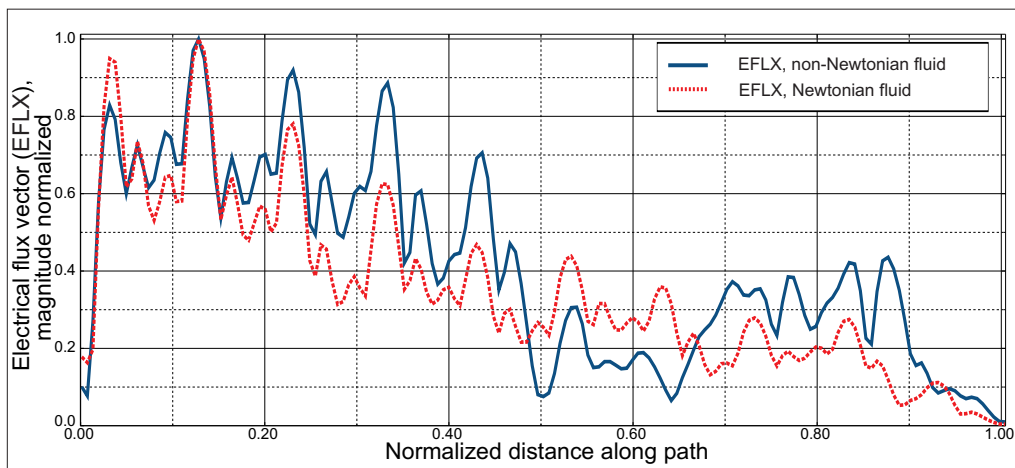


Figure 4.9: Comparison of influences of non-Newtonian and Newtonian fluid on the magnitude of the electrical flux vector

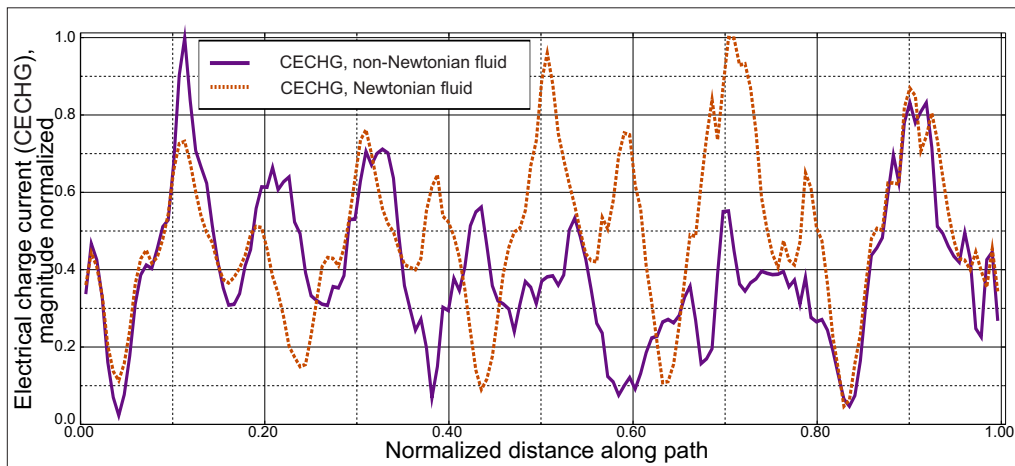


Figure 4.10: Comparison of influences of non-Newtonian and Newtonian fluid on the magnitude of the electrical charge current

the shell appeared under action of hydrodynamic pressure cause the polarization of the material, see Figs. 4.8–4.10. The inverting of this process gives us the possibility of calculation the required electric potential for the motion of the shell in the flow. This is of great interest since it gives the ability to predict and control the motion of such structures in the flow, see [41].

In the case of pseudoplastic behavior of the fluid the viscosity decreases in the neighborhood of the moving helix as a monotonic function of the velocity, which is predicted by the rheological equation (4.21) with $n = \frac{1}{2}$, Fig. 4.11. In Figs. 4.11 a) and b) is presented the distribution of the viscosity by the coupled

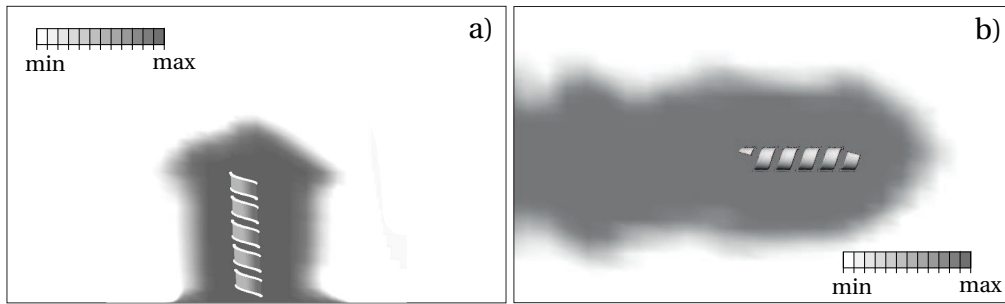


Figure 4.11: Viscosity field of non-linear viscous fluid: a) elastic piezoelectric shell, b) rigid shell

analysis of the fluid-structure interaction between an elastic piezoelectric or rigid shell and a laminar flow of a pseudoplastic fluid, respectively. Thus, it is possible to observe the so-called thixotropy effect⁶, see [52]. The results in Fig. 4.11 show the apparent effect of "fluidification", which cannot be regarded as the pure thixotropy effect, but it is close to it. The observed effect of decreasing viscosity is a result of the power law (4.21) and the rheological equation (4.23) for the viscosity due to the increased shear stress. The pure thixotropic fluid viscosity decreases with time at constant shear stress. In the presented case the change of the viscosity according to the rheological model (4.21)–(4.23) is caused by an increase in the velocity gradient of the fluid as a result of the shell at a rate greater than the velocity of the liquid. Because of chiral geometry of the structure and the pseudoplasticity of the environment one can have the possibility to observe the Weissenberg effect⁷, Fig. 4.11. For the fluid behavior it is a complex combination of two standard types of laminar flows (telescopic and torsional), see Figs. 2.3 c), d). The translational and rotational movable shell winds and roots some fluid chains by its path. It should be noted that the natural helix twist is reason for the motion of the shell in a fluid. The "fluidification" of pseudoplastic liquids can be applied in biomedicine and pharmaceuticals, in particular, in the treatment of cancer. Blood vessels of helical shape supplying the tumor are more porous than usual vessels and such nanostructures can easily penetrate into the area affected by cancer. The helical shape of the shell and the natural helical trajectory of the motion in the flow reduce the hydrodynamic resistance on the part of fluid surrounding the shell taking

⁶Thixotropy effect is the effect for viscous fluids, which consist in the time-decreasing of the viscosity by the constant shear stress [7].

⁷Weissenberg effect is a phenomenon that occurs when a spinning rod is inserted into a solution of liquid polymer, and instead of being thrown outward, the solution is drawn towards the rod and rises up around it [7].

into account the sufficiently large surface [43].

The computational algorithm is complicated since the finite volume and the finite element analysis are coupled. The presented calculations allow to design structures and predict their behavior with sufficient accuracy. The described above simulations are confirmed by the correctness of the properly posed and coupled fluid-structure interaction problem and the numerical implementation in approved software packages with numerical stability of the simulation.

4.3 Instability of a piezoelectric helical shell under electrical field action

In general, the thin helical shell is a geometrical non-linear structure. The geometrical non-linearity is the source of the buckling collapse by various types of loads [8, 84, 90, 93, 111, 113, 132]. The consideration of the geometrical non-linearity of the thin helical structure is an essential part in simulations of processes as the motion and interaction of the shell with the environment.

4.3.1 Problem statement

Let us consider the tape helix with a geometry as depicted in Fig. 1.3. The geometry of structure is defined by following values: layer thickness 20 nm, width of helix belt 3 μm , radius 6 μm , length of helix coils 10 μm , number of coils 5. Both material properties (Table 4.8) and the shape of the studied structure (Fig. 4.12) are the principal information allowing to investigate the resulting buckling behavior. Based on the presented in Chapter 2 relations the basic Lagrangian equations of electro-elastic bodies in the case of quasi-electrostatics and absence of external loads take the form:

1. Equation of motion:

$$\nabla \cdot [\boldsymbol{\sigma}_{\mathbf{P}_I} \cdot \mathbf{F}] = \mathbf{0} \quad (4.32)$$

2. Maxwell's relations for the electric displacement vector and electric field vector, respectively:

$$\nabla \cdot \mathbf{D} = 0 \quad (4.33)$$

$$\mathbf{E} = -\nabla\varphi \quad (4.34)$$

3. Finite deformation tensor:

$$\boldsymbol{\varepsilon} = \frac{1}{2} (\nabla\mathbf{u} + \nabla\mathbf{u}^T + \nabla\mathbf{u} \cdot \nabla\mathbf{u}^T) \quad (4.35)$$

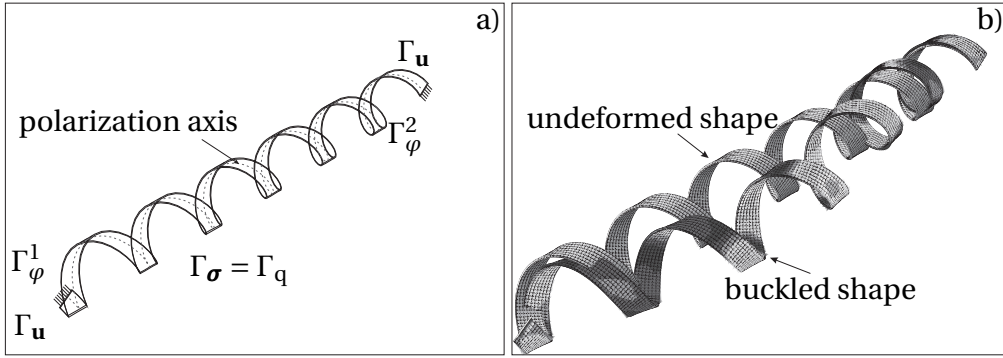


Figure 4.12: Helical shell buckling: a) Shape and boundary conditions; b) Initial and buckled shapes of the shell

Table 4.10: Electric properties of ZnO [128]

$e_{11} \left[\frac{\text{m}}{\text{V}} \right]$	$e_{12} \left[\frac{\text{m}}{\text{V}} \right]$	$e_{13} \left[\frac{\text{m}}{\text{V}} \right]$	$e_{24} \left[\frac{\text{m}}{\text{V}} \right]$	$e_{35} \left[\frac{\text{m}}{\text{V}} \right]$	d
$-543 \cdot 10^{-12}$	$-543 \cdot 10^{-12}$	$16.7 \cdot 10^{-12}$	$-113.4 \cdot 10^{-12}$	$113.4 \cdot 10^{-12}$	10.8

4. Constitutive equations:

$$\boldsymbol{\sigma} = {}^{(4)}\mathbf{C} \cdot \boldsymbol{\varepsilon} - {}^{(3)}\mathbf{e}^T \cdot \mathbf{E} \quad (4.36)$$

$$\mathbf{D} = \boldsymbol{\varepsilon} \cdot \boldsymbol{\varepsilon} - \mathbf{d} \cdot \mathbf{E} \quad (4.37)$$

5. Boundary conditions, Fig. 4.12:

$$\mathbf{u}|_{\Gamma_u} = \mathbf{0}, \quad (4.38)$$

$$\mathbf{n} \cdot \boldsymbol{\sigma}|_{\Gamma_\sigma} = \mathbf{0} \quad (4.39)$$

$$\begin{aligned} \varphi|_{\Gamma_{\varphi_1}} &= \varphi_0 \\ \varphi|_{\Gamma_{\varphi_2}} &= 0 \end{aligned} \quad (4.40)$$

$$-\mathbf{n} \cdot \mathbf{D}|_{\Gamma_q} = 0 \quad (4.41)$$

6. Initial conditions:

$$\begin{aligned} \mathbf{u}|_{t=0} &= \mathbf{u}_0 \\ \dot{\mathbf{u}}|_{t=0} &= \mathbf{v}_0 \end{aligned} \quad (4.42)$$

We will investigate the one-layer tape helical shell depicted in Fig. 4.12 and with material properties presented in Tables 4.8, 4.10 and 4.11.

Table 4.11: Elastic properties of ZnO [128]

$C_{11} = C_{22}$ [MPa]	C_{33} [MPa]	$C_{12} = C_{21}$ [MPa]	$C_{13} = C_{31}$ [MPa]
$1.90 \cdot 10^4$	$1.96 \cdot 10^4$	$1.10 \cdot 10^4$	$0.90 \cdot 10^4$
$C_{23} = C_{32}$ [MPa]	$C_{44} = C_{55}$ [MPa]	C_{66} [MPa]	
$1.10 \cdot 10^4$	$0.39 \cdot 10^4$	$0.45 \cdot 10^4$	

4.3.2 Stability of helical springs

Let us consider the stability problem for an elastic beam replacing the tape helix [48], see Fig. 1.3. Based on some considerations concerning the mechanical equivalence one can substitute the helix as an equivalent beam, Fig. 4.13, see also [17, 90]. The compression spring with the sufficiently great ratio length ℓ_0 to helix diameter $2R$ can lose the stability under the action of the load F .

For the determination of the critical load F_{cr} let us consider the analytical model of a beam, which is equivalent to the helix with a small angle of ascent, bending stiffness EI (where E is the Young's modulus and I is the second order area moment) and shear stiffness GA (where G is the shear modulus and A is the sectional area). By the static loading of the helix up to the buckling load F_{cr} the helix compresses to the length λ_{cr} , see Fig. 4.13.

Assuming small bending of the beam axis we take into account the following equation of equilibrium in the deformed configuration with respect to the pure beam bending:

$$\omega''(z) = -\frac{F\omega(z)}{EI} = -\frac{M}{EI} = \kappa \quad (4.43)$$

where M is the bending moment, κ is the curvature by the pure beam bending, which is opposite to the bending $\omega(z)$ [48]. In general, the beam bending $\omega(z)$ can be expressed only by the pure bending $\omega_b(z)$. In the case of the helical spring with low-helix drills the transverse force Q reflects the coil bending respective to the binormal of coils cross-section, see Fig. 4.13, that requires the adding an additional term to the bending function $\omega_s(z)$:

$$\omega(z) = \omega_b(z) + \omega_s(z) \quad (4.44)$$

The second derivative of $\omega(z)$ with respect to coordinate z can be expressed as follows:

$$\omega''(z) = \omega_b''(z) + \omega_s''(z)$$

The second term of $\omega(z)$ in (4.44) reflects the turn of the z axis as the result of the shear deformations. Then $\omega_s''(z)$ is the first derivative with respect to the angle of rotation of the z axis $\omega_s'(z) = \frac{Q}{GA}$. The following relation is valid assuming $GA = \text{const}$:

$$\omega_s''(z) = \frac{dQ}{dz} \frac{1}{GA}$$

where $Q = F\gamma$ is the transverse force and γ is the angle of rotation of the equivalent beam section, see Fig. 4.13.

Since the shear deformations of the beam cross-sections are almost parallel shifted, the angle γ is connected only with the deflections resulting from the bending. This means $\gamma = \omega_b'(z)$, therefore $Q = F\omega_b'(z)$ and

$$\omega_s''(z) = \frac{dQ}{dz} \frac{1}{GA} = \frac{F}{GA} \omega_b''(z)$$

With help of the Eqs. (4.43) and (4.44) the equation of beam deflection takes the following form:

$$\omega''(z) + \frac{F}{EI} \left(1 + \frac{F}{GA}\right) \omega(z) = 0$$

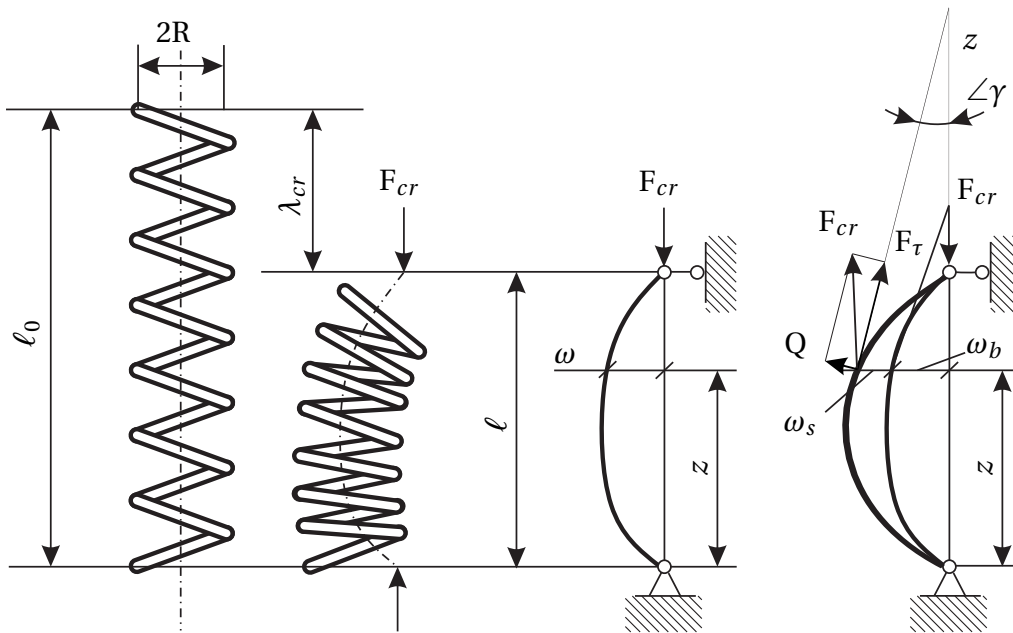


Figure 4.13: Mechanical model of the stability loss problem by equivalent beam (R is the radius of the helix, ℓ_0 and ℓ are the initial and actual lengths of the helix, respectively, F_τ is the tangential force component, $\lambda_{cr} = \ell_0 - \ell$ is the critical length change [90, 93])

with the standard solution [48]

$$\omega(z) = a \sin kz + b \cos kz$$

where

$$k^2 = \frac{F}{EI} \left(1 + \frac{F}{GA} \right) \quad (4.45)$$

Parameters a , b can be determined from the boundary conditions [48]. The most probable form of the curved axis shape with respect to the simply supported boundary conditions is the sinusoidal form. In this case by taking into account the

$$k = \frac{\pi}{\ell}$$

the relation (4.45) takes the form:

$$F^2 + AGF - EIAG \frac{\pi^2}{\ell^2} = 0 \quad (4.46)$$

By the loading up to F_{cr} the helix is compressed up to critical length change λ_{cr} . The most important feature comparing beam and helix is the fact that for the beam one can neglect the relation between the change of the initial beam length and the axial force. For the helix the possible change of the initial length l_0 should be considered. Then the bending and shear stiffness of the spring are

$$EI = \frac{2B_n \ell}{2\pi Ri \left(1 + \frac{B_n}{C} \right)}, \quad GA = \frac{8B_b \ell}{\pi(2R)^3 i}$$

They are functions of the current length⁸ $\ell = \ell_0 - \lambda$. Consider the Reuleaux⁹ formula:

$$F = Z\lambda$$

where

$$Z = \frac{4C}{\pi(2R)^3 i}$$

is the spring stiffness. Substituting the relations for the stiffnesses in Eq. (4.46) and expressing the force in terms of λ one can consider the following

⁸According to the geometry as depicted in Figs. 1.3 and 4.1 the coil stiffness by the bending are the $B_b = \frac{ba^3 E}{12}$, $B_n = \frac{ab^3 E}{12}$ and according to the rectangular shape of the profile (see Fig. 1.3) the torsional stiffness is $C = 0.33ba^3 G$ [48].

⁹Franz Reuleaux (September 30, 1829 – August 20, 1905) was a German mechanical engineer and a lecturer of the Berlin Royal Technical Academy, later appointed as the President of the Academy. He was often called the father of kinematics [87].

quadratic equation, representing the relation of the critical length change λ_{cr} to the initial helix length ℓ_0 :

$$\left(2 - \frac{C}{B_b}\right) \left(\frac{\lambda_{cr}}{\ell_0}\right)^2 - 2 \left(\frac{\lambda_{cr}}{\ell_0}\right) + \frac{\pi^2}{1 + C/B_n} \left(\frac{2R}{\ell_0}\right)^2 = 0 \quad (4.47)$$

The roots of Eq. (4.47) are

$$\begin{aligned} \left[\frac{\lambda_{cr}}{\ell_0}\right]_1 &= \frac{1}{2 - C/B_b} \left(1 - \sqrt{1 - \pi^2 \frac{2 - C/B_b}{1 + C/B_n} \left(\frac{2R}{\ell_0}\right)^2}\right) \\ \left[\frac{\lambda_{cr}}{\ell_0}\right]_2 &= \frac{1}{2 - C/B_b} \left(1 + \sqrt{1 - \pi^2 \frac{2 - C/B_b}{1 + C/B_n} \left(\frac{2R}{\ell_0}\right)^2}\right) \end{aligned}$$

The second root obviously does not satisfy the conditions $\lambda_{cr} < \ell_0$. Considering the first root $\left[\frac{\lambda_{cr}}{\ell_0}\right]_1$ one can note, that the expression $1 - \pi^2 \frac{2 - C/B_b}{1 + C/B_n} \left(\frac{2R}{\ell_0}\right)^2$ tends to a negative value if $\frac{\ell_0}{2R} = \sqrt{\pi^2 \frac{2 - C/B_b}{1 + C/B_n}}$. Then the critical value of the length change parameter λ_{cr} takes a complex value. This means that the real solution of Eq. (4.46) does not exist. Thus, the respective equilibrium state of the helix does not exist too. From the mechanical point of view this behavior corresponds to the loss of stability. The consequence of Eq. (4.3.2) is the relationship between stability of the helical structures and their mechanical parameters. Note that not all helical structures show buckling behavior, see [46, 93]. It depends on both geometry and material. Applying the simply supported boundary conditions on both ends of the tape helix one can present the limit value:

$$\left(\frac{\ell_0}{2R}\right)_\infty = \sqrt{\pi^2 \frac{2 - C/B_b}{1 + C/B_n}} \quad (4.48)$$

According to the limit value (4.48) only by conditions (4.49) the helix can lose stability:

$$\frac{\ell_0}{2R} \geq \left(\frac{\ell_0}{2R}\right)_\infty \quad (4.49)$$

$$\frac{\ell_0}{2R} < \left(\frac{\ell_0}{2R}\right)_\infty \quad (4.50)$$

Equation (4.50) gives us the condition for a accident-free case in the case of the spring geometry. As an example, helical structure has small angle of ascent or some specificity of the cross-section. Considering typical geometry of helical nanostructures one can see that the stability loss problem should be proved. Indeed, let us introduce the functional parameters of a typical nano-helix, see

Fig. 4.1 and Table 4.1. The principal property of the investigated structure is the large ratio of the initial length of the helix to the cross-section dimensions. This ratio can reach more than 10^3 . Let us perform the following calculations:

$$\left(\frac{\ell_0}{2R}\right) = 11.25$$

and

$$\left(\frac{\ell_0}{2R}\right)_\infty = \sqrt{\frac{\pi^2 \frac{2 - 12 \cdot 0.33 \cdot (5.34/11.9)}{1 + 12 \cdot 0.33 \cdot (5.34/11.9) \cdot \left(\frac{27 \cdot 10^{-3}}{3}\right)^2}}{}} \approx 1.5$$

$\left(\frac{\ell_0}{2R}\right)_\infty < \left(\frac{\ell_0}{2R}\right)$ and according to (4.49) the nanohelix can lose a stability.

In the case of mechanical loads the critical loads for the global loss of stability can be obtained [14]. But shell material under consideration is a piezoelectric one. Under electrical load the structure becomes deformed according to their polarization [44]. It means that one can obtain some critical electrical load, which is the reason of the stability loss of the piezoelectric helical nanoshell by the inverse piezoelectric effect. The principal question is: can we replace the electrical load by mechanical boundary conditions and use some simplified methods for their investigation. However, the problem of stability loss of the nanohelix under the action of an electric field, in general, can not be solved in terms of mechanical boundary conditions, Fig. 4.14. The deformations of the spiral body under electrical load according to the polarization are usually not similar to the deformations under mechanical forces. The critical loads can give different deformations, see Fig. 4.14. This complicates the

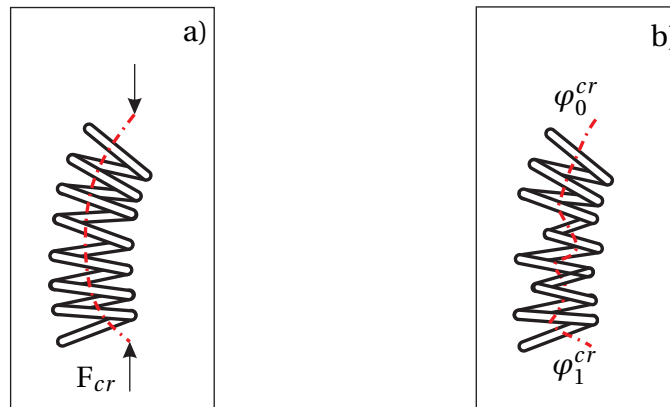


Figure 4.14: Simplified view of apparent effect of difference in buckling mode: a) Model of buckling mode for critical mechanical load F_{cr} ; b) Model of buckling mode for critical electrical field $\mathbf{E} = -\nabla\varphi$

possibility of analytical solutions, and requires the use of numerical and experimental methods for studying these processes.

By the investigation of some nanostructures the questions of the functional properties changes are very important [45, 88]. Macroproperties of the material usually cannot accurately describe the microbehavior of the material [28, 122, 123, 124, 131]. It is obviously to understand that properties of nano-structured materials are affected by the energy competition between the surface and the bulk properties [3, 5, 25, 27, 28, 30, 124]. The surface in this sense is related to the microlevel of the material behavior, while the bulk behavior is related to the macrolevel of material behavior [77, 78]. Hereby, one can confirm that in the majority of cases the expansion (4.51) can give us the scaling law, which describe the relations between the nano- and the bulk properties [20, 25]. On this moment a lot of papers are devoted to this problem [11, 20, 41, 116, 122, 129]. Most of them they are dedicated to experiments.

By using experimental data, which are obtained in tests with nanostructures, one can obtain some intrinsic length scale. The intrinsic length scale can be used for the recalculations of the unknown material properties on the nanoscale by bulk properties with the help of the scaling law (4.51), see Fig. 4.15. It should be noted that in the general case the intrinsic length scale and the scaling law are proper for various functional properties. But in case of the current study the assumption on pure elastic material properties is considered. The linear dependence between elastic and electric material parameters according to the constitutive equations (2.18) and (2.19) in Section 2.1.2 is assumed. These two assumptions make possible to accept the simplification and to use for the recalculation all material parameters, of cause, with taking into account the material anisotropy, the scaling law (4.51) and the intrinsic length scale (4.52):

$$\frac{F(L)}{F(\infty)} = 1 + \alpha \frac{\ell_{\text{in}}}{L} + O\left(\frac{\ell_{\text{in}}}{L}\right)^2 \quad (4.51)$$

$$\ell_{\text{in}} = \frac{\tau}{E} \quad (4.52)$$

where ℓ_{in} is the intrinsic length scale related to the surface properties, τ is the surface stress parameter, E is the Young's modulus of the bulk material, $F(L)$ is the function, which describes the material behavior on the micro-/nano-scale with the size-representative value L , $F(\infty)$ is the function, which describe the bulk material behavior, α is some non-dimensional factor. In the finite element simulation will be used the $^*[\mathbf{u} - \varphi]$ form of piezoelectric problem, see Table 2.1.

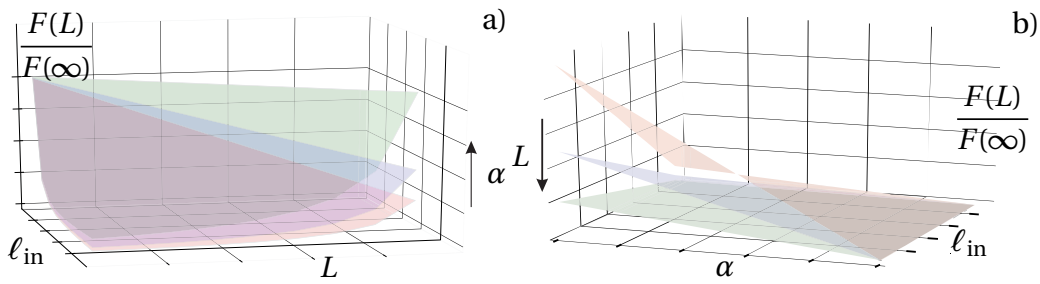


Figure 4.15: Schematic representation of scaling law: a) Relation $\frac{F(L)}{F(\infty)}$ vs. l_{in} and L with variation of the non-dimensional coefficient α ; b) Relation $\frac{F(L)}{F(\infty)}$ vs. l_{in} and α with variation of the size-representative value L

4.3.3 Results: Buckling problem in the case of IPE

The simulation of the problem is based on the FEM package ABAQUS[®], see Chapter 3. Abaqus/Standard allows the elastic buckling analysis by eigenvalue extraction [21]. Let us consider some special scheme for the solution of the buckling under electrical load problem shown in Fig. 4.12.

It is necessary to draw the attention that such numerical simulation with the Neumann boundary condition cannot be solved directly, that requires some modification of the analysis. Hereby, without loss of the physical meaning, one consider the problem statement in terms of the first type of boundary conditions and apply the electric potential instead of electric charge. The electrical charge is assumed to be close zero. Hereby, one can determine the value of critical electric potential, which causes buckling as the result of the inverse piezoelectric effect.

The morphology and the shell-structures growth should be taken into account in modeling, since we have anisotropic material properties. The axis along the turn of the helix is the polarization axis of the piezoelectric layer. According to this assumption, in the FEM-simulation the axes of the local coordinate system, which define the material orientation in the finite elements, is turned. 20-node quadratic finite elements carrying electrical degrees of freedom in the formulation of ABAQUS/CAE[®] (C3D20RE) are used. Thus, finite element allows the analysis of geometrical non-linear models. The total number of elements used in the simulation is 3031 with the total numbers of degrees of freedom 93680 (degrees of freedom plus maximal number of any Lagrange multiplier variables).

Let us describe more precise the simulation scheme:

- Material orientation:

The orientation of the material and the determination of the polarization axis are chosen (discrete assignment, normal axis direction - 2, primary axis direction - 1). The orientation of the material is given by the rotated local coordinate system, which determines the orientation of the material in each finite element.

- Analysis steps and boundary conditions, Table 4.12:

The analysis consists in three steps: the initial static step as standard predefined step in ABAQUS[®], the static analysis and the step of stability loss problem. In between, the statistical step artificially introduced to the possibility of modifying the boundary conditions in the calculation, Table 4.12.

The both ends of the spiral are fixed. The boundary conditions at each step of the analysis are stored. The surface charge is assumed to zero. The potential at both ends of the spiral shell at initial step be zero. After that at the followed step one of the helix ends is modified to a non-zero value and stored for the last step of the numerical simulation. Thus on the buckling step the electrical potential difference is created. This electrical field vector is the reason for the critical deformations of the shell by the inverse piezoelectric effect, see Table 4.12.

The following results are obtained. At first, one can see in Fig. 4.16 non-standard buckling mode for the mechanical type of load, see Fig. 4.14 b). The intrinsic length scale $\ell_{in} = 0.42$ is assumed for ZnO, after that all required material parameters are recalculated. The same geometry in the numerical experiment is performed.

In Fig. 4.17 is shown the distribution of the stress variable along the helical

Table 4.12: Sequence and characteristics of simulation steps

Load:			
Loads - Surface charge~ 0			
BCs			
BCs	Initial - St ₀	Static - St ₁	Buckling - St ₂
Pinned	✓	✓	✓
φ_1	0	Modified	✓
φ_2	0	✓	✓
Mesh:			
C3D20RE: A 20-node quadratic piezoelectric brick, reduced integration, Number of elements - 3031, ✓ denotes the conservation of boundary condition from previous step.			

path for the ZnO material is shown. The path along helixes according to the shell polarization is shown in Fig. 1.3. One can see the similar results with taking into account the linear and proportional response on the properties change. It should be noted that the material orientation is saved.

In Fig. 4.18 the conservation of the proportionality of the results in the case of elastic strain energy distribution is depicted. In spite of the conservation of the material orientation and polarization of the shell one can see the similar distribution of the von Mises stress by the resulting buckling modes with taking into account the nano-size effect, see Fig. 4.16. One can see the similar results of von Mises stress distribution in the case of taking into account the nano-size effect. One can notice that one can see no regular distribution of the stress in the shell cross-section.

In the Fig. 4.19 the result for the second material GaAs is presented by the

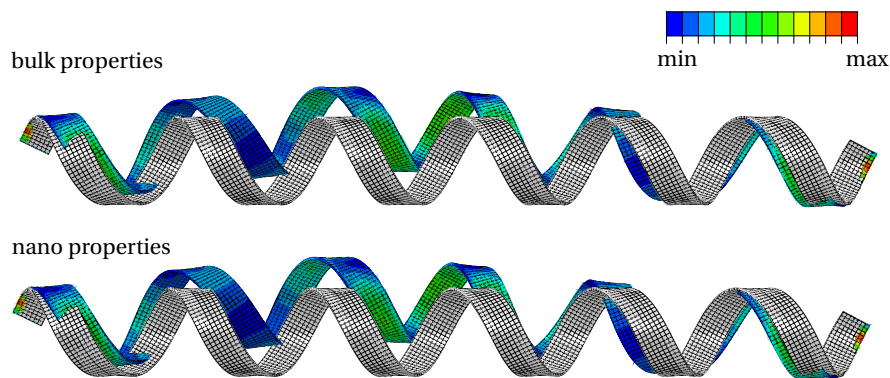


Figure 4.16: Buckling mode, von Mises stress distribution

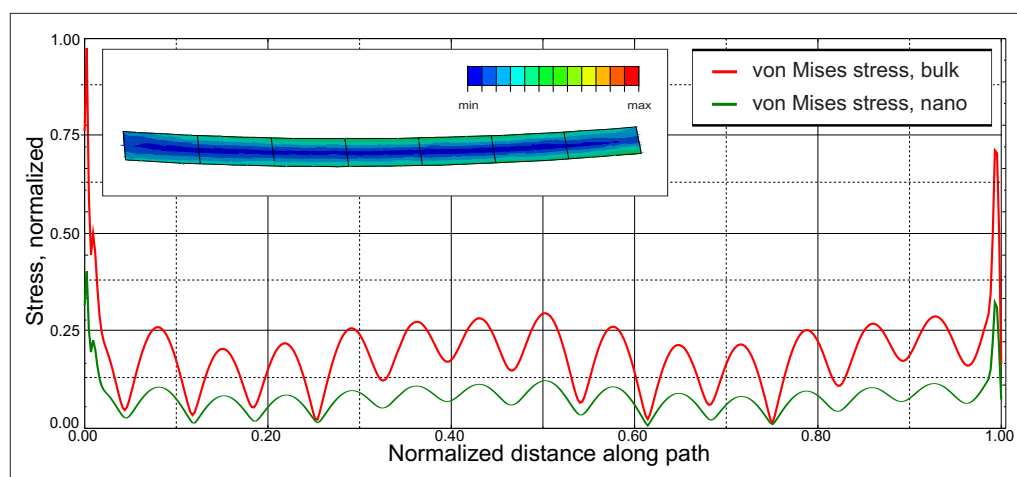


Figure 4.17: Von Mises stress distribution

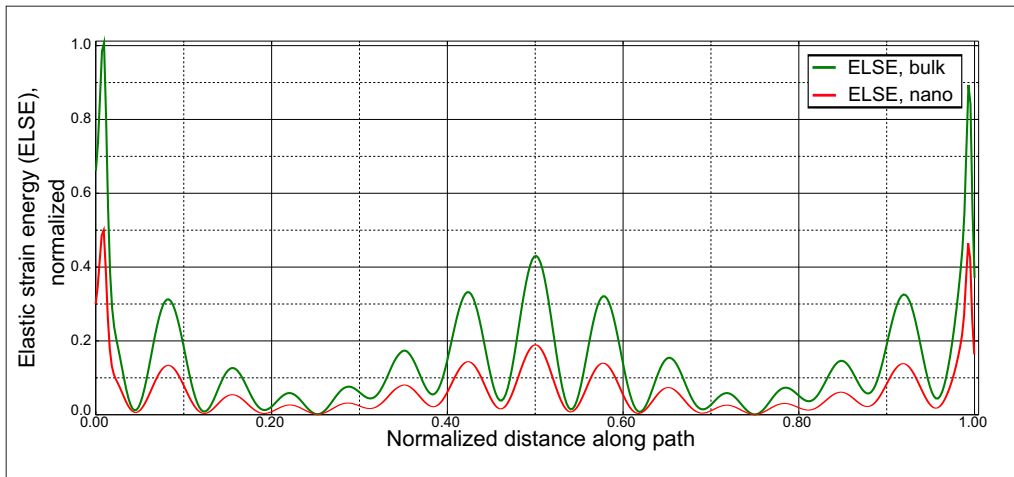


Figure 4.18: Elastic strain energy (ELSE)

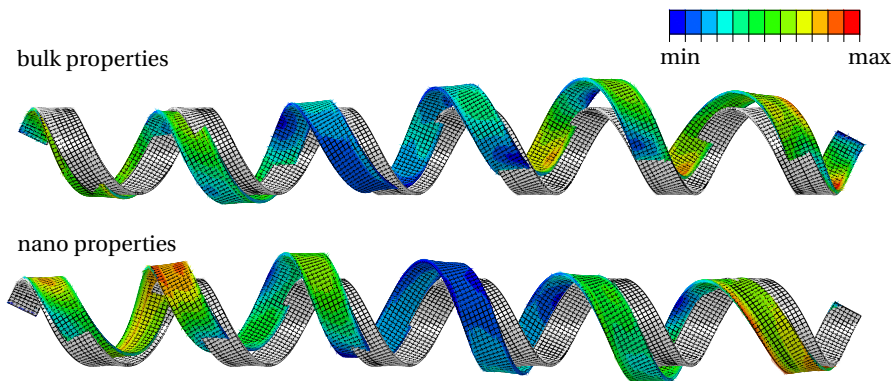


Figure 4.19: Buckling mode, von Mises stress distribution

preservation of all geometric characteristics, modeling scheme, etc. One can see the difference of the resulting buckling modes by influence of the nano-size effect, the intrinsic length scale is calculated as $\ell_{in} = 0.47$. The distribution of the stress variable along the helical path is shown in Fig. 4.20.

In Fig. 4.21 depicted the same situation in the case of the elastic strain energy distribution. In Fig. 4.22 one can see the striking change of the buckling mode with the reversal of the electrical potential gradient sign after recalculation the material parameters in the case of GaAs material of the shell. It does not appear in the case of ZnO consideration. It should be noted that the presented negative eigenvalue in Fig. 4.22 indicates that the structure would buckle if the load is applied in the opposite direction [21].

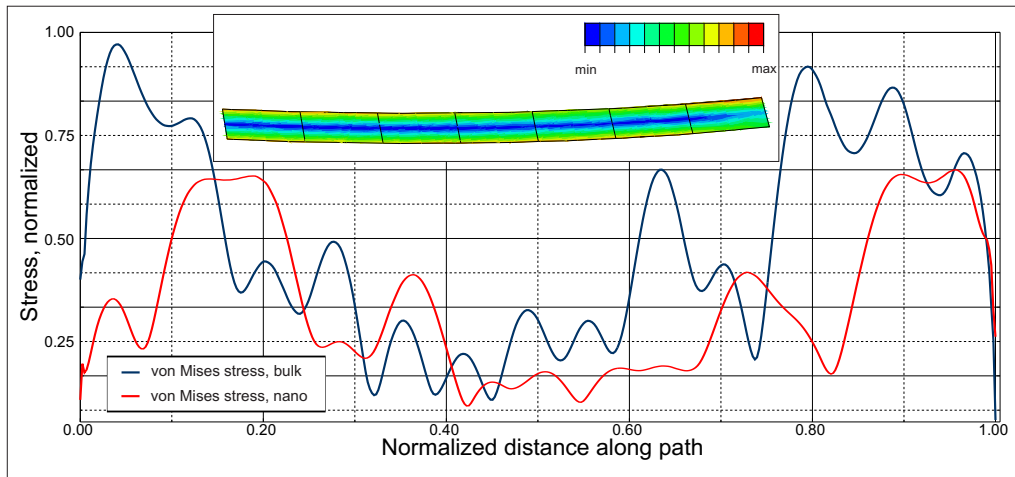


Figure 4.20: Von Mises stress distribution along helical path

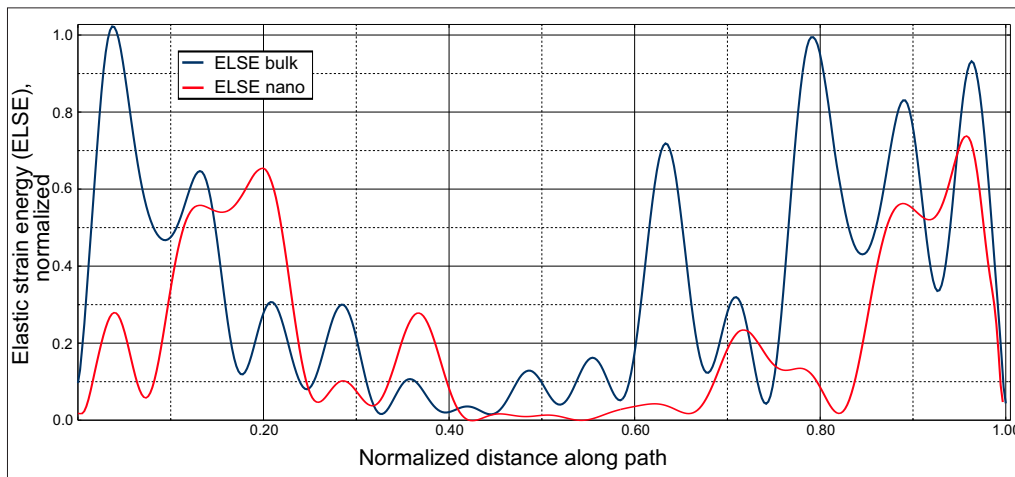


Figure 4.21: Strain energy magnitude (ELSE)

4.3.4 Piezoelectric response of investigated materials

The reasons, which can give such huge influence on the critical modes, are the different piezoelectric moduli distribution of ZnO and GaAs according to the difference in the wurtzite type of the crystal lattice of both materials, Figs. 4.23 – 4.25 and chirality of the geometry [91], which belongs to the specific of the crystalline structure.

The piezoelectric material produces electrical charges when subjected to pressure, and stretches or contracts when an electrical field is applied. The piezoelectric crystals have no center of symmetry, which induces spontaneous polarization. They belong to the 21 non-centrosymmetric classes of

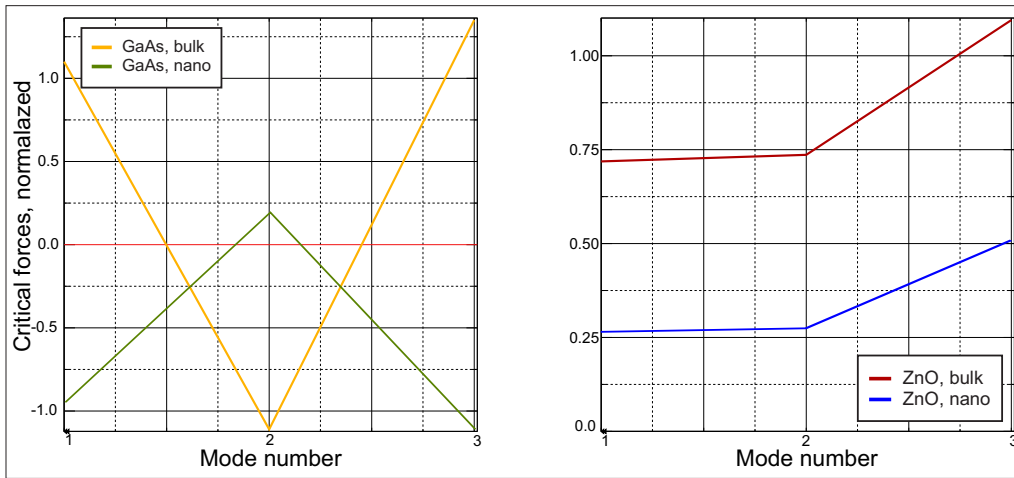


Figure 4.22: Critical forces

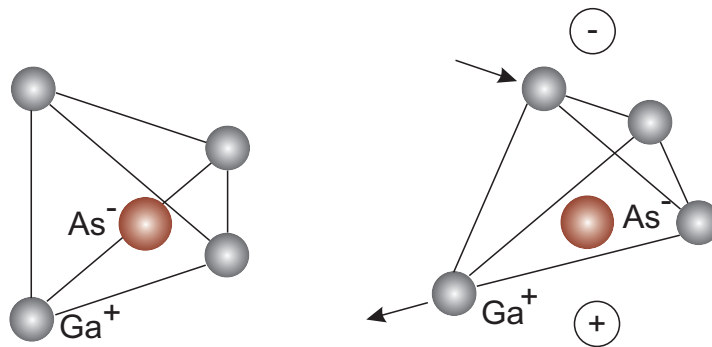


Figure 4.23: Nature of crystal deformations of GaAs

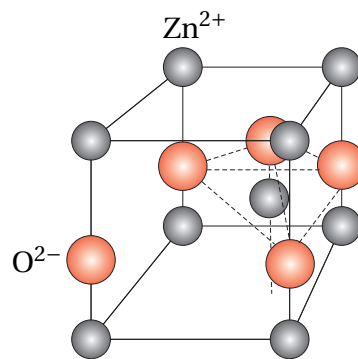


Figure 4.24: Structure of ZnO compound

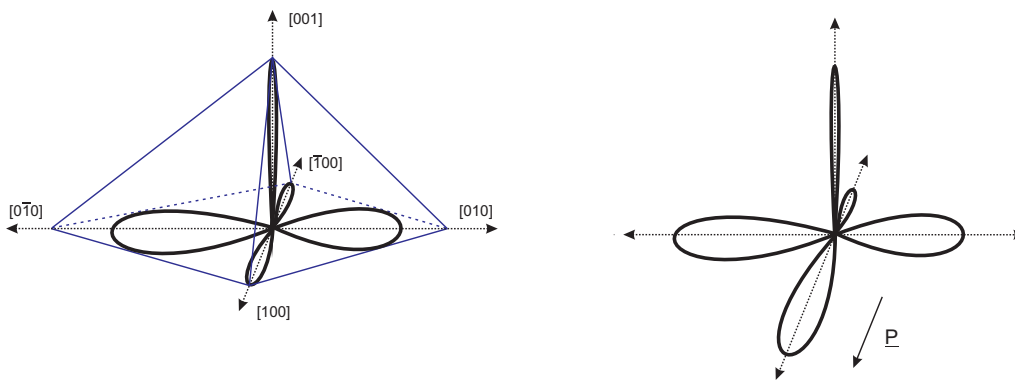


Figure 4.25: Piezoelectric modulus distribution

the 32 crystal classes. As an example in the Hermann-Mauguin notation one has $mm2$, $42m$, etc. [83, 119].

Let us discuss more accurately of piezoelectric deformation of the gallium arsenide. The gallium arsenide (GaAs) is a III/V semiconductor¹⁰. GaAs is an instance of a non-centrosymmetric classes according to piezoelectric constants distribution, see Fig. 4.23. It is the $\bar{4}3m$ and 23 classes by the Hermann - Mauguin notation [119]. This type of symmetry is close to the orthorhombic class 222 , but in the case of a cubic symmetry all of the piezoelectric moduli are equal [119], and it is used in the manufacture of devices such as microwave frequency integrated circuits, monolithic microwave integrated circuits, infrared light-emitting diodes, laser diodes, solar cells and optical windows [40, 60].

The nature of the piezoelectric response of GaAs can be explained by the consideration of the atomic arrangement in the GaAs structure, see Fig. 4.23, see also [120, 121]. Every anion As^- is surrounded by the four cations of Ga^+ . For this atomic arrangement the coordination polyhedron is the regular tetrahedron. Under applied electrical field, the anions move to the centrum of the polyhedron, at the same time move apart the cations of Ga^+ . The lower tetrahedron edge is stretching and the upper edge is shrinking, respectively. All tetrahedrons in the GaAs structure are equal and equally oriented. This is the reason for the general deformations of the crystal as the shrinking deformations without longitudinal strains in the defined direction [56, 73].

The same deformation process is apparent in the crystal ZnO according to the atomic arrangement in the wurtzite type of the crystalline lattice, see Fig. 4.24. Zinc oxide (ZnO) is an important semiconducting and piezoelectric ma-

¹⁰III/V semiconductor is a direct-gap semiconductor, according to the periodic table of elements it belongs to the complex: two-element type $A^{III}B^V$ [99].

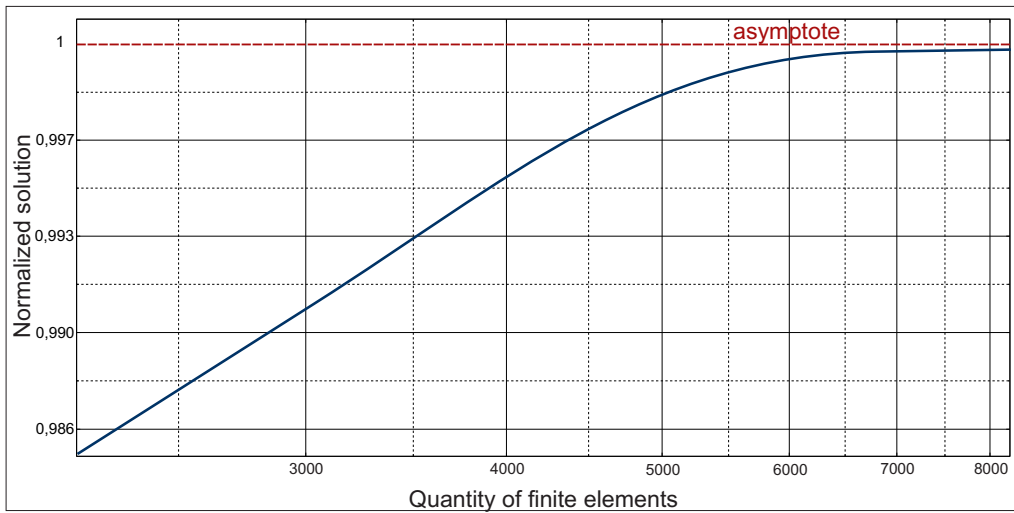


Figure 4.26: The numerical result of some eigenvalue ZnO, first critical mode, bulk properties

material, it has versatile applications in the field of optoelectronics, piezoelectric sensors, transducers and resonators [130]. In general, ZnO is a material that exhibits semiconducting, piezoelectric, and pyroelectric properties. Figure 4.25 shows the distribution of the piezoelectric modulus according to the [100] polarization.

According to the non-standard way of the modeling buckling collapse problems by the inverse piezoelectric effect the question of the numerical stability is very important. However, one can see that the numerical result of some eigenvalue in the case of ZnO material and first critical mode and the bulk properties, approaches the same value asymptotically by the increasing number of finite elements, see Fig. 4.26. It is not necessary to check the solution stability for the other simulations because of using the same modeling scheme.

Let us conclude the principal results and scientific novelty of analysis of piezoelectric helical shell stability with geometrical non-linearity. The critical value of the electric potential is determined, which causes loss of stability of the helicoidal shell. The result can be used in the investigation of the imperfection sensitivity of a nano-structure in MEMS/NEMS.

Investigation of metamaterials with chiral elements

Metamaterials are composite materials with properties, which are dependent on both the physical properties of individual components and the macrostructure [54]. As it is mentioned in Chapter 1, usually the individual components are the reason for the special effective macroscopic behavior of the structure [4, 16, 29, 57]. The investigation of artificial complex materials requires interdisciplinary knowledge and involves various fields of application areas such as development of MEMS/NEMS, solid state physics, optoelectronics, material science, theory of composite structures, nanoscience, etc. [16, 122, 130]. In this case the question of the micro-macro behavior of metamaterials is connected with the prediction of functional properties of such structures [81, 85, 109].

5.1 Problem statement

Below we investigate both the elastic and the electric properties of a chiral material and consider the composite structure made of a polymer matrix and anisotropic inclusions of GaAs taking into account the piezoelectric and dielectric properties of the composite. We estimate the functional properties of the composite. For the determination of functional properties of the artificial composite material we will consider the characteristic unit cell of the composite, see Fig. 5.1. Let us consider the tape helix with a geometry as depicted in Fig. 1.3. The geometry of helixes is defined by following values: layer thickness 7 nm, width of helix belt $0.35 \mu\text{m}$, radius $1.1 \mu\text{m}$, length of helix coils $1.2 \mu\text{m}$, number of coils 5. Unit cell from polymer is the cuboid with the width $3 \mu\text{m}$

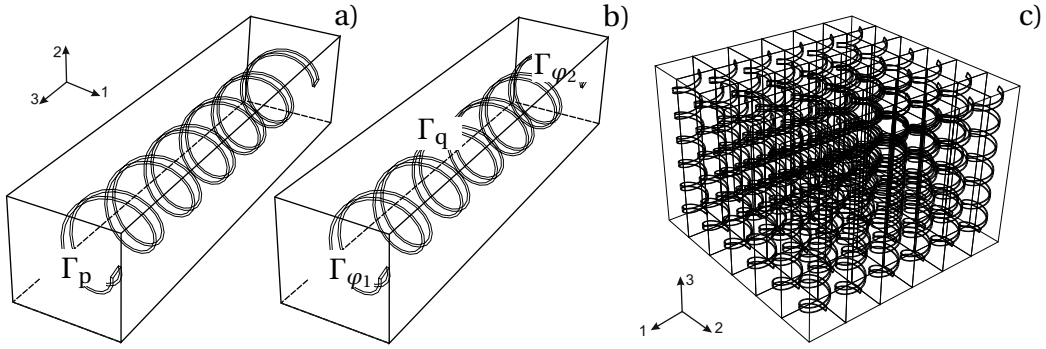


Figure 5.1: Problem statement: a) Boundary conditions for the direct piezoelectric effect; b) Boundary conditions for the inverse piezoelectric effect; c) Assembly of units in the composite material

and length $13 \mu\text{m}$. Both material properties (Table 4.8) and the shape of the studied structure (Fig. 4.12) are the principal information allowing to investigate the resulting buckling behavior.

Within the frame of electroelasticity one can consider the problem statement which requires the solution of the system of equations for the piezoelectric body (see Chapter 2):

1. Equation of motion:

$$\nabla \cdot \boldsymbol{\sigma} = \rho \frac{d^2 \mathbf{u}}{dt^2} \quad (5.1)$$

2. Maxwell's relations for the electric displacement vector and electric field vector, respectively:

$$\nabla \cdot \mathbf{D} = 0 \quad (5.2)$$

$$\mathbf{E} = -\nabla \varphi \quad (5.3)$$

3. Relation for strain tensor in the case of small deformations:

$$\boldsymbol{\varepsilon} = \frac{1}{2} (\nabla \mathbf{u} + \nabla \mathbf{u}^T) \quad (5.4)$$

4. Constitutive equations:

$$\boldsymbol{\sigma} = {}^{(4)}\mathbf{C} \cdot \boldsymbol{\varepsilon} - {}^{(3)}\mathbf{e}^T \cdot \mathbf{E} \quad (5.5)$$

$$\mathbf{D} = \boldsymbol{\varepsilon} \cdot {}^{(3)}\mathbf{e} - \mathbf{d} \cdot \mathbf{E} \quad (5.6)$$

5. Boundary conditions, Fig. 5.1:

$$\mathbf{u}|_{\Gamma_u} = \mathbf{u} \quad (5.7)$$

$$\mathbf{n} \cdot \boldsymbol{\sigma}|_{\Gamma_\sigma} = \mathbf{p} \quad (5.8)$$

$$\varphi|_{\Gamma_\varphi} = \varphi \quad (5.9)$$

$$-\mathbf{n} \cdot \mathbf{D}|_{\Gamma_q} = 0 \quad (5.10)$$

In addition, we take into account that the normal component of the electric flux vector \mathbf{D} is continuous on the matrix-inclusion interface.

We will consider a composite, which consists of a polyimide matrix (PI, see Table 5.1) with a periodic located array of helical shell-like structures with GaAs properties, see Table 5.2. The question of the choice of the alternative matrix material in the metamaterial is connected with the applications and the relative simple and cheap possibilities of synthesis of such structures, see Section 1.2. According to this, for the more precise understanding of the matrix influence on the composite behavior, we will conduct the simulation with an alternative matrix material Al_2O_3 , Table 5.3. The components of the metamaterial have the following properties. The polyimide structure is used because polyimide has particular thermal and mechanical properties [81]. The dielectric properties of such polymer material can be improved by reduction of the values of dielectric parameters [72, 85, 129]. The use of fluorinated polyimides can reduce the relative dielectric parameter value from 3.4 to 2.8. The inclusions in the polymer matrix are piezoelectric helical one-layer structures. The piezoelectric deformations of the inclusion material one can see in Section 4.3. It is obvious that the effect of inclusion deformation under applied electrical field is the reason of the deformation of the composite structure. Hereby, one can see the presence of the direct and inverse piezoelectric effects. This means that one can understand the resulting artificial composite material as a piezoelectric one. The deformation behavior of the composite structure, which is formed from described above materials, differ from the or-

Table 5.1: Properties of the fluorinated polyimide [81]

E [MPa]	ν	ρ_s $\left[\frac{\text{kg}}{\text{m}^3}\right]$	d
$2.30 \cdot 10^4$	0.27	1150	2.8

Table 5.2: Properties of GaAs-inclusions [128]

C_{11} [MPa]	C_{12} [MPa]	C_{44} [MPa]	ρ_s $\left[\frac{\text{kg}}{\text{m}^3}\right]$	e^e $\left[\frac{\text{m}}{\text{V}}\right]$	d
$11.9 \cdot 10^4$	$5.34 \cdot 10^4$	$5.96 \cdot 10^4$	5317	$-2.69 \cdot 10^{-12}$	12.9

Table 5.3: Properties of the matrix Al_2O_3 [128]

E [MPa]	ν	$\rho_s \left[\frac{\text{kg}}{\text{m}^3} \right]$	d
$3.00 \cdot 10^4$	0.20	3950	9.10

dinary electro-elastic systems because the source of stresses is the deformation of the piezoelectric shells.

The problem of the determination of the effective values of the metamaterial requires the application of the homogenization methods [19]. Let us consider this problem with particular features of the symmetry type of the composite material and the influence of the size-effect on the piezoelectric response of the composite.

5.2 Results: Behavior of the chiral material

The composite material can be considered as a local orthotropic composite with a symmetry axis directed tangential to the surfaces of the helices, see Fig. 5.2 a). It is necessary to suppress the unique mirror reflection according to the consideration of the geometry type and arrangement variation of the inclusions 5.2 b). The orthorhombic class of symmetry for the piezoelec-

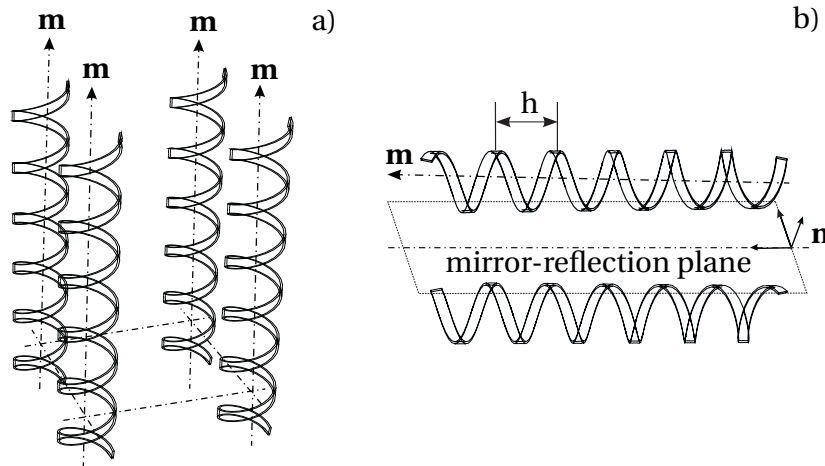


Figure 5.2: Representation of shells in a composite arrangement, \mathbf{m} is orthogonal to the plane of symmetry: a) Lattice arrangement; b) Right/left-hand twist of the helices (\mathbf{n} is the normal vector according to the plane of the mirror reflection)

tric response of the investigated material (class mm2, [100]) will be assumed. Hereby it is necessary to define 7 independent constants, which form the stiffness matrix of the resulting chiral material. For the description of the electric properties one should obtain 5 independent constants of a piezoelectric tensor in the matrix form (2.21) and 3 independent constants of the dielectric matrix (2.23).

Considering Eqs. (5.1)–(5.10) the determination of the functional elastic and electric parameters can be performed as in Table 5.4. Here we accept as nonzero components of the strain tensor and vector of the electrical field only thus which are indicated in Table 5.4. The subtasks with nonzero components of the strain reflect the DPE-analysis and the other tasks are connected with the IPE-problem. It should be noted that the determination of the engineering constants is possible too. The coefficients of the stiffness matrix can be expressed in terms of Young's moduli and Poisson's ratios. Hereby one can retrieve the stiffness matrix by the determination Young's moduli E_i and Poisson's ratios ν_{ij} , $i, j = 1 \div 3$. Then the missing in Table 5.4 coefficients of the stiffness matrix can be calculated by (4.12).

Based on the unit cell analysis with the finite element package Simulia ABAQUS[®], we define the material of the matrix as a piezoelectric material. The material is composed of inclusions and matrix material with zero piezo-

Table 5.4: Determination of the effective properties based on the $[\mathbf{u} - \varphi]$ type relations for the piezoelectric problem. $\langle \cdot \rangle$ denotes the averaged values for each finite element

$\varepsilon_{11} \neq 0$	$C_{11}^{\text{eff}} = \frac{\langle \sigma_{11} \rangle}{\langle \varepsilon_{11} \rangle}$	$e_{11}^{\text{eff}} = \frac{\langle D_1 \rangle}{\langle \varepsilon_{11} \rangle}$
$\varepsilon_{22} \neq 0$	$C_{22}^{\text{eff}} = \frac{\langle \sigma_{22} \rangle}{\langle \varepsilon_{22} \rangle}$	$e_{21}^{\text{eff}} = \frac{\langle D_2 \rangle}{\langle \varepsilon_{22} \rangle}$
$\varepsilon_{33} \neq 0$	$C_{33}^{\text{eff}} = \frac{\langle \sigma_{33} \rangle}{\langle \varepsilon_{33} \rangle}$	$e_{31}^{\text{eff}} = \frac{\langle D_3 \rangle}{\langle \varepsilon_{33} \rangle}$
$\varepsilon_{12} \neq 0$	$C_{44}^{\text{eff}} = \frac{\langle \sigma_{12} \rangle}{\langle \varepsilon_{12} \rangle}$	$e_{42}^{\text{eff}} = \frac{\langle D_2 \rangle}{\langle \varepsilon_{12} \rangle}$
$\varepsilon_{13} \neq 0$	$C_{55}^{\text{eff}} = \frac{\langle \sigma_{13} \rangle}{\langle \varepsilon_{13} \rangle}$	$e_{53}^{\text{eff}} = \frac{\langle D_3 \rangle}{\langle \varepsilon_{13} \rangle}$
$E_1 \neq 0$		$d_{13}^{\text{eff}} = \frac{\langle D_3 \rangle}{\langle E_1 \rangle}$
$E_2 \neq 0$		$d_{22}^{\text{eff}} = \frac{\langle D_2 \rangle}{\langle E_2 \rangle}$
$E_3 \neq 0$		$d_{33}^{\text{eff}} = \frac{\langle D_1 \rangle}{\langle E_3 \rangle}$

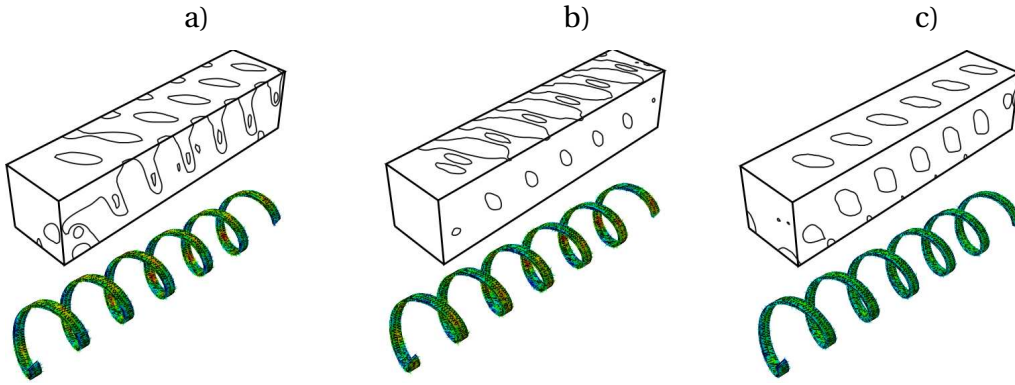


Figure 5.3: Direct piezoelectric effect: a) Determination of e_{11}^{eff} and C_{11}^{eff} by non zero ε_{11} component; b) Determination of e_{12}^{eff} and C_{22}^{eff} by non zero ε_{22} component; c) Determination of e_{13}^{eff} and C_{33}^{eff} by non zero ε_{33} component

electric properties. Only in this case we can use finite elements having electric degrees of freedom. Introducing both displacement and electrical potential as nodal variables it possible to discuss all required types of boundary conditions for the matrix and on the interface region of different materials, see Fig. 5.1 b). It should be noted that matrix and inclusions are meshed with the same type of finite elements as a 4-node linear piezoelectric tetrahedron, see Fig. 5.3.

For the definition of all functional moduli, which describe the material behavior of a chiral material, it is necessary to implement 6 tests with mechanical boundary conditions and 3 tasks for the inverse piezoelectric effect, see Fig. 5.3. By the implementations of the described above tests for the direct and inverse piezoelectric effect are estimated the material properties of the composite material. The coefficients of the stiffness matrix in the case of transversal anisotropy:

$$\begin{aligned} C_{11} &= 2.318 \cdot 10^4 \text{MPa}, & C_{12} &= 0.937 \cdot 10^4 \text{MPa}, & C_{13} &= 1.169 \cdot 10^4 \text{MPa}, \\ C_{22} &= 2.286 \cdot 10^4 \text{MPa}, & C_{23} &= 1.172 \cdot 10^4 \text{MPa}, & C_{33} &= 2.284 \cdot 10^4 \text{MPa}, \\ C_{44} &= 0.901 \cdot 10^4 \text{MPa}, & C_{55} &= 0.900 \cdot 10^4 \text{MPa}, & C_{66} &= 0.900 \cdot 10^4 \text{MPa} \end{aligned}$$

The obtained piezoelectric coefficients and dielectric constants are following:

$$\begin{aligned} e_{11} &= 2.54 \cdot 10^{-10} \frac{\text{m}}{\text{V}}, & e_{12} &= -7.82 \cdot 10^{-9} \frac{\text{m}}{\text{V}}, & e_{13} &= -1.84 \cdot 10^{-10} \frac{\text{m}}{\text{V}}, \\ e_{24} &= -3.06 \cdot 10^{-9} \frac{\text{m}}{\text{V}}, & e_{35} &= -7.22 \cdot 10^{-12} \frac{\text{m}}{\text{V}}, \\ d_{11} &= 2.8, & d_{22} &= 2.8, & d_{33} &= 2.79 \end{aligned}$$

All other coefficients are equal to zero. It should be noted that the consideration of engineering constants is more usable for the description of the elastic

behavior of the material. However, the engineering constants for the structure polyimide/GaAs one can see in the Table 5.5. For understanding the material choice influence we perform the same simulation with a more harder matrix and the same material of the inclusions. The averaged functional properties for a matrix of Al_2O_3 and GaAs-inclusions one can see in Table 5.6. They are based on the initial properties for the matrix Al_2O_3 indicated in Table 5.3. In both cases of the polymeric matrix and the matrix of Al_2O_3 , which is more stiff than the polymer one, the same anisotropy type is observed. Table 5.6 shows the similar behavior of the material to the results in the case with polyimide. However, the elastic properties of the source matrix give an influence on the resulting elastic response. This influence is significant in the plane of symmetry direction of the inclusions, see Fig. 5.2 a).

Let us consider the model of the chiral material with the left-hand twist of the inclusions. It should be noted that the inclusion volume fraction is not changed and the model is completely the same as it is described above for the polyamide/GaAs components. By the consideration of the result elastic properties, piezoelectric coefficients and relative dielectric parameters, presented below, one can make conclusions about the differences of the behavior of the chiral material with the right/left-hand twists of the helices. The matrix components are now:

$$\begin{aligned}
 C_{11} &= 2.30 \cdot 10^4 \text{MPa}, & C_{12} &= 1.18 \cdot 10^4 \text{MPa}, & C_{13} &= 0.971 \cdot 10^4 \text{MPa}, \\
 C_{22} &= 2.29 \cdot 10^4 \text{MPa}, & C_{23} &= 0.965 \cdot 10^4 \text{MPa}, & C_{33} &= 2.30 \cdot 10^4 \text{MPa}, \\
 C_{44} &= 0.907 \cdot 10^4 \text{MPa}, & C_{55} &= 0.907 \cdot 10^4 \text{MPa}, & C_{66} &= 0.906 \cdot 10^4 \text{MPa} \\
 e_{11} &= -6.26 \cdot 10^{-10} \frac{\text{m}}{\text{V}}, & e_{12} &= -6.82 \cdot 10^{-11} \frac{\text{m}}{\text{V}}, & e_{13} &= -4.04 \cdot 10^{-10} \frac{\text{m}}{\text{V}}, \\
 e_{24} &= -2.67 \cdot 10^{-11} \frac{\text{m}}{\text{V}}, & e_{35} &= -1.59 \cdot 10^{-10} \frac{\text{m}}{\text{V}}, & &
 \end{aligned}$$

Table 5.5: Engineering constants for polyimide/GaAs composite

E_1	$2.318 \cdot 10^4 \text{MPa}$	ν_{12}	0.264	ν_{21}	0.268
E_2	$2.286 \cdot 10^4 \text{MPa}$	ν_{23}	0.265	ν_{32}	0.265
E_3	$2.284 \cdot 10^4 \text{MPa}$	ν_{13}	0.259	ν_{31}	0.262

Table 5.6: Engineering constants for tAl_2O_3 /GaAs composite

E_1	$2.395 \cdot 10^4 \text{MPa}$	ν_{12}	0.126	ν_{21}	0.127
E_2	$2.388 \cdot 10^4 \text{MPa}$	ν_{23}	0.285	ν_{32}	0.456
E_3	$1.491 \cdot 10^4 \text{MPa}$	ν_{13}	0.283	ν_{31}	0.454

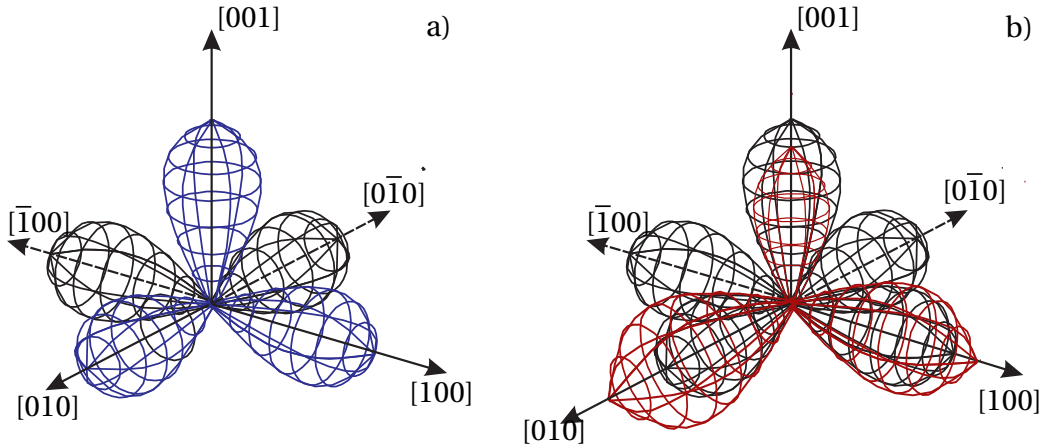


Figure 5.4: Schematic representation of the twist influence of the inclusions on the polarization vector according to the piezoelectric modulus distribution: a) Right-hand twist of the chiral elements; b) Left-hand twist of the chiral elements

$$d_{11} = 2.80, d_{22} = 2.80, d_{33} = 2.82$$

One can see that the elastic behavior of the material is not strongly changed as well as the dielectric properties. The dielectric properties as first case present the isotropic behavior. One can see that the twisting changing of the inclusions does not reflect a considerable change of the symmetry of the composite according to the elastic properties. All isotropic properties are preserved. But the twist type of the piezoelectric helices can reflect the difference in the polarization of the resulting material, particularly one can have a scaling of the polarization vector \mathbf{P} . Figure 5.4 schematically presents the polarization change of the piezoelectric material according to the piezoelectric moduli distribution for the orthotropic class of material symmetry. One can see by consideration of the piezoelectric constants matrix that the following equation for the polarization vector is valid:

$$\mathbf{P} = \boldsymbol{\sigma} \cdot \mathbf{e}$$

The question about the size effect influence, stated in Section 4.3, requires to take into account some size-dependence for the nano-structured composites. Let us consider the influence of the size effect by the transition from the macrolevel to the microlevel of the material description. The surface characteristics represent the microlevel and bulk properties describe the macroresponse [77, 78]. We confirm again that the scaling law (4.51) gives us the relations between the nano and bulk material properties [20, 25]. We use the

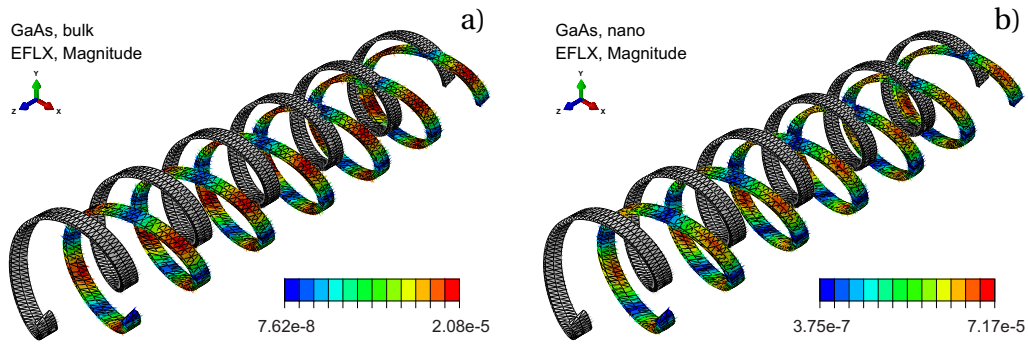


Figure 5.5: Distribution of the electrical flux vector magnitude with the deformation of the shell-inclusion under applied electrical potential

same intrinsic length scale (4.52) calculated for the GaAs-material according to the experimental data from the literature [40, 73, 121]. This intrinsic length scale can be used for the recalculations of all material properties by the initial bulk properties with the help of the scaling law (4.51). Note that in the general case the intrinsic length scale and the scaling law are not proper in the same manner to describe all functional properties. But in our case we assume the linear dependence between elastic and electric material parameters. According to the constitutive equations (6.5)–(6.6) the recalculation scheme can be simplified. So we can apply for both the elastic and electric properties the same intrinsic length scale (4.52) and scaling law in form (4.51). In the described above nano-structured composite only inclusions have a size beyond the macrolevel (thickness of the shell layer). This requires the recalculation only of the material parameters for the inclusions [77, 78]. For the polymer matrix is not necessary to take into account the size-effect.

Let us consider some averaging results of the functional properties in the case of the left-hand twist of the helical inclusions embedded in the polymer matrix with taking into account the size effect for the inclusions basic material. Figure 5.5 shows the deformations of the interior inclusions under the influence of the electric potential. This test belongs to the inverse piezoelectric effect and denotes the similar deformations of the shell with the proportional change of all resulting variables. In the Fig. 5.5 the distribution of the electrical flux vector magnitude is presented. By finite element triangulation (general quantity of elements in the model is 137738) the finite element mesh of matrix with the element type C3D4E is used, the same type of element is applied for meshing the inclusions [21]. The parameters of the stiffness matrix, the piezoelectric coefficients and the dielectric constants are computed

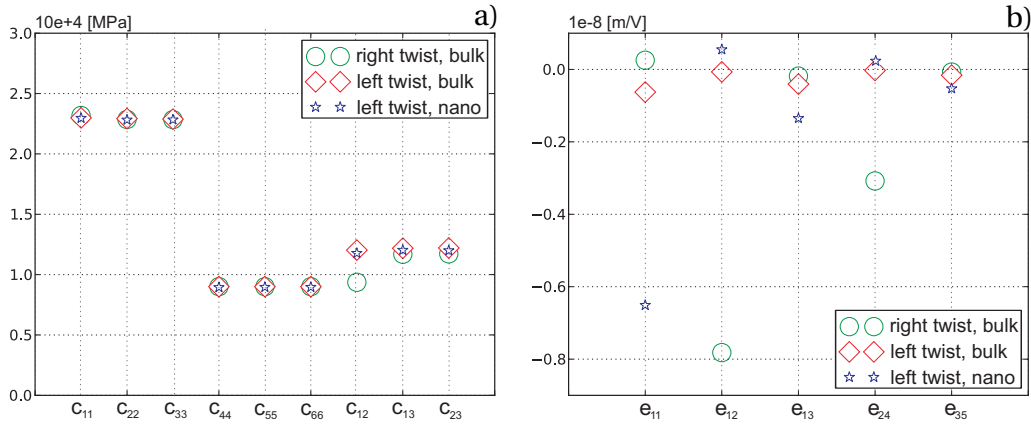


Figure 5.6: Comparison of the obtained results by change of the input characteristics: a) Coefficients of the stiffness matrix; b) Coefficients of the matrix of the piezoelectric moduli

considering the influence of the size effect:

$$\begin{aligned}
 C_{11} &= 2.30 \cdot 10^4 \text{MPa}, & C_{12} &= 1.178 \cdot 10^4 \text{MPa}, & C_{13} &= 1.204 \cdot 10^4 \text{MPa}, \\
 C_{22} &= 2.29 \cdot 10^4 \text{MPa}, & C_{23} &= 1.20 \cdot 10^4 \text{MPa}, & C_{33} &= 2.30 \cdot 10^4 \text{MPa}, \\
 C_{44} &= 0.895 \cdot 10^4 \text{MPa}, & C_{55} &= 0.896 \cdot 10^4 \text{MPa}, & C_{66} &= 0.897 \cdot 10^4 \text{MPa} \\
 e_{11} &= -6.51 \cdot 10^{-10} \frac{\text{m}}{\text{V}}, & e_{12} &= 5.49 \cdot 10^{-11} \frac{\text{m}}{\text{V}}, & e_{13} &= -1.35 \cdot 10^{-10} \frac{\text{m}}{\text{V}}, \\
 e_{24} &= 2.15 \cdot 10^{-11} \frac{\text{m}}{\text{V}}, & e_{35} &= -5.28 \cdot 10^{-11} \frac{\text{m}}{\text{V}}, \\
 d_{11} &= 2.80, & d_{22} &= 2.80, & d_{33} &= 2.80
 \end{aligned}$$

As in the case of the twisting change, the size effect has not given the particular changes according to the permittivity matrix, the isotropic behavior and the values of the dielectric properties are the same. As stated above, the influence of the application of the size law to the recalculation of the elastic properties is significant only by the consideration of the tangential stresses, Fig. 5.6 a). The reason is the packing arrangement of the thin-walled shell in the isotropic matrix according to the concentration of the inclusions material. Figures 5.7 and 5.8 denote some particular results of the analysis of the inverse and direct piezoelectric effect, according to Table 5.4. It should be noted that the values are considered along the full loft of the upper surface of the chiral shell. This is the more characteristic helical path and more accurately describes the influence of the chiral geometry on the distribution of the desired quantities.

Based on the supposition about the orthorhombic class of properties symmetry in the case of the piezoelectric modulus one can see that the polarization of the composite is changed by the the nano-size effect influence,

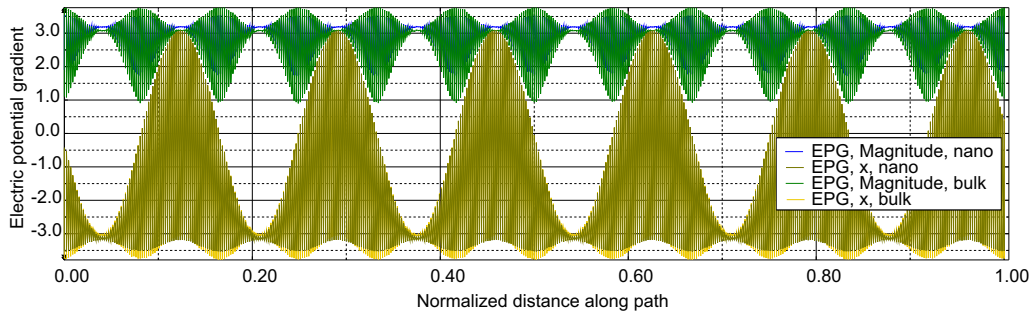


Figure 5.7: Distribution of the electrical flux vector along typical helical trajectory (inverse piezoelectric effect)

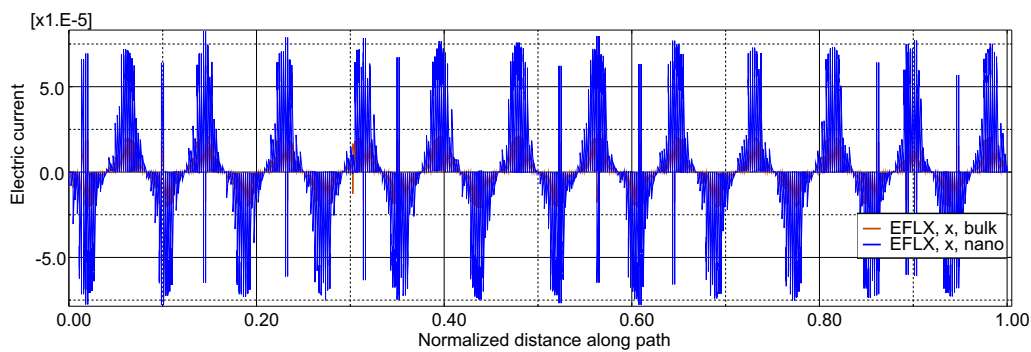


Figure 5.8: Distribution of the electrical potential gradient vector along typical helical trajectory by the direct piezoelectric effect

Fig. 5.6 b). Figure 5.9 schematic demonstrates the polarization change of the piezoelectric material. Particularly, the polarization vector is scaled in two directions, in the third direction the reflection and scaling of the third component is obvious. Hereby, the pyramid, described the piezoelectric modulus distribution, is rotated around one axis about angle of 180 degrees and stretched in all directions as the result of the size-effect influence. This is the principal result because it makes possible to construct the polarization of the artificial chiral materials and govern of the piezoelectric response of the composite.

Let us conclude the results of described above simulation. The finite element simulation of the chiral composite unit cell is implemented and the difference of the chiral material behavior results by variation of the functional properties of the basic components and the twisting of the helical inclusions is noted. The presence of the anisotropy according to mechanical and electrical behavior in the composite is established. The twisting of the helixes reflects the considerable changes only in case of piezoelectric properties of the ma-

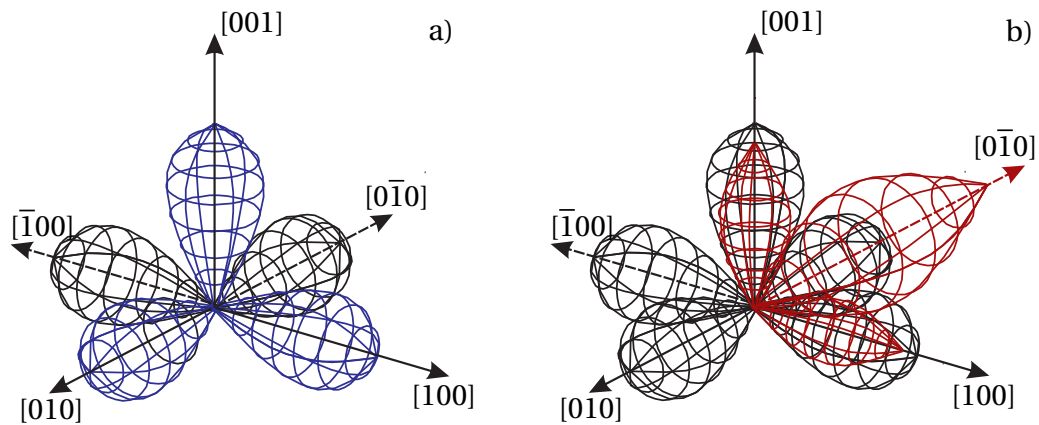


Figure 5.9: Schematic representation of the size-effect influence on the polarization vector according to the piezoelectric moduli distribution, see Figs. 5.6 a, b: a) By the consideration of the bulk properties of the inclusion material; b) By the taking into account size-effect for the inclusion material

terial. The size-effect by the investigation of the material properties makes the important amendment in the result behavior of the nano-structured composite, especially by the consideration of the electrical response of the material. By consideration of packing variations of the helical inclusions one can have the supposition that the geometry of the helical inclusions as the shell width, packing density, quantity of the spiral turns, etc. have a significant influence on electrical properties averaging. As an example, by the increasing helix length or quantity of the spiral turns (in the case of polarization described above) one can receive more evident piezoelectric effect in a chiral material, but the increasing only shell width not improves the piezoelectric characteristics of the composite structure. It is obviously that the questions of the shape optimization for this structures are more complicated and should be considered according to the optimization problem [85]. The results of this work can be used for the designing of a metamaterial structure with the chiral properties and for the prediction of its mechanical and electrical response.

Crystal/fiber arrays on multilayer substrates

Arrays of micro- and nanofibers or tubes made of semiconductors or piezoelectric materials belong to the perspective structures microelectronics. They are studied intensively, see e.g. [49, 98]. The investigation of nanofiber/nanorod arrays on substrates should be based on the consideration of the synthesis processes of nanostructures [49, 59, 98, 129]. The number of nanocrystals on substrates is usually high, see Fig. 6.1. Hereby, one can consider these structures as an anisotropic continuum with effective (homogenized) properties [1]. The estimation of the effective properties is obviously interesting, because it makes possible a prediction of the particular behavior of the nano-crystals arrays working in microelectronics and nanophotonics devices at various conditions.

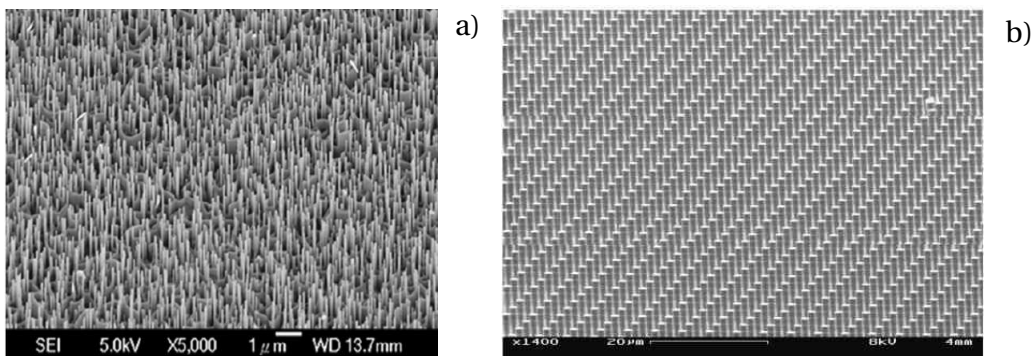


Figure 6.1: Example of the quasi-periodic array of crystals/fibers: a) Self-grown system of ZnO crystals [124]; b) Nanocrystals created by the stamp process [92]

6.1 Problem statement

Let us consider an array of nanocrystals on a multilayer substrate with a geometry and material components as depicted in Fig. 6.2. Within the frame of electroelasticity one can formulate the problem statement which requires the solution of the system of equations for a piezoelectric body. However, let us consider the basic equations for electro-elastic bodies with the tessellated boundary to subregions for the application of boundary conditions (Fig. 6.2).

1. Equation of motion:

$$\nabla \cdot \boldsymbol{\sigma} = \rho \frac{d^2 \mathbf{u}}{dt^2} \quad (6.1)$$

2. Maxwell's relations for the electric displacement vector and electric field vector, respectively:

$$\nabla \cdot \mathbf{D} = 0 \quad (6.2)$$

$$\mathbf{E} = -\nabla \varphi \quad (6.3)$$

3. Relation for strain tensor in case of small deformations:

$$\boldsymbol{\varepsilon} = \frac{1}{2} (\nabla \mathbf{u} + \nabla \mathbf{u}^T) \quad (6.4)$$

4. Constitutive equations:

$$\boldsymbol{\sigma} = {}^{(4)}\mathbf{C} \cdot \boldsymbol{\varepsilon} - {}^{(3)}\mathbf{e}^T \cdot \mathbf{E} \quad (6.5)$$

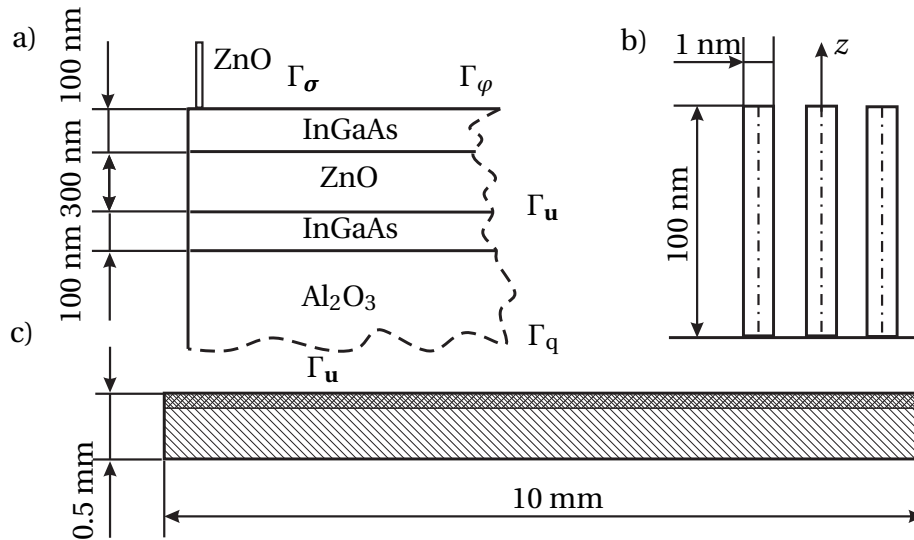


Figure 6.2: Example of the standard model of crystals/fibers: a) Distribution of material properties of the structures with the approximate size of layers; b) Approximate size of nanocrystals/nanorods; c) Macroview of crystal/rod/fiber arrays on substrates

Table 6.1: Properties of the layer made of $\text{In}_{0.14}\text{Ga}_{0.86}\text{As}$ [128]

E [MPa]	ν	ρ_s $\left[\frac{\text{kg}}{\text{m}^3}\right]$
$8.06 \cdot 10^4$	0.32	5500

$$\mathbf{D} = \boldsymbol{\varepsilon} \cdot \cdot^{(3)} \mathbf{e} - \mathbf{d} \cdot \mathbf{E} \quad (6.6)$$

5. Boundary conditions (Fig. 6.2):

$$\mathbf{u}|_{\Gamma_u} = \mathbf{u}_0 \quad (6.7)$$

$$\mathbf{n} \cdot \boldsymbol{\sigma}|_{\Gamma_\sigma} = \mathbf{p} \quad (6.8)$$

$$\varphi|_{\Gamma_\varphi} = \varphi_0 \quad (6.9)$$

$$-\mathbf{n} \cdot \mathbf{D}|_{\Gamma_q} = 0 \quad (6.10)$$

We will investigate ZnO nanocrystals on the substrate ZnO/InGaAs/Al₂O₃ with the properties of each component indicated in Tables 4.11, 5.3 and 6.1. It should be noted that usually Al₂O₃ is used as an absorbent and catalyst for the processes of nanocrystal growing [98]. As is mentioned above for nanocrystal/fiber arrays the density of elements on the substrate can be large in the case of identical dimensions and constant mechanical and electrical properties [129]. This allows us to consider a model based on the continuous distribution of nanoobjects [26, 98]. However, the simulation of the real structure, where the number of crystals on the substrate can reach 10¹⁵, is connected with large computational costs. Thus by the creation such model it is rational to simulate the nanocrystal array by a continuous layer with averaged material parameters. Let us discuss the possibilities of analytical averaging of the functional properties taking into account the specificity of the crystal arrangement.

6.1.1 Case of quasi-periodic array of nanocrystals

Let us consider a periodic array of nanocrystals (Fig. 6.1). We introduce instead of the model of the real structure a simplified model: a unidirectional fibre composite, which consists of some matrix and a regular array of piezoelectric crystal inclusions. The interior between the fibers is modeled as inclusions consist of air. For averaging of the nanocrystal array we will use the methods of the classical theory of fibre-reinforced composites [19, 55]. According to these methods on the border of a partition between crystal/fiber

and the interior of the fiber we accept the conditions of ideal contact. This means that the continuity for the displacements, stresses, potentials and currents is fulfilled.

Let us select the representative element of a nanoarray structure with the volume V and the N number of the inclusions. This representative volume is the element of structure, in which all averaged components of stress and strain tensors are equal according to the respective values in the whole array. In the case of the applied uniform stress field or strain field one can present the averaged stress and strain by the volume element:

$$\langle \sigma_{ij} \rangle = \frac{1}{V} \int_V \sigma_{ij}(x_i) dv, \quad \langle \varepsilon_{ij} \rangle = \frac{1}{V} \int_V \varepsilon_{ij}(x_i) dv \quad (6.11)$$

$$\sigma = \frac{1}{V} \int_{V - \sum_{n=1}^N V_N} \sigma_{ij} dv + \frac{1}{V} \sum_{n=1}^N \int_{V_N} \sigma_{ij}(x_i) dv \quad (6.12)$$

$$\langle \sigma_{ij} \rangle = C_{ijkl} \langle \varepsilon_{kl} \rangle \quad (6.13)$$

Here the analytical expressions for the stress and strains are not presented, because their representation is possible only in the cases of a special geometry with absolute periodicity of the components in the investigated structure (Fig. 6.1). The main part of the determination of the functional properties is the estimation of material characteristics by obtaining of the "upper" and "lower" limits of the possible variation of the functional properties. Such an estimation of the effective moduli first was suggested by Hashin and Rosen [55].

The averaged layer of the ZnO crystals can be considered as a transversely isotropic material. For the description of mechanical properties one should determine 5 independent parameters. Let us introduce the axis z as the axis of isotropy. This axis is perpendicular to symmetry plane, see Fig. 6.2. One can consider the following relations between the engineering constants and the components of the stiffness matrix \mathbf{C} [19]:

$$\begin{aligned} C_{11} &= C_{22} = E_1(1 - \nu_{13}\nu_{32})K_{23} \\ C_{12} &= E_1(\nu_{13}\nu_{32} + \nu_{12})K_{23} \\ C_{13} &= C_{23} = E_1(\nu_{12}\nu_{32} + \nu_{32})K_{23} \\ C_{33} &= E_3(1 - \nu_{12}^2)K_{23} \\ C_{44} &= C_{55} = \mu_{23}, \quad C_{66} = \mu_{12} \end{aligned} \quad (6.14)$$

where E_i is the modulus of elasticity along the axis i , ν_{ij} is the Poisson's ratio corresponding to the contraction in the direction j if the stress is applied in



Figure 6.3: Suggested models: a) and b) Polydisperse model with cylindrical inclusions; c) Three-phase model with cylindrical inclusions

direction i , K_{23} is the bulk modulus by plane strain state in the plane 23, μ_{ij} is the shear modulus related to the material response in the ij -plane.

For the determination of the unknown constants we consider the polydisperse model with cylindrical inclusions [55], Figs. 6.3 a) and b). According to this model we can obtain 4 unknown engineering parameters. The last one, the shear modulus in the isotropy plane, can be obtained by the three-phase model with cylindrical inclusions, see Fig. 6.3 c) [19].

If we solve the boundary value problem (6.1)–(6.10) with the stress boundary condition (6.8) and applying the theorem of minimum of potential energy one can obtain the stress state in the volume element. Thereby, the calculated energy for this stress state is an upper bound of the unknown stress state. Then the modulus E^l is the lower bound of the unknown modulus. By analogy we can estimate E^u , which is the upper bound. Similarly, if we will observe the displacement field for one compound cylinder, the boundary condition in displacements is (6.7), and one can obtain that the result of integration is the upper value E^u . Using the estimate $E^l \leq E \leq E^u$ we obtain the approximate values [19]:

$$E_3 = cE_F + (1-c)E_{3M} + \frac{4c(1-c)(\nu_F - \nu_{32M})^2 \mu_{32M}}{\frac{(1-c)\mu_{32M}}{K_M + 1/3\mu_{32M}} + \frac{c\mu_{32M}}{k_F + 1/3\mu_{32M}} + 1} \quad (6.15)$$

$$\nu_{32} = (1-c)\nu_{32M} + c\nu_F + \frac{c(1-c)(\nu_F - \nu_{32M}) \left[\frac{\mu_{32M}}{k_M + 1/3\mu_F} - \frac{\mu_{32M}}{k_F + 1/3\mu_F} \right]}{(1-c) \frac{\mu_F}{k_F + 1/3\mu_F} + \frac{\mu_{32M}}{k_M + 1/3\mu_{32M}} + 1} \quad (6.16)$$

$$K_{23} = k_M + 1/3\mu_{32M} + c \left[k_F - k_M + 1/3(\mu_F - \mu_{32M}) + \frac{1-c}{k_M + 4/3\mu_{32M}} \right] \quad (6.17)$$

$$\mu_{32} = \mu_{32M} \left[\frac{\mu_F(1+c) + \mu_{32M}(1-c)}{\mu_F(1-c) + \mu_{32M}(1+c)} \right] \quad (6.18)$$

$$\mu_{12} = 1 + \frac{c}{\frac{\mu_{12M}}{\mu_F - \mu_{12M}} + \frac{k_F + 7/3\mu_{12M}}{2k_F + 8/3\mu_{12M}}} \quad (6.19)$$

where the index M denotes the matrix, the index F denotes the inclusion,

$$c = \left(\frac{a_i}{b_i} \right)^2 = \text{const}, \quad \forall i \in N$$

is the volume concentration of inclusions, a_i and b_i are the radius of an inclusion and an inclusion hull, respectively.

The expressions (6.15)–(6.19) are sufficient to describe the transversely isotropic material. For the remaining parameters one should estimate by standard relations according to the basis vector \mathbf{e}_3 , which is perpendicular to the symmetry plane:

$$\frac{\nu_{31}}{E_3} = \frac{\nu_{32}}{E_3} = \frac{\nu_{13}}{E_1} = \frac{\nu_{23}}{E_2}$$

ν_{23} can be determined by analogy to ν_{32} , see Eq. (6.16). In addition, we have

$$\nu_{12} = \frac{E_1}{2\mu_{12}} - 1$$

Thereby, one can recalculate the elastic properties of the averaged layer of the tubes/fibers on the substrate [19, 55].

6.1.2 Stochastic array of nanocrystals

The assumption about the regularity of the crystal array does not reflect the specificities of the various crystal/fiber structures. One possible way to overcome the estimation scatter is to apply the principles of fractal analysis and the multifractal formalism, because the theory of elastic/fractal properties is an example of the macroscopic description of a scale invariant irregular structure [82]. In the considered structures of stochastic crystal/fiber arrays on the substrate the array components and the internal environment have enough topology and fractal properties to consider them as fractal objects, Fig. 6.4. The analysis of an array structure shows us the following items:

- the structure formation is the result of a self-organized growth;
- the structures are self-similar and hierarchic, which means that the large crystal agglomerates are formed from the individual components as the fractal agglomerates should be formed from the small fractal elements.

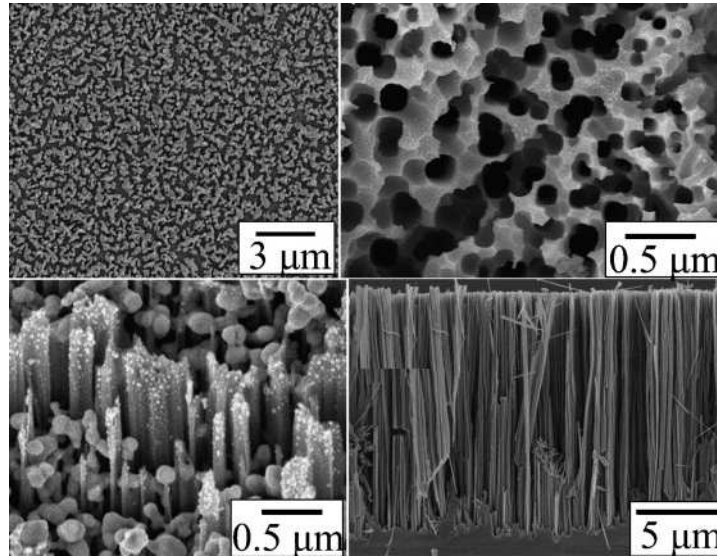


Figure 6.4: Example of SEM images of silver nanoclusters [59, 104]

Thereby, one can consider a model of a crystal/fiber array as a solid-state fractal structure. For the problem description of the material properties estimation in the case of solid-fractal structure taking into account the piezoelectric characteristics of nanocrystals we use the expansion of the Euclidean space E^3 topology with the dimension d to the Hausdorff space X with the unknown dimension D . Because the agglomerate characterization the Euclidean geometry cannot be used to describe the complex shapes of many ambient crystals.

The fractal dimension is the principal characteristics of the fractal structures. This value can be defined by the following expression:

$$n = \left(\frac{R}{a}\right)^D \quad (6.20)$$

where n is the number of fractal elements in the fractal aggregate, R is the rate of the aggregate, a is the rate of the fractal element in the aggregate. It is necessary to consider the definition of the fractal Hausdorff-Besikovitch dimensionality¹:

Let us accept the fractal set consisted of the enumerable aggregates $\cup A_i, i = 1 \div k$, Fig. 6.6, then

$$\begin{aligned} \forall A_i : \text{diam}(A_i) < \delta, \forall \delta > 0, \forall i \in N \Rightarrow \exists m^p = \sup_{\delta} \inf_i \sum_i \text{diam}(A_i)^p \\ \Rightarrow D := \sup_{m^p > 0} p \end{aligned} \quad (6.21)$$

¹The Hausdorff-Besicovitch dimension is an extended non-negative real number associated with any metric space. The Hausdorff dimension generalizes the notion of the dimension of a real vector space [10].

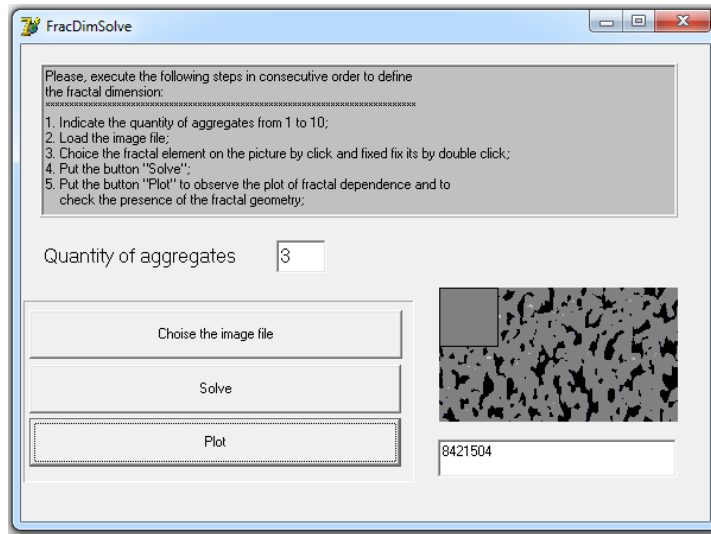


Figure 6.5: Fractal Dimension Solver

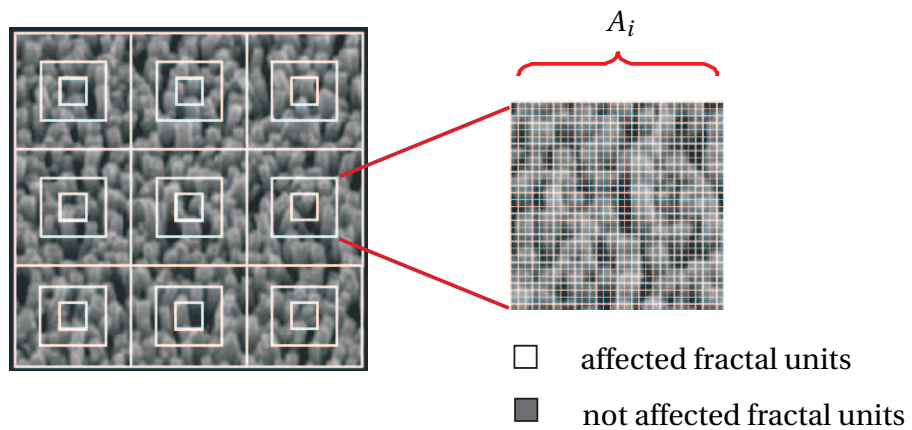


Figure 6.6: Determination of the fractal dimension by the method of nested squares with decomposition of the fractal system on the fractal aggregates (A_i) and determination of the fractal dimension of the one fractal aggregate with the k_i squares and k'_i squares with the fractal element

$D = \sup_{m^p > 0} p$ is called the fractal Hausdorff-Besicovitch dimensionality. For the determination of the fractal dimension one can use the Fractal Dimension Solver (FDS), which is prepared for this thesis by the application of the open source object-oriented programming, see Fig. 6.5. This application is based on the method of the embedded squares, see Fig. 6.6 [10].

According to this method one can observe and check the fractal geometry of various nanocrystal structures. For the above mentioned algorithm the fractal dimension for the ZnO array is shown in Figs. 6.6 and 6.7.

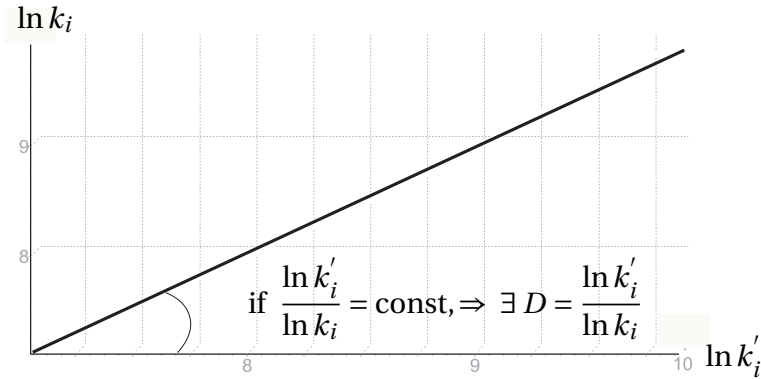


Figure 6.7: Example of the determination of the fractal dimension by the consideration of the dependence between the square numbers k_i and the total numbers of the units affected fractal structure k'_i

The dimension is equal to $D = 2.024$. Balankin [9, 10] obtained the relation between elastic properties and fractal dimension in the case of isotropic material.

6.2 Results: Analysis of applied methods

Let us compare the difference between the obtained results of the applied methods by the material parameters estimation. The fractal method, which allows to estimate the functional properties, is resembled to the way of taking into account the size-effect in the process of the comparison of the micro- and macrolevel. For example one can consider a relationship between the intrinsic length scale and the fractal dimension of the fractal aggregate. The parameters of the stiffness matrix, which are not presented in Table 6.2, are equal to zero. In the rows ZnO FA and ZnO PM the averaged elastic properties of the transversal isotropic material are shown. In the row ZnO FA the results, which were obtained with the fractal analysis, are shown and the row ZnO PM presents the results based on methods of classical theory of fiber-reinforced composites (polydisperse model with cylindrical inclusions and three-phase model with cylindrical inclusions).

After averaging of the material parameters of the homogeneous layer of the crystals on the substrate indicated in the Table 6.2 the numerical experiments of the eigenvalue problem and the case of a shear loading are of interest, because these experiments can show us more accurately the difference between the elastic response in the layer by using of two methods of the ma-

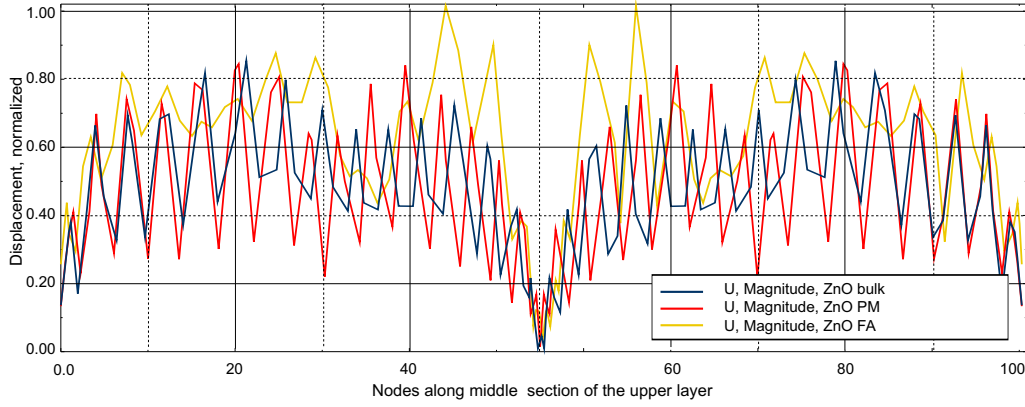


Figure 6.8: Comparison of the displacement change between averaged layer and not averaged layer by eigenvalue analysis (case of 3rd mode)

terial parameters estimation. In the Fig. 6.8 the plots with change of displacement along a middle-section of the layer in case of eigenvalue $2.05e + 7$ Hz and respective eigenmode are depicted. In Figs. 6.8, 6.10 -6.11 one can see the qualitative coincidence of the displacements and stresses in the case of identical eigenmodes and equal loads, respectively. The principal differences consists in the value of the local variations according to the remainder of the maximal and minimal values of considered functions, which describe the presented processes in the indicated intervals. Figure 6.9 shows the difference between material behavior in the case of the averaged layer and in the case of the original material parameters as the result of the shear traction. Even in this case the qualitative coincidence of the results by the various modifications of the layer material can be observed.

All presented pictures have a horizontal and vertical symmetry of the stress

Table 6.2: Mechanical properties of elastic layer

C [MPa]	$C_{11} = C_{22}$	$C_{12} = C_{21}$	$C_{13} = C_{31}$	
ZnO bulk	$1.90 \cdot 10^4$	$1.10 \cdot 10^4$	$0.90 \cdot 10^4$	
ZnO FA	$5.10 \cdot 10^3$	$0.60 \cdot 10^3$	$1.70 \cdot 10^3$	
ZnO PM	$4.30 \cdot 10^3$	$2.00 \cdot 10^3$	$1.60 \cdot 10^3$	
C [MPa]	$C_{23} = C_{32}$	C_{33}	$C_{44} = C_{55}$	C_{66}
ZnO bulk	$1.10 \cdot 10^4$	$1.10 \cdot 10^4$	$0.39 \cdot 10^4$	$0.45 \cdot 10^4$
ZnO FA	$1.17 \cdot 10^3$	$7.8 \cdot 10^3$	$3.9 \cdot 10^3$	$4.5 \cdot 10^3$
ZnO PM	$1.16 \cdot 10^3$	$1.13 \cdot 10^3$	$3.1 \cdot 10^3$	$1.02 \cdot 10^3$

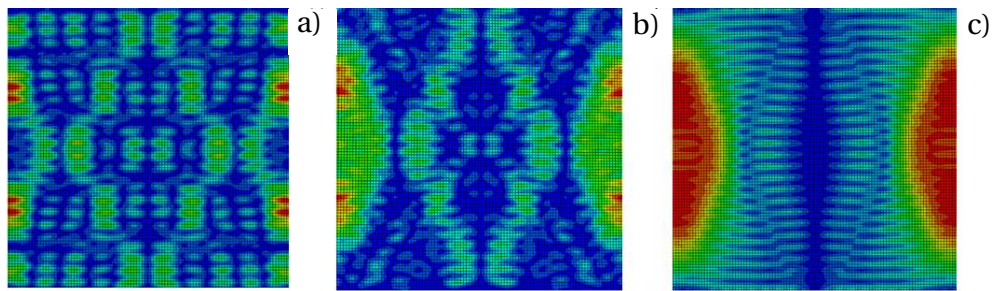
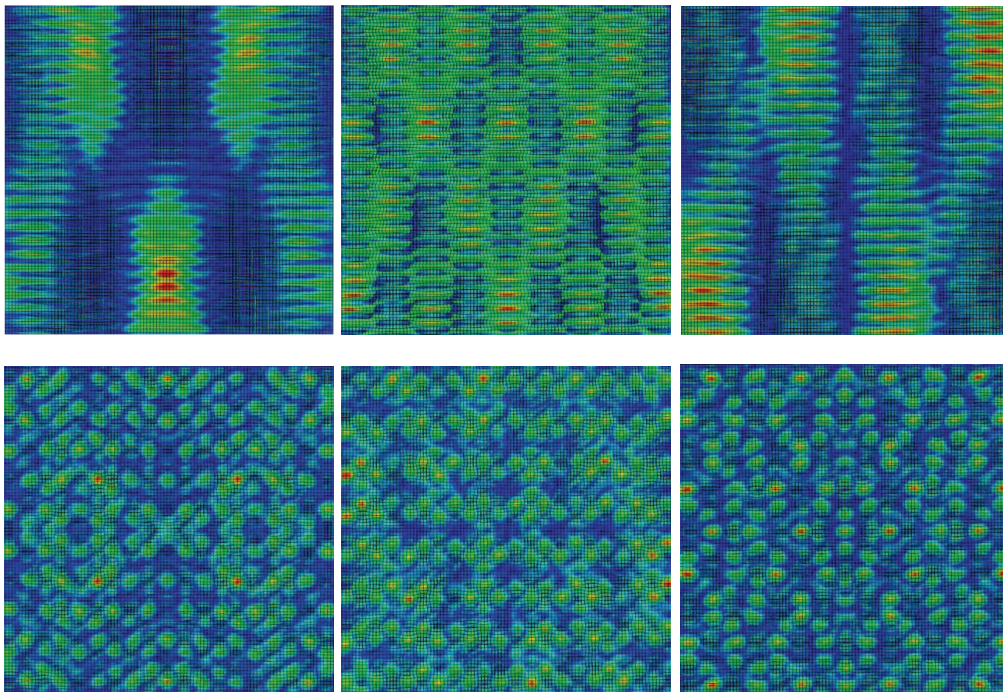


Figure 6.9: Von Mises stress distribution: a) ZnO properties; b) Averaged properties with the fractal analysis; c) Averaged properties with the methods of classical mechanic of fiber composites



Averaged layer with general ZnO properties Recalculated properties (polydisperse model) Recalculated properties (fractal analysis)

Figure 6.10: First two eigenmodes of crystal layer with different material properties

distributions in the case of the shear load, Fig. 6.9. The figures have the minimum stress in their center and equal quantity of the pronounced area of stress variations with the comparable stress amplitude. Such material behavior can be explained by the preservation of a transversely isotropic type of symmetry

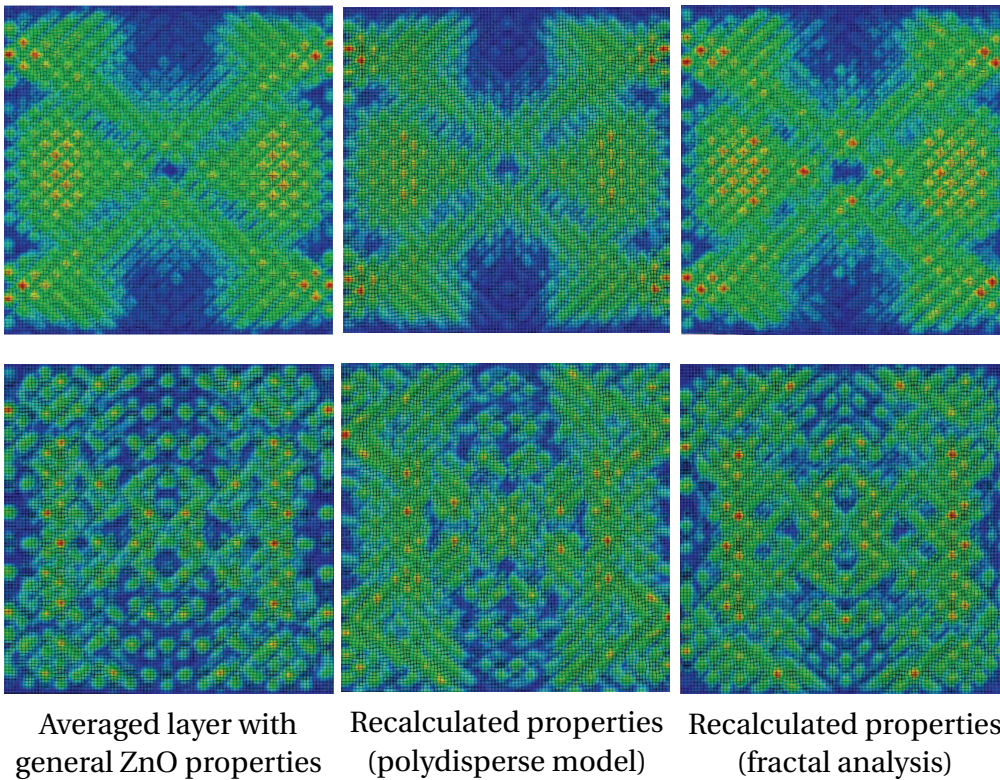


Figure 6.11: Second two eigenmodes of crystal layer with different material properties

of the averaged material according to the recalculated stiffness matrix. The use of the polydisperse and three-phase models with cylindrical inclusions is connected with a more complicated implementation. With help of these methods one can obtain exact results only in the case of the special geometry. In other cases the experimental verification of the stiffness matrix is required. The realization of the second method of the mechanical properties estimation is easier in the case of a geometry with fractal topology. Nevertheless, the possibility of the recalculation of the functional properties of an array of nanocrystals with both methods of fiber-reinforced composite mechanics and fractal analysis is given. This makes it possible to use simplified FEM simulation in investigation of crystal/fiber array structures and implementation of the simulation results in the production of MEMS/NEMS based on crystal/fiber piezoelectric arrays.

Conclusions

7.1 Summary

The main result of the presented thesis is the development of methods of analysis of spiral piezoelectric multilayer shells and shells/crystal arrays. In addition, simulations of their behavior are presented, especially under the consideration of the particular influence of the environment. Obviously, this investigation requires the implementation of software packages for the solution of the governing equations. In particular, the following results for the models of nanostructures with chiral elements are obtained:

- A model of one- and multi-layer shell with a helical geometry and particular properties of the active layers is constructed. The mathematical model is based on the principles of continuum mechanics. With help of numerical methods several physical problems concerning the features of the nanoshell behavior are investigated.
- The simulation of both the direct and the inverse piezoelectric effects with consideration of various types of piezoelectric properties is provided. As a result the structure behavior under mechanical and electrical loads, the influence of the polarization type and the complex geometry of the belt by the electro-elastic task is considered.
- The basic unknown parameters of the system are obtained by numerical calculations. The eigenvalue analysis with the determination of the eigenvalues and respective eigenmodes of a nanoshell is performed. The obtained results can find practical applications in the determination of functional properties of multi-layer shells and some structures

which contain agglomerates of helical shells. It should be noted that the results of the above described eigenvalue problem gave a good agreement with results, that were published before cf. [31, 32, 36].

- The problem of the interaction of a piezoelectric shell with a non-linear environment is completely solved. It should be noted that this complicated problem is solved numerically by using the two-way exchange between finite element and finite volume method.
- The different influence of a Newtonian and non-Newtonian fluid in the context of the obtained fields of unknown variables is investigated. At once two models for the parametric analysis of an interaction of a helical membrane with external environment are proposed. As an additional feature of the considered processes the particular effects in a non-linear fluid are mentioned, for example, the Weissenberg effect, thixotropy, etc. As a consequences of the results, that are obtained by the coupled hydroelastic analysis the possibility of a contactless control of the shell motion is offered.
- The most interesting question is the stability loss problem under the influence of the electric field in the process of inverse piezoelectric effect. Taking into account the physical linearity of the material behavior the reason of the stability loss is based on the finite strain theory. As a consequence of the buckling problem modeling in the case of the inverse piezoelectric effect the values of the critical potentials, buckling modes, distributions of the principal variables are obtained. Moreover, one of the principal results of the present work is the detection of the possible influence on the results of the stability loss problem. The difference of the results of two different materials with different piezoelectric modulus distributions by considering the size-effect is revealed. Also the advanced supposition that buckling under the electrical fields cannot be modeled by effective mechanical loads in general, is supported by numerical experiments. This principal conclusion exposes the necessity of a further development of a numerical or natural analysis for the design of the precise-working systems made from singular chiral structure or assemblies.
- The model of a composite with chiral-shell inclusions and the model of an array of crystals on a substrate are constructed. By the consideration of a characteristic unit cell of a composite with chiral inclusions the principal material characteristics are numerically obtained. However, the principal differences of the functional properties of a general composite by changing the twisting of the interior helixes, initial prop-

erties of the matrix and inclusions, etc. are detected. The most attractive feature is the increase of changes of relative to a general material symmetry according to the elastic and electric properties. The detection of this opens a new possibility to produce effective devices with chiral elements.

- The behavior of crystal arrays on a substrate is investigated. In this case the determination of the functional properties of the general structure is performed. However, for the estimation of the functional properties the theoretical methods of the classical composite mechanics and the fractal theory are used. The fractal theory is the suitable for investigated structures, because such agglomerates of crystals conserve the attributes of a fractal structure.
- Due to the fact, that the system of crystals/fibers array on the substrate is modeled as a homogeneous multi-layer structure, the question of the wave distribution as transport of energy without transport of matter is investigated. The unusual wave front distribution on the active wave surface (homogeneous layer of crystals) by consideration of various types of boundary conditions is mentioned. The results of this part of the work can be used for the design of a metamaterial structure with chiral properties and for prediction of their mechanical and electrical response.

7.2 Outlook

In the field of the present research a lot of other questions are still open (see Fig. 7.1, green boxes). For example, such questions can be the dynamic simulations of the twisting of nanofilms made from nanobelts under the residual stress, taking into account the analysis of the influence of different types of anisotropy and polarization of the shell. Another problem is the separation of laminated films, forming multilayer structures. The processes of a multilayer shell creation involve the considerable internal stresses as the reason of the distortion of the shell crystalline lattice [97, 103]. Obviously, it is important to identify the conditions for such exfoliation and to try to optimize the cases of possible structure disintegration. However, the consideration of nanofilm adhesion to the layers and to the substrate is required.

In Section 4.2 there is mentioned, but not completely studied the question of the specifics of complex behavior of non-linear fluid interacting with a piezoelectric shell. Obviously, there are more problems of the proper mod-

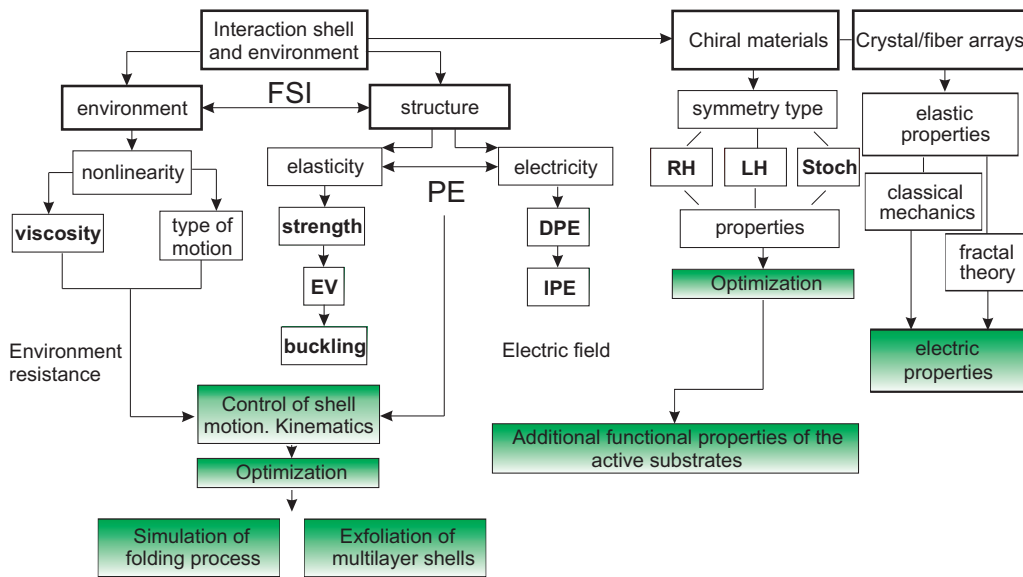


Figure 7.1: Overview and outlook of the problems discussed in the thesis

eling and they require special investigations, especially with respect to the real properties of the shell environment. The control of the kinematics of the piezoelectric shell under consideration of the environment effects is important for the production of nanostructures as elements of MEMS/NEMS. As a consequence, the kinematics control opens additional possibilities in optimization of the shape and material parameters of the structure.

In Chapter 5 the particular properties of a metamaterial are investigated. These investigations were restricted to the case of piezoelectric properties of chiral elements in the source matrix. However, at the present time one of the most perspective applications of the metamaterials is the application in solar cell. For the simulation of such processes it is necessary to consider photoelectric materials composed of helical shells. At present time applications are in the field of the solar cell modeling.

The modeling of the above described open issues can significantly influence the development of nanotechnology in the area of using shell-like helical structures and their assemblies. Thus, the set of the problems solved in the present work, as well as the above described open issues, see Fig. 7.1, allow to construct a complete model of helical nanostructures and to open new opportunities for their application in practice with development of the modern nanotechnologies.



Bibliography

- [1] H. Altenbach. *Kontinuumsmechanik - Eine elementare Einführung in die materialunabhängigen und materialabhängigen Gleichungen*. Springer, Heidelberg, 2. edition, 2012. [16, 17, 20, 83]
- [2] H. Altenbach, J. Altenbach, and W. Kissing. *Mechanics of Composite Structural Elements*. Springer, Berlin, 2004. [39, 42]
- [3] H. Altenbach and V. A. Eremeyev. On the shell theory on the nanoscale with surface stresses. *Int. J. Eng. Sci.*, 49:1294 – 1301, 2011. [62]
- [4] H. Altenbach and V. A. Eremeyev, editors. *Generalized Continua: from the Theory to Engineering Applications*. Number 541 in CISM Courses and Lectures. Springer, Wien, New York, 2012. [16, 71]
- [5] H. Altenbach, V. A. Eremeyev, and N. F. Morozov. Mechanical properties of materials considering surface effects. In A. Cocks and J. Wang, editors, *IUTAM Symposium on Surface Effects in the Mechanics of Nanomaterials and Heterostructures*. IUTAM Bookseries, pages 105 – 115. Springer, 2013. [62]
- [6] ANSYS, Inc., Canonsburg. *ANSYS Workbench User's Guid*, v. 13.0 edition, 2010. [34]
- [7] G. Astarita and G. Marrucci. *Principles of non-Newtonian Fluid Mechanics*. McGraw-Hill, Maidenhead, 1974. [26, 27, 28, 29, 46, 54]

- [8] A. E. Babenko and B. Soltaninia. Solution of the geometrically nonlinear problem on the deformation of a helical spring by variational methods (in Russ.). *Vestn. NTUU "KPI", Mashinostroenie*, (5):47 – 51, 2007. [55]
- [9] A. S. Balankin. Quantum statistical approach to dynamic problems of solid mechanics. *Revista Mexicana de Fisica*, 41:147 – 180, 1995. [91]
- [10] A. S. Balankin. Elastic behavior of materials with multifractal structures. *Phys. Rev. B.*, 53:5438 – 5443, 1996. [14, 89, 90, 91]
- [11] D. J. Bell, L. X. Dong, B. J. Nelson, M. Golling, L. Zhang, and D. Grützmacher. Fabrication and characterization of three-dimensional InGaAs /GaAs nanosprings. *Nano Lett.*, 6:7 – 25, 2006. [11, 62]
- [12] D. J. Bell, Y. Sun, L. Zhang, L. X. Dong, and D. Grützmacher. Three-dimensional nanosprings for electromechanical sensors. *Sens. Actuators A: Physical*, 54:130 – 131, 2006. [3, 10, 11]
- [13] B. Bhushan (Ed.). *Handbook of Nanotechnology*. Springer, Berlin, 2007. [5, 39]
- [14] V. L. Biderman and V. N. Shitikov. Tension and torsion on cylindrical ribbon spring in the presence of large displacements (in Russ). *Izv. AN SSSR. Mekhanika Tverdogo Tela*, (1):137 – 141, 1970. [61]
- [15] P. R. Buseck, S. J. Tsipursky, and R. Hettich. Fullerenes from the geological environment. *Science*, 257:215 – 217, 1992. [1, 3]
- [16] F. Capolino. *Theory and Phenomena of Metamaterials*. CRC Press, Boca Raton, 2009. [4, 71]
- [17] N. A. Chernyishev. *Stability of Compression Springs (in Russ.)*. Mashgiz, Moskva, 1946. [57]
- [18] A. Y. Cho and J. R. Arthur. Molecular beam epitaxy. *Prog. Solid State Chem.*, 10:157 – 192, 1975. [8]
- [19] R. Christensen and K. Lo. Solutions for effective shear properties in three phase sphere and cylinder models. *J. Mech. Phys. Solids*, 27(4):315 – 330, 1979. [42, 74, 85, 86, 87, 88]
- [20] S. Cuenot, C. Fretigny, S. Demoustier-Champagne, and B. Nysten. Surface tension effect on the mechanical properties of nanomaterials measured by atomic force microscopy. *Phys. Rev. B*, 69:165410–1 – 165410–5, 2004. [62, 78]

- [21] Dassault Systemes. *ABAQUS User's Manual*, v. 6.12 edition, 2012. [14, 34, 36, 42, 45, 63, 66, 79]
- [22] T. Delclos, C. Aim, and E. Pouget. Individualized silica nanohelices and nanotubes: Tuning inorganic nanostructures using lipidic self-assemblies. *Nano Lett.*, 8:1929 – 1935, 2008. [6]
- [23] G. Demazeau. Solvothermal reactions: an original route for the synthesis of novel materials. *J. Mater. Sci.*, 43:2104 – 2114, 2008. [7]
- [24] M. V. Donadon, S. F. M. Almeida, and A. R. de Faria. Stiffening effects on the natural frequencies of laminated plates with piezoelectric actuators. *Compos. B Eng.*, 5:335 – 342, 2002. [39]
- [25] H. L. Duan, J. Wang, Z.P. Huang, and B. L. Karihaloo. Size-dependent effective elastic constants of solids containing nano-inhomogeneities with interface stress. *J. Mech. Phys. Solids*, 53:1574 – 1596, 2005. [62, 78]
- [26] H. L. Duan, J. Wang, and B. L. Karihaloo. Eshelby formalism for nano-inhomogeneities. *Proc. R. Soc. Lond. A*, 461(2062):3335 – 3353, 2005. [85]
- [27] H. L. Duan, J. Wang, and B. L. Karihaloo. Nanoporous materials can be made stiffer than non-porous counterparts by surface modification. *Acta Mater.*, 54(11):2983 – 2990, 2006. [62]
- [28] H. L. Duan, J. Wang, and B. L. Karihaloo. Theory of elasticity at the nanoscale. In E. van der Giessen and H. Aref, editors, *Advances in Applied Mechanics*, volume 42, pages 69 – 252. Academic Press, London, 2008. [3, 6, 10, 62]
- [29] N. Engheta and R. W. Ziolkowski, editors. *Metamaterials: Physics and Engineering Explorations*. Wiley, Hoboken, 2006. [3, 71]
- [30] V. A. Eremeyev, H. Altenbach, and N. F. Morozov. The influence of surface tension on the effective stiffness of nanosized plates. *Dokl. Phys.*, 54:98 – 100, 2009. [62]
- [31] V. A. Eremeyev, E. A. Ivanova, N. F. Morozov, and A. N. Soloviev. On the determination of eigenfrequencies for nanometer-size objects. *Dokl. Phys.*, 51:93 – 97, 2005. [40, 44, 96]
- [32] V. A. Eremeyev, E. A. Ivanova, N. F. Morozov, and A. N. Soloviev. Method of determining the eigenfrequencies of an ordered system of nanoobjects. *Tech. Phys.*, 52:1 – 6, 2007. [39, 40, 96]

- [33] V. A. Eremeyev, E. A. Ivanova, N. F. Morozov, and S. E. Strochkov. Natural vibrations of nanotubes. *Tech. Phys.*, 52:431 — 435, 2007. [39]
- [34] V. A. Eremeyev, E. A. Ivanova, N. F. Morozov, and S. E. Strochkov. The spectrum of natural oscillations of an array of micro- or nanospheres on an elastic substrate. *Dokl. Phys.*, 52:699 — 702, 2007. [39, 44]
- [35] V. A. Eremeyev, E. A. Ivanova, N. F. Morozov, and S. E. Strochkov. Natural vibrations in a system of nanotubes. *J. Appl. Mech. Tech. Phys.*, 49:291 — 300, 2008. [39]
- [36] V. A. Eremeyev and W. Pietraszkiewicz. Stiffening effects on the natural frequencies of laminated plates with piezoelectric actuators. *J. Elasticity*, 85:125 – 152, 2002. [42, 96]
- [37] A. Erturk and D. J. Inman. Appendix E: Numerical data for PZT-5A and PZT-5H piezoceramics. In *Piezoelectric Energy Harvesting*, Chichester, 2011. John Wiley and Sons. [41, 42]
- [38] L. B. Freund. Substrate curvature due to thin film mismatch strain in the nonlinear deformation range. *J. Mech. Phys. Solids*, 48(6 – 7):1159 – 1174, 2000. [39]
- [39] L. B. Freund and H. T. Johnson. Influence of strain on functional characteristics of nanoelectric devices. *J. Mech. Phys. Solids*, 49(9):1925 – 1935, 2001. [39]
- [40] K. Fricke. Piezoelectric properties of GaAs for application in stress transducers. *J. Appl. Phys.*, 70:914 – 918, 2000. [69, 79]
- [41] A. Ghosh and P. Fischer. Controlled propulsion of artificial magnetic nanostructured propellers. *Nano Lett.*, 9:2243 – 2245, 2009. [11, 39, 40, 46, 53, 62]
- [42] C. T. Gibson, D. A. Smith, and C. J. Roberts. Calibration of silicon atomic force microscope cantilevers. *Nanotechnology*, 16:234 – 238, 2005. [3]
- [43] A. A. Girchenko, V. A. Eremeyev, and H. Altenbach. Interaction of a helical shell with a nonlinear viscous fluid. *Int. J. Eng. Sci.*, 61:53 – 58, 2012. [55]
- [44] A. A. Girchenko, V. A. Eremeyev, and N. F. Morozov. Modelling of spiral nanofilms with piezoelectric properties. *Phys. Mesomech.*, 13:5 – 10, 2010. [45, 61]

- [45] W. A. Goddard, D. W. Brenner, S. E. Lyshevski, and G. J. Iafrate. *Handbook of Nanoscience, Engineering and Technology*. CRC-Press, Boca Raton, 2003. [39, 62]
- [46] M. V. Goncharenko and V. V. Goncharenko. Geometric nonlinearity of mechanical behaviour as a consequence of large deformations of springs. *J. Engng. Phys. Thermophys.*, 82:1229 – 1234, 2009. [60]
- [47] H. Grabert and M. H. Devoret, editors. *Single Charge Tunneling: Coulomb Blockade Phenomena in Nanostructures*. Plenum Press, New York, 1992. [10]
- [48] K.-H. Grote and J. Feldhusen, editors. *Dubbel – Taschenbuch für den Maschinenbau*. Springer, Berlin, 2007. [57, 59]
- [49] Z. Gu, M. P. Paranthaman, M. P. Xu, and Zh. W. Pan. Aligned ZnO nanorod arrays grown directly on zinc foils and zinc spheres by a low-temperature oxidization method. *ACS Nano*, 3:273–281, 2009. [2, 83]
- [50] I. G. Gurrie. *Fundamental Mechanics of Fluids*. McGraw-Hill, Hightstown, New York, 1993. [27, 29]
- [51] M. Yu. Gutkin and I. F. Ovid’ko. *Physical Mechanics of Deformed Nanostructures*. Yanus, St. Petersburg, 2003. [26, 39]
- [52] D. W. Hadley and J. D. Weber. Rheological nomenclature. *Rheologica Acta*, 14:1098 – 1109, 1975. [54]
- [53] A. Hajati and K. Sang-Gook. Ultra-wide bandwidth piezoelectric energy harvesting. *Appl. Phys. Lett.*, 99(8):083105–1 – 083105–3, 2011. [5, 44]
- [54] B. Q. Han, Lavernia I., and Mohamed F. A. Mechanical properties of nanostructured materials. *Rev. Adv. Mater. Sci.*, 9:1 – 16, 2005. [71]
- [55] Z. Hashin and B. W. Rosen. The elastic moduli of fiber-reinforced materials. *J. Appl. Mech.*, 31:223 – 232, 1964. [14, 85, 86, 87, 88]
- [56] H. Hauptman and J. Karle. Solution of the phase problem I. The centrosymmetric crystal. *Acta Cryst.*, 8(6):365 – 366, 1955. [69]
- [57] L. H. He, C. W. Lim, and B. S. Wu. A continuum model for size-dependent deformation of elastic films of nano-scale thickness. *Rev. Adv. Mater. Sci.*, 41(3-4):847 – 857, 2004. [71]

- [58] L. L. Hench and J. K. West. The sol-gel process. *Chem. Rev.*, 90:33, 1990. [7]
- [59] A. Hochbaum and P. Yang. Semiconductor nanowires for energy conversion. *J. Am. Chem. Soc.*, 110:527 – 546, 2010. [5, 83, 89]
- [60] Y. W. Hsu, S. S. Lu, and P. Z. Chang. Piezoresistive response induced by piezoelectric charges in n-type GaAs mesa resistors for application in stress transducers. *J. Appl. Phys.*, 85:333 – 340, 1991. [69]
- [61] S. S. Huang and X. Zhang. Extension of the stoney formula for film-substrate systems with gradient stress for MEMS applications. *J. Microelectromech. Microeng.*, 16(2):382 – 389, 2007. [5, 6]
- [62] S. S. Huang and X. Zhang. Gradient residual stress induced elastic deformation of multilayer MEMS structures. *Sens. Actuators A. Phys.*, 134:177 – 185, 2007. [4, 5, 6]
- [63] W. L. Hughes and Z. L. Wang. Piezoelectric single-crystal nanorings and nanobows. *J. Am. Chem. Soc.*, 126(21):6703 – 6709, 2004. [6]
- [64] C. Hwang, G. Dockendorf, D. J. Bell, L. X. Dong, H. Hashimoto, D. Poulikakos, and B. J. Nelson. 3-d InGaAs/GaAs helical nanobelts for optoelectronic devices. *Int. J. Optomech.*, 2(2):88 – 103, 2008. [1, 2]
- [65] G. Hwang and H. Hashimoto. Development of human-robot shared tele-tweezing system. *IEEE Trans. on Cont. Syst. Tech.*, 15(5):960 – 966, 2007. [1, 2]
- [66] T. Ikeda. *Fundamentals of Piezoelectricity*. Oxford University Press, New York, 1990. [22, 25, 26, 46]
- [67] T. Ishikawa. Effect of non-newtonian property of blood on flow through a stenosed tube. *Fluid Dynamics Research*, 22:251 – 264, 1998. [4, 26, 46, 48, 49]
- [68] E. A. Ivanova and N. F. Morozov. An approach to the experimental determination of the bending stiffness of nanosize shells. *Dokl. Phys.*, 50:83 – 98, 2005. [13, 40, 45]
- [69] E. A. Ivanova, N. F. Morozov, B. N. Semenov, and A. D. Firsova. Determination of elastic moduli of nanostructures: Theoretical estimates and experimental techniques. *Mech. Solids*, 40:60 – 72, 2005. [13, 45]

- [70] S. Y. Jeong, J. Y. Kim, H. D. Yang, A. N. Yoon, S. H. Choi, H. K. Kang, C. W. Yang, and Y. H. Lee. Synthesis of silicon nanotubes on porous alumina using molecular beam epitaxy. *Adv. Mater.*, 15:1172 – 1176, 2003. [8]
- [71] M. Kaltschmitt, H. Hartmann, and H. Hofbauer. *Energie aus Biomasse. Grundlagen, Techniken und Verfahren*. Springer, Berlin, 2009. [7]
- [72] J. H. Koo. *Polymer Nanocomposites. Processing, Characterization, and Applications*. McGraw-Hill, New York, 2006. [4, 73]
- [73] J. Lagowski, H. C. Gatos, and Sprolesand E. S. Surface stress and the normal mode of vibration of thin crystals: GaAs. *Appl. Phys. Lett.*, 26(9):493 – 495, 1975. [69, 79]
- [74] L. D. Landau and E. M. Lifshitz. *Fluid mechanics, Course of Theoretical Physics*. Pergamon Press, New York, 1987. [17, 26, 27, 28, 31]
- [75] M. Law, J. Goldberger, and P. Yang. Semiconductor nanowires and nanotubes. *Annu. Rev. Mater. Sci.*, 34:83 – 122, 2004. [2, 8]
- [76] R. J. LeVeque. *Numerical methods for conservation laws / Randall J. LeVeque*. Birkhäuser Verlag, Boston, 1990. [35]
- [77] C. W. Lim and L. H. He. Size-dependent nonlinear response of thin elastic films with nano-scale thickness. *Int. J. Mech. Sci.*, 46(11):4631 – 4647, 2004. [62, 78, 79]
- [78] P. Lu, L. H. He, H. P. Lee, and C. Lu. Thin plate theory including surface effects. *Int. J. Solids Struct.*, 43(16):4631 – 4647, 2006. [62, 78, 79]
- [79] A. I. Lurie. *Nonlinear Theory of Elasticity*. North-Holland, Amsterdam, 1990. [19]
- [80] A. I. Lurie. *Theory of Elasticity*. Springer, Berlin, Heidelberg, 2005. [16, 18, 19]
- [81] Z.-Z. Mai, Y.-W. and Yu. *Polymer Nanocomposites*. Woodhead Publishing Limited, Cambridge, 2006. [71, 73]
- [82] B. Mandelbrot. *The Fractal Geometry of Nature*. W. H. Freeman Company, New York, 1988. [88]
- [83] G. A. Maugin. *Continuum Mechanics of Electromagnetic Solids*. North-Holland, Amsterdam, 1988. [15, 16, 17, 22, 25, 46, 69]

- [84] G.I. Mikhasev and P.E. Tovstik. Stability of conical shells under external pressure. *Mech. Solids*, 25(4):106 – 119, 1990. [55]
- [85] V. Mittol. *Optimization of Polymer Nanocomposite Properties*. Wiley-VCH, Weinheim, 2010. [4, 71, 73, 82]
- [86] Ch. Mohammad, T. Pall, and A. S. John. Gram-scale production of graphene based on solvothermal synthesis and sonication. *Nature Nanotech.*, 4(1):3 – 30, 2008. [7]
- [87] F. C. Moon. Franz Reuleaux: Contributions to 19th century kinematics and theory of machines. *Applied Mechanics Reviews*, 56(2):261–285, 2003. [59]
- [88] H. S. Nalwa. *Handbook of Nanostructured Materials and Nanotechnology*. Academic Press, New York, 2000. [10, 62]
- [89] A. V. Nasedkin. Finite element modeling of hydroacoustic piezoelectric semiconductor transducers (in Russ.). *IGM NAN Ukraini. Zhovtnya*, 1(3):159 – 164, 2003. [25, 26]
- [90] Ya. G. Panovko and I. I. Gubanova. *Stability and Oscillations of Elastic Systems: Current Concepts, Paradoxes and Errors (in Russ.)*. Nauka, Moskva, 1987. [55, 57, 58]
- [91] J. Pendry. A chiral route to negative refraction. *Science*, 306:1353 – 1355, 2004. [67]
- [92] Q. Peng and Yu. Qin. ZnO nanowires and their application for solar cells. In S. Suzuki, editor, *Physical and Chemical Properties of Carbon Nanotubes*. Springer, 2013. [83]
- [93] S. D. Ponomarev and L. E. Andreeva. *Design of Elastic Elements of Machines and Devices (in Russ.)*. Mashinostroenie, Moskva, 1980. [55, 58, 60]
- [94] V. Y. Prinz, D. Grützmacher, A. Beyer, C. David, B. Ketterer, and E. Deckardt. A new technique for fabricating three-dimensional micro- and nanostructures of various shapes. *Nanotechnology*, 12:399 – 402, 2001. [1, 6, 8, 48]

- [95] V. Y. Prinz, D. Grützmacher, A. Beyer, C. David, B. Ketterer, and E. Deckardt. A new concept in fabricating building blocks for nanoelectronic and nanomechanic devices. *Microelectron. Eng.*, 69:466 — 475, 2003. [1]
- [96] V. Y. Prinz and V. Ya. Prinz. Application of semiconductor micro- and nanotubes in biology. *Surf. Sci.*, pages 532 — 535, 2003. [4, 5]
- [97] V. Y. Prinz and V. A. Seleznev. Nanoscale engineering using controllable formation of ultra-thin cracks in heterostructures. *Microelectron. Eng.*, 30:439 – 442, 1996. [4, 6, 7, 8, 10, 97]
- [98] V. Y. Prinz, V. A. Seleznev, and A. K. Gutakovsky. Nanohelices and their arrays. *Physica E*, 6:828 – 831, 2000. [1, 48, 83, 85]
- [99] V. Ya. Prinz. New precise nanostructures: semiconductor shells and their well ordered arrays. In *Chemistry and Application of Nanostructures*, pages 471 – 474, Hackensack, 2003. World Scientific. [6, 7, 69]
- [100] V. Ya. Prinz. New ultra-precise semiconductor and metal nanostructures: tubes, shells and their ordered arrays. In *Nanotechnology, 2003. IEEE-NANO 2003. 2003 Third IEEE Conference on*, volume 1, pages 199 – 204, 2003. [1, 7]
- [101] V. Ya. Prinz. A new concept in fabricating building blocks for nanoelectronic and nanomechanic devices. *Microelectron. Eng.*, 69:2 — 4, 2006. [7, 8]
- [102] V. Ya. Prinz and S. V. Golod. Elastic silicon-film-based nanoshells: Formation, properties, and applications. *J. Appl. Mech. Tech. Phys.*, 47:2 — 4, 2006. [4, 7, 8]
- [103] V. Ya. Prinz, V. A. Seleznev, and A. K. Gutakovsky. Application of controllable crack formation for nanoelectronic device elements fabrication. *Inst. Phys. Conf. Ser.*, 155:49 — 54, 1996. [6, 97]
- [104] T. Qiu and P. K. Chu. Self-selective electroless plating: An approach for fabrication of functional 1D nanomaterials. *Materials Science and Eng.: R: Reports*, 61(1 – 6):59 – 77, 2008. [89]
- [105] U. Rabe, K. Janser, and W. Arnold. Vibrations of free and surface-coupled atomic force microscope cantilevers: Theory and experiment. *Rev. Sci. Inst.*, 67:3281 – 3293, 1996. [3]

- [106] M. Reiner and S. Blair. *Rheology Terminology*. Academic Press, New York, 1967. [46]
- [107] M. Remskar. Inorganic nanotubes. *Adv. Mater.*, 16:1497 – 1504, 2004. [8]
- [108] W. Ritz. *Neue Methode zur Lösung gewisser Randwertaufgaben*. Gesellschaft der Wissenschaften zu Göttingen, Göttingen, 1908. [35]
- [109] V. G. Shevchenko. *Fundamentals of Physics, Polymer Composite Materials*. Springer, Berlin, 2010. [71]
- [110] Tesis, Moscow. *FlowVision 3.xx.xx (-HPC), Software Manual*, 2009. [32, 34, 36, 37]
- [111] S. P. Timoshenko. *Theory of Elastic Stability*. McGraw-Hill, New York, 1961. [17, 19, 25, 55]
- [112] E. F. Toro. *Riemann Solvers and Numerical Methods for Fluid Dynamics*. Springer Verlag, Berlin, 2009. [35]
- [113] P. E. Tovstik. *Stability of Thin Shells (in Russ.)*. Nauka, Moskva, 1995. [55]
- [114] C. Tropea, A. L. Yarin, and J. E. Foss. *Principles of non-Newtonian Fluid Mechanics*. Springer, Berlin, 2007. [26, 28, 29, 46]
- [115] C. Truesdell. *The Elements of Continuum Mechanics*. Springer, New York, 1966. [15, 16, 17, 18, 19, 20, 21, 25]
- [116] Z. C. Tu, Q. X. Li, and X. Hu. Theoretical determination of the necessary conditions for the formation of ZnO nanorings and nanohelices. *Phys. Rev. B*, 73:115402–1 – 115402–6, 2006. [62]
- [117] A. V. Turik and G. S. Radchenko. Maxwell – Wagner relaxation in piezoactive media. *J. Phys. D: Appl. Phys.*, 35:1188 – 1192, 2002. [14]
- [118] R. Vasilescu and Dancila D. S. Modeling and analysis of active flap using coiled bender piezoelectric actuators. *J. Intell. Mater. Syst. Struct.*, 15:9 – 10, 2004. [5]
- [119] W. Voigt. *Lehrbuch der Kristallphysik*. Teubner, Leipzig, 1928. [20, 23, 24, 69]
- [120] E. A. Vopilkin, V. I. Shashkin, Yu. N. Drozdov, V. M. Daniltsev, A. Yu. Klimov, V. V. Rogov, and I. Yu. Shuleshova. Piezoelectric anisotropic effect in MEMS, based on the epitaxial heterostructures $\text{Al}_{0.5}\text{Ga}_{0.5}\text{As}/\text{AlAs}$. *J. Intell. Mater. Syst. Struct.*, 10(1):75 — 79, 2009. [69]

- [121] S. Voronov and Yu. Poplavko. Piezo- and pyroelectric GaAs sensors integrated in one crystal with GaAs fet. *J. of Vibroengineering*, 12:119 – 224, 2009. [69, 79]
- [122] B. Wang, J. Zhou, T. Koschny, M. Kafesaki, and C. Soukoulis. Chiral metamaterials: simulations and experiments. *J. Opt. A: Pure Appl. Opt.*, 11:1 – 10, 2009. [2, 3, 62, 71]
- [123] J. Wang, H. L. Duan, Z. P. Huang, and B. L. Karihaloo. Zinc oxide nanostructures: Synthesis and properties. *Nano Lett.*, 3:16 — 25, 2004. [2, 3, 7, 10, 62]
- [124] J. Wang, H. L. Duan, Z. P. Huang, and B. L. Karihaloo. A scaling law for properties of nano-structured materials. *Proc. R. Soc. A*, 462:1355 — 1363, 2006. [3, 62, 83]
- [125] Y. Xia, P. Yang, Y. Sun, Y. Wu, B. Mayers, B. Gates, Y. Yin, F. Kim, and H. Yan. One-dimensional nanostructures: synthesis, characterization, and applications. *Adv. Mater.*, 15:353 – 389, 2003. [1]
- [126] X. Yang and J. Ni. Electronic properties of single-walled silicon nanotubes compared to carbon nanotubes. *Phys. Rev. B*, 72:195426–1 – 195426–5, 2005. [8]
- [127] G. C. Yi, Ch. Wang, and W. I. Park. ZnO nanorods: synthesis, characterization and applications. *Semicond. Sci. Technol.*, 20(4):22 – 34, 2005. [1, 2]
- [128] G. Zegrya, N. Gunko, and A. Polkovnikov. New semiconductor materials. characteristics and properties, 2001. [41, 48, 56, 57, 73, 74, 85]
- [129] Y. Zhang, Y. Chi-Wei, A. Taylor, and S. Yang. Replica molding of high-aspect-ratio polymeric nanopillar arrays with high fidelity. *Langmuir*, 22:8595 – 8601, 2006. [62, 73, 83, 85]
- [130] M. Zhao, Zh. Wang, and S. X. Mao. Characterization of individual zinc oxide nanobelt probed by piezoresponse force microscope. *Nano Lett.*, 4:587 – 590, 2004. [6, 70, 71]
- [131] L. G. Zhou and H. C. Huang. Are surfaces elastically softer or stiffer? *Appl. Phys. Lett.*, 84(11):1940 – 1942, 2004. [62]
- [132] L. M. Zubov. The exact theory of tension and twisting of screw springs. *Dokl. Phys.*, 47(8):623 – 628, 2002. [55]